Universidade do Minho
Escola de Engenharia

Nuno Martins Magalhães

Impedance Control Applied to Robotic Platforms

Dissertação de Mestrado

Mestrado em Engenharia Eletrónica Industrial e Computadores

Trabalho efetuado sob a orientação da

Professora Doutora Cristina P. Santos

Dezembro de 2018

ACKNOWLEDGEMENTS

Anything worth doing takes work and this thesis was a lot of work. This work, however, would not be possible if not for the time and effort of some people.

First and foremost, I would like to express my deepest gratitude to my advisor Prof. Cristina Santos, who gave me a chance. I am extremely grateful for her dedication, support and motivation, providing me with an excellent atmosphere to complete my thesis. I am sincerely grateful for her excellent guidance and perseverance, encouraging me to tackle the different problems of this research. The help provided allowed to finish this work and become a more capable person for the future.

Second, I would like to thank the Ph.D. student, the engineer César Ferreira, who aided Prof. Cristina Santos in supervising my work. It was thanks to him that I was able to overcome some of the hardest hurdles during the thesis, by always being there with helpful (most of the times) criticism and guidance.

I also would like to thank the University of Minho and all my professors for giving me an education of excellence and providing me the tools I needed to follow this path. They helped me build the boat in which I sailed during this journey.

My friends and laboratory colleagues that helped in moments of more stress and tension with their jokes and stories. They were definitely the breadth of fresh air whenever I needed.

Last, but not least, the support from my family was always constant. They were the anchor that held me and allowed me to rest, providing me financial and emotional support throughout my entire life. Its thanks to them that I even got the opportunity to start this journey in the first place, and for that, I will be forever grateful.

RESUMO

A perda de um membro pode criar dificuldades significativas nas tarefas quotidianas de uma pessoa, sendo pior em situações mais incomuns, como correr ou saltar. Isso cria problemas com pessoas que precisam de passar por uma amputação, prejudicando o seu bem-estar. Com as dezenas de milhões de amputados no mundo e este número aumentando a cada ano, o desenvolvimento de dispositivos prostéticos capazes de emular um membro humano torna-se uma necessidade cada vez mais importante. O desenvolvimento de próteses tem melhorado consideravelmente ao longo dos anos, no entanto a maioria das próteses comercialmente disponíveis hoje em dia, são passivas e, portanto, não são capazes de fornecer a quantidade necessária de energia para recriar uma marcha humana adequada. Para superar esse problema, próteses ativas estão sendo pesquisadas em todo o mundo.

Esta tese foca-se no desenvolvimento de um controlador de uma prótese transtibial com base no conceito de controlo de impedâncias. Este tipo de controlador tenta recriar o tipo de controlo presente em humanos, onde a impedância de saída de um membro pode ser alterada para permitir um movimento mais adaptável. A prótese foi projetada para funcionar como um dispositivo autónomo e usar os seus sensores e uma máquina de estado para alterar a impedância de saída do dispositivo. O protótipo da prótese foi projetado para ser usado pelo robô humanoide Darwin-OP, que tem uma marcha ambulante semelhante à de um humano.

O controlador requer a otimização de vários parâmetros. Para esta tarefa, um algoritmo genético foi empregue para ajudar na determinação dos parâmetros do controlador, bem como a dos parâmetros para o controlador da marcha do Darwin-OP, sendo este baseado num controlador de Geração de Padrões Central.

Uma comparação entre adicionar ou não, um modelo dinâmico do corpo do atuador para o controlador, foi realizada. Essa comparação forneceu informações sobre as vantagens e desvantagens do uso de um modelo no controlador e levou à escolha do controlo sem o modelo na prótese transtibial.

No final, a otimização foi capaz de determinar os parâmetros para o controlador da prótese e o robô simulado de Darwin-OP, com o dispositivo. O humanoide foi capaz de andar para frente, embora a uma velocidade menor do que o humanoide sem a prótese. Em relação ao controlador, este foi capaz de detetar com precisão as fases de *Stance* e *Swing* do dispositivo. Testes ao controlador foram realizados em simulação usando o Webots ™.

Palavras Chave:
Controlo de Impedâncias, Robô Bípede, Prótese Transtibial, Algoritmo Genético

ABSTRACT

A loss of a limb can create significant difficulties in the everyday tasks of a person, being worse in more uncommon situations such as running or jumping. This creates problems with people that need to undergo an amputation, taking a toll on their wellbeing. With the tens of millions of amputees in the world and their number increasing every year, the development of prosthetic devices that are able to emulate a human limb becomes a necessity. The development of prostheses has improved over the years, by a considerable amount, however, most prostheses commercially available nowadays, are passive and therefore are not able to provide the necessary amount of energy to recreate proper human gait. To overcome this problem, active powered prostheses are being researched across the world.

This thesis focuses on the development of a powered transtibial prosthesis's controller based on the concept of impedance control. This type of controller tries to recreate the type of control found in humans, where a limb's output impedance can be altered to allow for a more adaptable motion. The prosthesis was designed to work as a standalone device and use its sensors and a finite state machine to alter the output impedance of the device. The prosthesis' prototype was designed to be worn by the Darwin-OP humanoid robot, which has a walking gait similar to that of a human.

The controller requires the optimization of several parameters. For this task, a genetic algorithm was employed to help determine the controller parameters, as well as the parameters for the Darwin-OP waking motion controller, this one being based on Central Pattern Generators.

A comparison between adding or not, a dynamic model of the actuator's body to the controller, was performed. This comparison provided information about the advantages and disadvantages of using a model on the controller and led to the choice of foregoing the model in the transtibial prosthesis.

In the end, the optimization was able to determine the parameters for the prosthesis controller and the simulated Darwin-OP robot, with the device. The humanoid was able to walk forward, albeit at a slower speed than the humanoid without the prosthesis. In regard to the controller itself, it was able to accurately detect the stance and swing phases of the device. Tests of the controller were performed in simulation using Webots™.

Keyword:
Impedance Control, Bipedal Robot, Transtibial Prosthesis, Genetic Algorithm Optimization

TABLE OF CONTENTS

LIST OF FIGURES

LIST OF TABLES

Acronyms

CPG	**C**entral **P**attern **G**enerator
DOF	**D**egree **of** **F**reedom
CNS	**C**entral **N**ervous **S**ystem
COM	**C**entre **of** **M**ass
GRF	**G**round **R**eaction **F**orce
FSR	**F**orce **S**ensor **R**esistor
PID	**P**roportional–**I**ntegral–**D**erivative
DC	**D**irect **C**urrent
PWM	**P**ulse **W**idth **M**odulation
GA	**G**enetic **A**lgorithm
SBX	**S**imulated **B**inary **C**rossover
MIT	**M**assachusetts **I**nstitute of **T**echnology
CPR	**C**ounts **P**er **R**evolution
IMU	**I**nertial **M**easuring **U**nit
ZMP	**Z**ero **M**oment **P**oint
UART	**U**niversal **A**synchronous **R**eceiver-**T**ransmitter
AEDA	**A**ccelerometry-based **E**vent **D**etection **A**lgorithm
ACPO	**A**mplitude **C**ontrolled **P**hase **O**scillator
KAG	**K**nee **A**ngle **G**enerator
COP	**C**enter **of** **P**ressure
EMG	**E**lectro**m**yo**g**raphy
FSI	**F**inite **S**tate **I**mpedance
EEA	**E**xplosive **E**lastic **A**ctuation
VSA	**V**ariable **S**tiffness **A**ctuation
SEA	**S**eries **E**lastic **A**ctuators
SEAPS	**S**eries **E**lastic **A**ctuation with **P**arallel **S**pring
PAM	**P**neumatic **A**rtificial **M**uscles
CF	**C**onventional **F**eet
ESR	**E**nergy-**S**toring-and-**R**eturning

CHAPTER 1 INTRODUCTION

This thesis was developed in the Mestrado Integrado em Engenharia Eletrónica Industrial e Computadores (MIEEIC) in the Departamento de Eletrónica Industrial (DEI) of the Universidade do Minho (UM), more specifically in the branch Control, Automation and Robotics (CAR).

This work addresses the field of artificial devices that replace a missing body limb, focusing on a prosthesis for the ankle-foot. The goal of this work is the development of a controller for an active transtibial prosthesis, using the concepts from impedance control. The implemented controller was tested, both in a simulated environment, using a simulated humanoid biped robot and the Webots ™ robotic simulator, and in a real environment, using the same biped robot and a prototype of the prosthesis develop by an element of the laboratory's team.

1.1 Motivation, Scope and Problem Statement

Limb amputation is still a hard choice to make, for both doctors and patients alike. Since that human-like motion is still unavailable, having a lost limb replaced by a prosthetic device, with their slow and awkward motions, will still negatively effect on the wearer's ability to perform even the basic of human activities.

With over 30 million amputees in the world (Alcaide-Aguirre, Morgenroth and Ferris, 2013) and thousands of new cases every year, mainly due to war, cancer, birth defects, accidents and vascular diseases, especially diabetes (Torrealba, Fernández-López and Grieco, 2008), the development of limb prostheses becomes crucial as it can improve the lives of these millions of people. From the several causes, defective blood supply is the main one and as it is related to patient age, more than half of amputees are older than 65 years old, with just 25% of amputees being younger than 54 (Windrich *et al.*, 2016).

Focusing on the lower limb amputation as they represent 90% of new amputations, 39% are transfemoral, 53% are transtibial. Thus, the development of lower limb prostheses is important as it can lead to an increase in life quality of millions of people by restoring their mobility (Windrich *et al.*, 2016).

Due to their necessity, prostheses have evolved significantly, over the years. Research on the creation of prostheses is now focused on prostheses that function as extensions of the human body structurally, neurologically and dynamically (King *et al.*, 2017) and not lifeless mechanisms. The goal of these researches is the synthetization of a mechanism that will functionally mimic the missing part of an anatomical leg and, therefore, restore the normal gait and be able to perform several tasks of daily living, such as climbing stairs, walking up and down a slope or simply balancing their legs. Some important technological advances that have had a significant impact on the improvement of prostheses are the creation of energy-storing ankle-foot complexes, the integration of microprocessors in the prostheses control, the development and use of more efficient actuators technologies (like series elastic actuators) and the improvement of control frameworks that exploit principles of bio-inspired movements. Current prostheses are still far from perfect. They still present some shortcomings, mainly related to the control strategies.

A major problem of current prostheses is the increase in the amount of effort needed to use one. It is known that the ankle joint is essential to be able to walk, as it is responsible for a significant amount of the net work involved in walking, substantially more than the knee and the hip joint. In (1990), Winter showed that the ankle flexors produce 80% of the mechanical power generated during normal walking. However, most of the existing commercial transtibial prostheses are energetically passive and do not provide actuation, thus being unable to provide net power at the joints. This presents lower limb amputees with an extraordinary loss in power generation. Because of their passive builds, these types of prostheses can cause an increase of 20 to 30% of metabolic energy for the amputee, when compared to able-bodied individuals while walking at comparable speeds (Collins and Kuo, 2005).

The development of new actuators and new control methods allows for the creation of prosthesis capable of motions closer to that of a human. These advances, in prosthetics devices and their controllers, are an important research field as it can improve the quality of life of millions of individuals.

1.2 Research Goals and Research Questions (RQ)

The objective of this thesis is to develop a controller for a transtibial prosthesis, designed for the humanoid robot Darwin-OP. To achieve this main goal, an extensive survey of the state of the art on impedance control on legged robots and in ankle prosthesis was done, several goals achieved, and research questions answered. To achieve the final objective, the following goals need to be addressed:

(Goal 1): Find the advantages and disadvantages of using the impedance controller with and without a dynamic model of the device. This goal will help justify the use or not of the dynamic model of the device, on the controller.

(Goal 2): Develop a controller which uses impedance control to actuate a transtibial prosthesis. This goal aims to design the impedance controller and optimize it, by means of a genetic algorithm optimizer.

(Goal 3): Develop the controller hardware for the physical prosthesis prototype. After developing the controller, the hardware for the prosthesis controller needs to be implemented. This goal can be divided into smaller tasks such as the selection of the hardware, comprising od sensors, actuators and electronics to be incorporated in the prototype, the analysis of the walking gait to generate the required control in real time, as well as the delineation of the experiments to validate the prototype.

The following research questions (RQ) are expected to be answered:
(RQ1): What are the advantages and disadvantages of using a dynamic model on an impedance controller?
(RQ2): Is it possible to substitute the ankle pitch joint of the Darwin-OP robot with an impedance-controlled prosthesis?
(RQ3): Is a two-state finite state machine impedance controller sufficient to control the transitions of the prosthesis for the humanoid robot?

1.3 Report Structure

This document is organized as follows. The first chapter introduces the thesis with the motivation for the work and the structure of the thesis. It is followed by the literature review, where works relating to the interaction control history, impedance control in legged robots and in active ankle prostheses are analyzed. Chapter 3 presents the work done with the impedance control and its implementation on a two-link planar robotic arm. This chapter showcases the benefits and problems of using the robot's dynamic model in the controller. In Chapter 4, the controller used for the generation of the gait motion for the healthy individual and the healthy joints for the individual robot is explained. This chapter also includes the optimization method used to determine the parameters for the Central Pattern Generator controller and the impedance Controller. Chapter 5 focus in the Impedance controller for the prosthesis, presenting the results of the simulation tests. The conclusions and future work can be found in the last chapter.

CHAPTER 2 STATE OF THE ART

To better understand the work that has already been done in the area of impedance control in prosthesis controllers, several works were studied. Impedance control can be classified as an interaction control method, and therefore to better comprehend it, a brief history of interaction control is also presented. This chapter is divided as such, the first part is on the history of interaction control, followed by impedance control in legged robots and finally an overview of the state of the art of active powered lower limb prosthesis.

2.1 Interaction Control History

Understanding movement and manipulation as well as how they may be best controlled could be seen as a fundamental problem in robotics and in several other different fields, for example, neurophysiology. Understanding the strategies employed by the central nervous system in the control of movement, such as normal controls and movement commands in a human, is one of the several endeavors of neurophysiology. This aids in the development of artificial prosthesis and orthosis and how they may be best implemented, providing better tools to rehabilitate people with functional disabilities. It also aids in the development of robots with homologous body parts to a human being.

In the cases previously mentioned, the prosthetics and the human-like body parts for robots, as well as a large number of industrial robots, require manipulation in some faction. For manipulation to occur, by any reasonable definition of physical manipulation, mechanical interaction with the object or multiple objects is required. This may be especially true if a human-like nature is to be emulated. If mechanical interactions are involved, then the manipulation action can be classified by the magnitude of the mechanical work exchanged between the manipulator and its environment (Hogan, 1985).

In some cases, the interactions forces are negligible, allowing for the manipulator to be treated as an isolated system, and having the control, and consequently the motion, being handled by its position, velocity or acceleration as the controlled variables. Position control has been the base, generally, of some industrial robots, and some more successful applications have been restricted to this type of control, for example, spray-painting and welding. (Whitney, 1977).

In other situations, the manipulator may encounter constraints in its environment and the resulting interactions are may not negligible. However, while being kinematically coupled with the environment, dynamic interactions could still be absent. One of such examples is a motion alongside a pure (i.e. frictionless) kinematic constraint. In this case, an appropriate control method could be the combination of motion control along the tangent of the constraint and force control along the normal (Raibert and Craig, 1981). This approach to manipulator control has been termed “compliance” or “force control” (Mason, 1981), being more properly named “accommodation” (Nevins and Whitney, 1972). Although being a topic that is currently being researched considerably, it has not yet seen a widespread industrial application.

The most general case is when the dynamic interactions are neither zero or negligible. As examples of this situation, in an industrial setting, we have a large class of manufacturing operations, such as drilling, bending, grinding, or any task that requires work to be done on the environment. In general, any task that involves the use of a tool can also be given as an example. (Hogan, 1985). The daily activities of a prosthesis or an orthosis user can also be included as an example, where the dynamic interactions are not negligible since prostheses are made to replace the missing limb and orthoses, to help a weak or malfunctioning limb. Both of these devices are designed to interact with the environment, directly or indirectly, and exchange work with it.

Due to the non-negligible dynamic interactions, present in most cases, the manipulator may no longer be treated, for the control purposes, as an isolated system, and thus the strategies usually employed for the control, for example, position or velocity, will be inadequate. Is then necessary to utilize a control method which is able to handle the mechanical work exchange between the manipulator and its environment. This control method must manage the effects the interactions have in the controlled variables. These effects can vary between a loss of performance to, more importantly, the loss of stability. The loss of stability is known as coupled or contact instability and can be found even in simple systems with basic controllers, when in contact with basic environments. (Hogan and Buerger, 2005). The vulnerability to coupled instability can be partially attributed to the fact that the actuators and the sensors are not co-located and the difficulty to design a robot with no significant dynamics interposed between its actuators and the points at which it contacts with the environment (Tilley and Cannon Jr, 1986; Sharon, Hogan and Hardt, 1988).

The development of a controller that is insensitive or even able to ignore the properties of an environment can bring other benefits other than the prevention of coupled instability. Take for an example, an assembly robot, that might pick up a component, move it across free space, bring it into contact with a kinematic constraint used to guide placement of the component, move it along the constraint, release the component, and return to get another. In this scenario three different stability challenges are presented, the movement of the unload robot, the transport of the component and the movement complying with the kinematic constraint. In this situation, a different controller is necessary for each moment, therefore the system must decide which controller to use at each instant and manage the transitions between them. Taking in account that easiest way to identify an environment is to interact with it, is clear to see that a single controller that can perform satisfactorily within all expected contexts without compromising stability, would have significant advantages, over a system involving multiple controllers and a transition event handler.

Control theory offers several tools to give controllers the ability to deal with unknown or poorly characterized interference (Levine, 1996). Some of the most relevant, that are not base in controlling the interactions, are the following:

- Disturbance Rejection.
- Modeling Uncertainty.

Disturbance Rejection

One of the possible tools is the rejection of disturbances, where the dynamics of the environment is included as a disturbance (Zhiqiang Gao, 2006). Design by J. Hans as a way out of the robust control paradox, it was first coined in (Gao, Huang and Han, 2001). This technique depends on the limitations of the perturbing forces. The forces of perturbation must be considerably smaller than the forces of the robot, which, in several applications where there are interactions with the environment, does not happen. In some situations, the perturbations can be equal or even exceed the forces of the robot. The fact that interaction forces depend on the state of the robot and the forces of non-perturbations also a reason why this technique is not adequate to deal with interactions.

Modeling Uncertainty

Another method to address interactions without interaction control is to model the environment as an uncertain part of the robot and using robust control tools (Levine, 1996). Interaction with the environment effectively changes the dynamics of the robot by adding a combination of elastic, dissipative and inertial properties, or kinematic constraints. If the alteration of the parameters of the robot is the only effects of the interaction (i.e. adding a mass to the endpoint), then this method is a viable choice. However, this method can suffer an unacceptable loss of performance, when trying to create a controller robust to a large range of environmental parameters, and its applicability is undermined, when it is possible to alter the structure of the model (i.e. the addition or reduction of degrees of freedom of the parts contacting a constraint).

2.1.1 Interaction Control

Instead of trying to overwhelm the consequences of interaction by building robustness, a different approach where design to regulate the interactions themselves, by controlling the robot's dynamic behavior at the points, also called ports, where the interactions occur. The most common forms of interaction control regulate the manipulator's impedance or admittance. Some of the most studied methods that regulate impedance are the:

- Explicit force control.
- Hybrid Position/Force Control.
- Impedance Control.
- Direct Impedance Modulation.

Explicit force control

The most direct approach, when trying to regulate interactions, is explicit force control. Explicit force control involves the direct measurement and command of force values, with the goal of having the output follow the input as closely as possible. The most commonly discussed force-based techniques usually employ some form of PID control and some simple form of filtering. In Paljug *et al.* (1992), it is shown, that explicit force control tries to accomplish a non-causal relation, thereby creating problems (Goldenberg, 1992; Grabbe *et al.*, 1992).

Hybrid Position/Force Control

A conceptually simple approach to controlling compliant motions of a robot manipulator. This technique is described as a hybrid, as it combines force and torque information with positional data to satisfy simultaneous position and force trajectory constraints specified in a convenient task related coordinate system (Raibert and Craig, 1981). Considering the presence of constrained and unconstrained directions of a robot in contact with an environment, this control approach has the unconstrained directions as a position control problem, while the constrained ones are force controlled. Although this technique addresses some of the problems of the position/velocity controllers, it still requires a well-defined environment. Since this method uses both position and force control, it may suffer from both kinematic instability and dynamic instability. (Fedele, Fioretti and Ulivi, 1992)

Impedance Control

One early attempt to an implementation of an impedance controller was proposed by Hogan (Hogan, 1985). This approach, termed “simple” impedance control, has been used with considerable success. It is based on the driving of an intrinsically low friction mechanism with force or torque-controlled actuators, and the use of motion feedback to increase output impedance. From a controller design point of view, the simple impedance control law closely resembles a PD motion controller acting on the error between the actual and desired trajectory. As mentioned, the use of this approach, requires the use of an intrinsically low friction mechanism, because the controller makes no attempt to compensate for any physical impedance in the mechanism, resulting in the actual output impedance consisting in the sum of the controller impedance and the internal impedance due to the mechanism.

Although it is primitive, a “simple” impedance controller goes a long way toward solving the stability problem, and its performance gets better as the inherent robot impedance is reduced. In practice, though this implementation performs well in some applications, it has limitations. Several factors make the controller impedance not passive, including discrete-time controller implementation and unmodeled dynamics between actuator and sensor.

Direct Impedance Modulation

A complementary approach to implementing interaction that does not fall back on feedback is to modulate impedance directly. This method relies on the fact that apparent inertia is readily modulated by taking advantage of kinematic redundancies in the robot mechanism. Using the human muscular-skeletal system as an example, the mechanical impedance may be varied by using different body segments as the interaction port and/or by varying the pose of the rest of the muscular-skeletal system. For example, with the phalanges partially flexed the fingertips present an extremely low mechanical impedance to their environment, while with the elbow fully extended, the arm presents a high impedance along the line joining hand to shoulder.

Impedance modulation can also be achieved by taking advantage of actuator redundancies. In the human muscular-skeletal system, muscle only pulls, so they are generally arranged in opposition about the joints so that positive and negative torques may be generated. Not only this but the fact that the number of muscles substantially exceeds the number of skeletal degrees of freedom. Per Hogan (1990), the torque contributions of different muscles may counteract each other, impedance contributions of said muscles always add to the joint impedance, resulting in direct mechanical impedance modulation without adjusting its pose.

2.1.2 Improving Low Impedance Performance

By having the ability to control the desired impedance or admittance of a robot, a large class of applications which require more complaint controls (i.e. having the ability to give way to an external force, and return to the desired position afterward), can be achieved. This can be done by employing robots with low mechanical impedance. An example of this type of applications are robots that interact with humans. To achieve a low impedance robot, the most direct and recommended approach is to design low impedance hardware and use a simple impedance control algorithm, for example, the “Simple” Impedance Controller. However, due to the difficulty in the design of low impedance hardware, especially with complex geometries and large force or power outputs, this approach can still be hard to implement. Therefore, the need for controllers to reduce the apparent endpoint impedance of interactive robots has been the subject of considerable effort. The most direct control method to accomplish this is by employing force feedback.

Force Feedback

Force feedback is probably the most appealing approach for reducing apparent impedance since this method minimizes the deviation between the actual end-point force and the desired force. This approach, however, has some fundamental limitations. Some of the control approaches previously stated refer themselves as an alternative to force feedback, since its implementation is not simple. This coupled to the fact that, theoretically the largest force feedback gain is desirable to minimize undesirable components provided by the intrinsic robot behavior, for example, nonlinear friction and that large force feedback will lead to instability in almost every case, shown by Colgate (1988). Colgate stated that, because any real robot will almost inevitably exhibit resonance, under force feedback the system becomes non-passive with a force feedback loop gain greater than unity, making it vulnerable to coupled instability. To overcome this problem, a few other methods, such as the Natural Admittance Control and the Series Dynamics Actuation, were proposed.

Natural Admittance Control

To overcome some of the problems caused by the Force Feedback, more specifically the loss of passivity, Newman proposed the Natural Admittance Control or NAC (Newman, 1992). This approach is based on the fact that, under force feedback, the system becomes non-passive when the apparent inertia is reduced, but the passivity is not compromised by the elimination of friction. Natural admittance control specifies a desired inertia that is close to that of the physical system (the “natural admittance”) and focuses on reducing friction as much as possible, preserving passivity.

Series Dynamics Actuation

An alternative to stabilizing interactions with force feedback is to place compliant and/or viscous elements in series between the manipulator and its environment. This method has been used since the early attempts at robot force control (Whitney, 1977), followed by other implementations using springs incorporated within force control actuators to facilitate force feedback and absorb impacts (Pratt and Williamson, 1995). Series Elastic Actuators (SEA) are a departure from the traditional approach of rigid actuation. The addition of the elastic element provides unique properties to the actuator when comparing to rigid actuators, which include lowering the mechanical output impedance, increasing the tolerance to impact loads, increasing the peak power output and providing passive mechanical energy storage. These properties align with the requirements of robustness, high-power output and energy efficiency of legged actuation systems, resulting on SEAs being widely adopted within the fields of legged robotics and human orthosis (Paine, Oh and Sentis, 2014).

2.2 Legged Robots

The methods previously mentioned were developed to increase the versatility of robotic devices in environments with inaccurate, poorly accurate or inexistent models. Looking at humans and animals, it can be inferred that robots endowed with arms and/or legs are more adequate to assist or even replace humans in dangerous, non-stimulating or plain just unpleasant jobs. While legs allow the robot to move with agility, in environments normally only accessible to humans or animals, the arms allow the execution of the required functions or tasks with the dexterity of a human.

Even with a long history and a considerable amount of research on these types of robots, they are still mostly confined to research labs and a few prototype demonstrations on controlled situations. With these limitations, one can argue with the versatility of said robots (Semini *et al.*, 2015). To be considered versatile, a robot must be able to be utilized in different situations, especially in situations other similar robots cannot be used, such as difficult terrain or human-engineered environments, as a factory floor or a house.

As it was mentioned previously, position controllers are the type of controllers that have seen the wider spread of applications in industry. However, an automatous robot can only have a precise model of the environment it is inserted if this environment is heavily controlled. In cases were, this type of environment isn't possible, it being too complex or being in constant change, a controller capable in dealing with collisions and harder contacts, in a safe and robust manner is highly desirable. This desire led to controllers that use the previously mentioned methods for interaction control.

The physical laws governing interaction dynamics show that it is essential to control the joint torques and/or the contact forces during interactions with the environment (Hogan, 1985). Studies have shown that humans and animals are able to accomplish this type of joint control, thanks to muscle pairs that act in reverse of each other. The elasticity of the tendons in combination with muscle control allows the adjustment of both the passive and active joint impedance (Hogan, 1984; Shadmehr and Arbib, 1992; Tee *et al.*, 2010). Active impedance for the hand or the foot is obtained essentially the same way (Burdet *et al.*, 2001; Franklin *et al.*, 2003; Selen, Franklin and Wolpert, 2009), and as per Kandel et al (2000) and Geyer and Herr (2010), this control is normally delayed by few tens of milliseconds or more.

The different ways to cope with interactions forces resulting from contacts with the environment, develop over the years by several pieces of research, can be divided by the type of impedance they employ. This can be passive impedance, active impedance or a combination of the two types. The types of impedance can be characterized as such:

2.2.1 Passive Impedance

The approaches that rely on passive impedance, use passive dynamics of mechanical or pneumatic springs, to govern the interactions dynamics (Raibert, 1986; Buehler *et al.*, 1998). By using the resonant frequency of the resulting spring-mass system, walking, resonant hopping and running motions can be achieved, as seen in (Pratt and Williamson, 1995), where SEA, series elastic actuators, were proposed. This type of actuator has, usually stiff, springs, that are tasked to control the joint forces, absorb impact peaks and temporarily store energy. The use of springs in electrically actuated robots is popular, as they can also protect gears from damage.

These springs, however, introduce low-frequency resonant modes, as well as the, previously mentioned, passive dynamics, in the system, and therefore have to be tuned for a certain purpose. While this is fine for a single-purpose machine, it can drastically reduce the versatility, and thus usefulness of said machine.

To overcome this problem, researchers proposed variable stiffness actuators (VSAs), that can vary their stiffness with the help of a smaller second actuator (Vanderborght *et al.*, 2013). While some progress has been made in this field, the actuators are still bulky, complex and often not able to absorb high energy impacts, due to the limited size of the springs.

Legged robots controlled with passive impedance

There are several examples of robots that utilize these types of actuators. For example, the quadruped Hyq (Hydraulically powered quadruped robot) (Figure 1) (Semini *et al.*, 2011). Develop in the Istituto Italiano di Technologia, as a test platform, it provides a way to study various aspects of quadrupedal locomotion, this robot stands 1 meter tall and weighs roughly 91 Kg.

The Hyq robot has a combination of hydraulically and electrically actuated joints controlling the four articulated legs and the torso frame. Each of the legs has three active joints, which control the hip and knee's DOFs, with a passive ankle joint and foot.

The addition of a spring for the passive ankle joint helps in the reduction of impact forces peaks at foot touch-down during running and rough terrain locomotion. The spring is also used to estimate the ground contact forces, by measuring the spring's compression using a linear potentiometer. Additional shock absorbance was also achieved by the viscous-elastic rubber foot. The overall stiffness of the leg is a combination of active and passive components and can be adjusted by the torque-controlled joints.

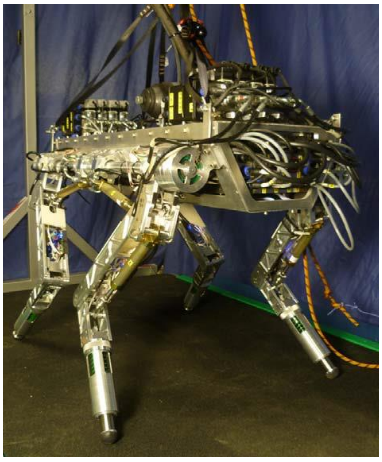

Figure 1: Picture of the hydraulically and electrically actuated quadruped robot HyQ on a laboratory treadmill (Semini *et al.*, 2011).

For a bipedal robot example, the M2V2 (Figure 2) can be pointed out (Pratt and Krupp, 2008). As the name may imply, this robot is the second version of a biped robot called M2. M2 was first developed at MIT Leg Laboratory by Dan Paluska, Gil Pratt and colleagues, with M2V2 building upon it to address some problems typically found in first version prototypes.

Using the same mechanical joint anatomy similar to its predecessor, the robot has twelve DOFs for its legs and no upper-body DOFs as its main goal is bipedal walking research. The actuators used in M2V2 are SEAs with integrated force and positioning sensors, which allows for easier integration and control of the actuators.

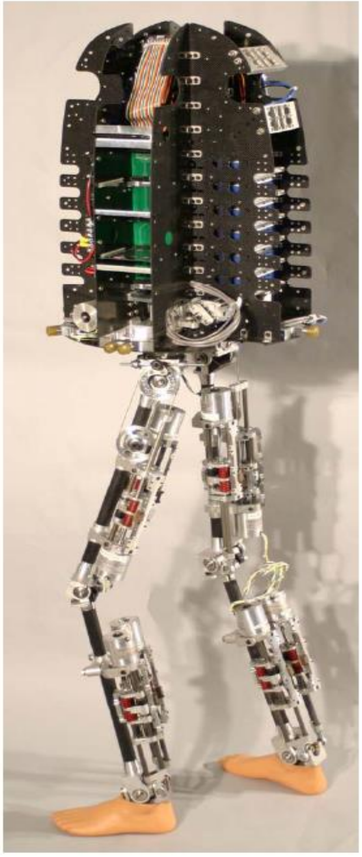

Figure 2: M2V2 side view of the assembled robot body and legs. Not shown are batteries and cable harnesses to the 12 Series Elastic Actuators. (Pratt and Krupp, 2008)

Another biped robot is MABEL (Figure 3), a testbed at the University of Michigan's EECS Department (Grizzle *et al.*, 2009). This robot grew out of a collaboration effort between the University of Michigan and the Robotic Institute of Carnegie Mellon University. Unlike the M2V2, MABEL is a planar bipedal robot comprised of five links assembled to form a torso and two legs with knees and with the legs terminating in point feet. The planar nature of the robot is manifested in the hips, which are constrained to only operate in the sagittal plane. Although being attached to a boom, forcing a circle trajectory, if the circle has a sufficiently large radius, the trajectory can be approximated to a straight line. One MABEL differs from other biped robots in several ways. One of the different aspects of MABEL, other than the lower number of DOFs on the legs, is the location of the actuators for said DOFs. These are located in the torso, so as to make the legs as light as possible. Another difference is the fact that the actuators of each leg do not correspond to the knee and hip angles, but rather to a collection of differentials. These differentials connect the two motors, with one motor control the angle of the virtual leg and the other connected in series, in order to control the length or shape of the virtual leg. The springs used in MABEL are also unilateral in the sense that they compress but do not extend beyond their nominal resting length.

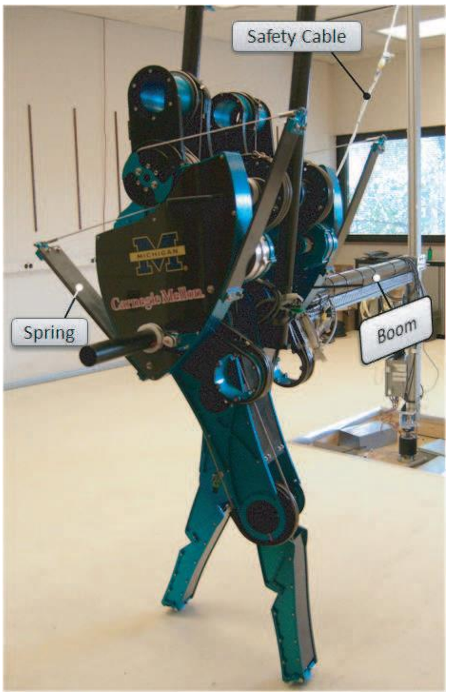

Figure 3: MABEL Robot (Grizzle *et al.*, 2009)

2.2.2 Active Impedance

Active impedance is a promising alternative that does not require any physical springs, since the required stiffness and damping can be controlled by software, using for example, impedance control by Hogan(1985), operational space control by Khatib (Khatib, 1987), and virtual model control by Pratt *et al.*(2001), and by using torque-controlled actuators This allows the real-time selection of any stiffness and damping, while within the limitations of the actuation control system, whether it be the end-effector or for each joint independently (Boaventura *et al.*, 2013). This approach has most of the advantages of VSA without the aforementioned limitations. An experimental comparison was performed by Boaventura et al. (2013), between passive and active compliance. Their results show that active impedance joints can emulate passive elements in the dynamic range needed for locomotion and interaction with the environment in general, showing no relevant difference between the actively controlled system and its fully passive counterpart.

Legged robots controlled with active impedance

Within the literature, there are only a few examples of purely impedance-controlled legs with an internal torque control loop. Ott et al. (2012) presented a bipedal robot denominated as DLR-Biped (Figure 4), since its torque-controlled electric motors actuators, with integrated joint torque sensors, are based on the modular drives of the DLR Lightweight Robot II (Hirzinger *et al.*, 2001).

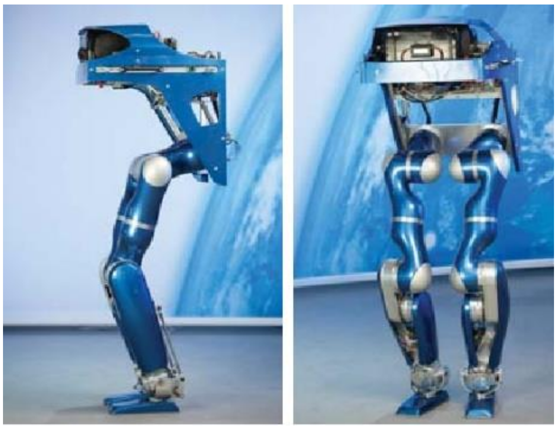

Figure 4: DLR-Biped, (Ott *et al.*, 2012)

Designed to allow research on walking based on joint control, the drive system is also stiff enough to allow comparison with position-based walking control algorithms. For the leg kinematics, a non-redundant configuration with six degrees of freedom per leg was chosen. This robot is equipped with motor position and joint torque sensors, as well as a pair of two six-axis force/torque in the feet, for the ability to compare bipedal walking controllers-based admittance control. It also employs an IMU (Inertial Measuring Unit), for the measure of the orientation of the trunk, and a stereo camera system to allow research on autonomous navigation. To achieve a walking motion, an underlining ZMP (Zero Moment Point) controller approach was followed, and in the end, the work showed that the robot was successful in demonstrating a walking motion on flat ground, as well as balancing and posture control. The work also showed promising results in experiments with stairs.

Another, electrically actuated, is the four-legged with purely impedance-controlled joints, MIT cheetah robot (Figure 5). Hyun *et al.* (2014) presented a quadruped robot with joint torque control implemented with electric motors with low gear ratio and current control, without the need for springs and torque sensing elements in their approach. In Hyun et al., (2014) the robot successfully demonstrated a running gait on a treadmill with reliable impedance control on a joint level, while supported by a beam.

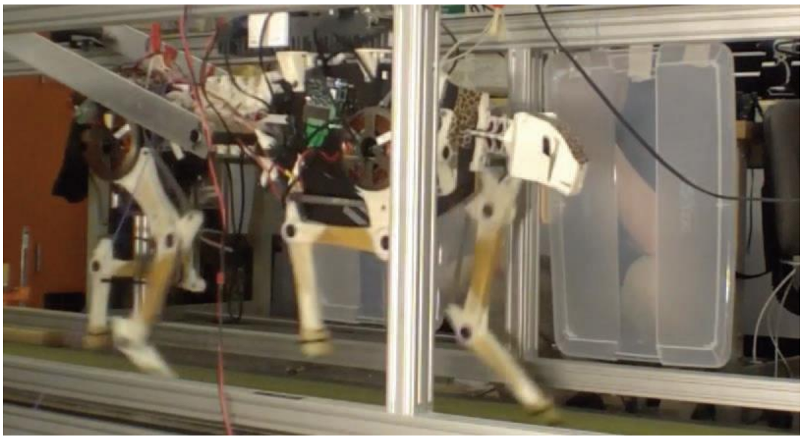

Figure 5: MIT Cheetah on the treadmill (Hyun *et al.*, 2014)

A similar method was employed by Buchli *et al* (2009) with LittleDog (Figure 6), a quadruped robot, developed by Boston Dynamics, which had joint level torque control based on electric motor current control. The paper showed how a feedforward torque term obtained by inverse dynamics can reduce the position gains and allow for successful disturbance rejection of unperceived obstacles. However, the implementation of well-controlled dynamic gaits was difficult due to the high gear ratio and the non-robust gears utilized, as well as the low control bandwidth.

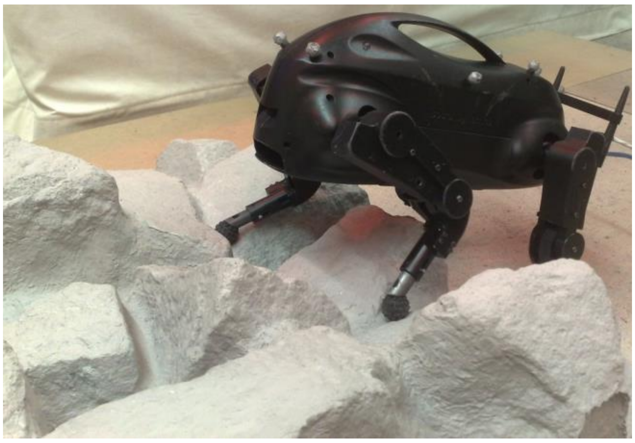

Figure 6: The quadruped robot LittleDog and a sample terrain to be crossed (Buchli *et al.*, 2009)

There are also a few examples of hydraulically actuated robots with only active impedance. A few torque-controlled humanoid robots, able to demonstrate balancing and simple stepping experiments, were developed by SARCOS, and later used in Hyon (2009), Stephens and Atkeson (2010) (Figure 7) and Herzog *et al.* (2014), at Advance Telecommunications Research Institute International, Carnegie Mellon University and University of Southern California, respectively.

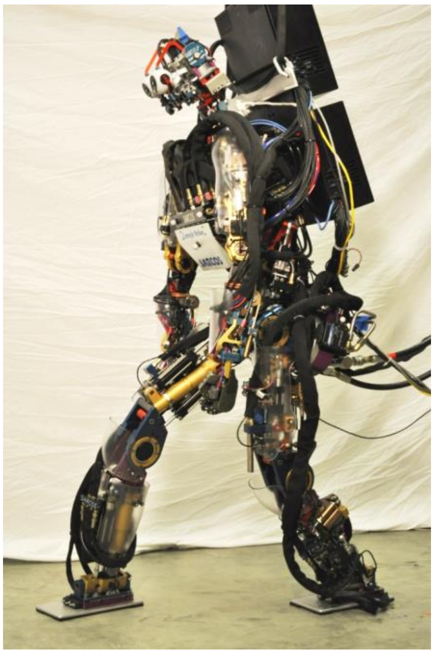

Figure 7: Sarcos Robot (Stephens and Atkeson, 2010)

2.3 Active Ankle Prostheses

Prostheses can be regarded, functionally speaking, as the same as a joint in a robot. The main differences are the controls and the restrictions that need to be applied. For the controls, the main goal for a prosthetic device is to emulate a healthy joint, so the prosthetic joint needs to, not only be able to act as a human joint but also to be controlled by the user in some manner. In regards to the restrictions, the prosthetic device needs to have a similar size to the healthy limb and most importantly the weight and power output of a healthy human joint.

As such, in the past decades, researchers have been studying pathological and nonpathological gait in terms of kinematics, dynamics, and energy expenditure, in order to understand the human's joint motions during walking and other motions like ascending and descending stairs. These efforts have resulted in the development of limb prosthetic devices aimed at raising the control and comfort for amputees, as well as the cosmetics of the prostheses. This research has resulted in a new design for semi-active prosthesis as well as an active prosthesis that have shown promising results when compared to passive prostheses (Cherelle *et al.*, 2014).

2.3.1 Actuator Designs

Semi-active prostheses improve on passive prostheses, by being able to modify the stiffness and/or damping properties of the device to allow for better foot placement in different scenarios. Incorrect foot placement can lead to an increase in falls, and as common passive prostheses tend to be designed to operate on even ground. This can result in a significant decrease in the walking stability of an amputee compared to an able-bodied person when an uneven ground is encountered. Because of this, passive prosthesis wearers usually have trouble when ascending and descending slopes, stairs and even when stepping in a rock or the curb of the road (Lapre and Sup, 2011). Some semi-active prosthesis may also use position control to position the foot, during the swing, locking it during stance (Alimusaj *et al.*, 2009), instead of adjusting stiffness or damping. In the literature, there are several examples of active ankle prosthesis that employ some form of impedance control, some of which are the following.

Active prostheses differ from their passive counterparts by having an actuator element that is able to provide energy to the user, thereby aiding the wearer. By having a net positive work generated by the prosthesis, the prosthesis can help overcome the extra metabolic energy that an amputee needs to exert while walking. Commercially available passive prostheses are comprised of spring structures that store and release elastic energy throughout each walking stance period. Although improved from past iterations, recent passive prostheses will always have as a net negative work, resulting on the missing energy being provided by the user, using a healthy joint, such as the knee or the hip. This will, in turn, result in a lower self-selected walking speed and difficulties in certain situations, such as uneven terrain. Therefore, the extra energy is important to achieve a more natural gait (Cherelle *et al.*, 2014).

Currently, most of the active prostheses available are still at the research level but have shown promising results when compared to passive prostheses. There are, however, some active prosthesis commercially available. These prostheses are the iWalk BiOM foot or the emPower from BionX, previously iWalk (*Prosthetic Technology – Ottobock, Ossur | MCOP Prosthetics*, no date) or the Spring Active Odyssey from a partnership from Spring Active Inc and Össur (*SpringActive – Innovative Solutions to Powered Human Assistance*, no date).

Over the past decades, the evolution of transtibial prostheses as seen remarkable steps forward. This evolution can be attributed to various factors. Some of these factors are the technological improvements in mechanical engineering, advances in computer-aided design and simulation software, the decrease of both price and size as well as the increase of performance of microcontroller technology and the more recent development of several types of compliant actuators such as pneumatic artificial muscles, series elastic actuators, variable stiffness actuators and explosive elastic actuators (Cherelle *et al.*, 2014).

In Cherelle *et al* (2014) prosthetic feet/ankle are classified into three main categories: conventional feet (CF), energy-storing-and-returning feet (ESR) and bionic feet. The authors further subcategorize the ESR feet into three categories, the early ESR, advance ESR and the articulated ESR. The bionic feet were also subdivided into stabilizing and propulsive devices as shown in Figure 8.

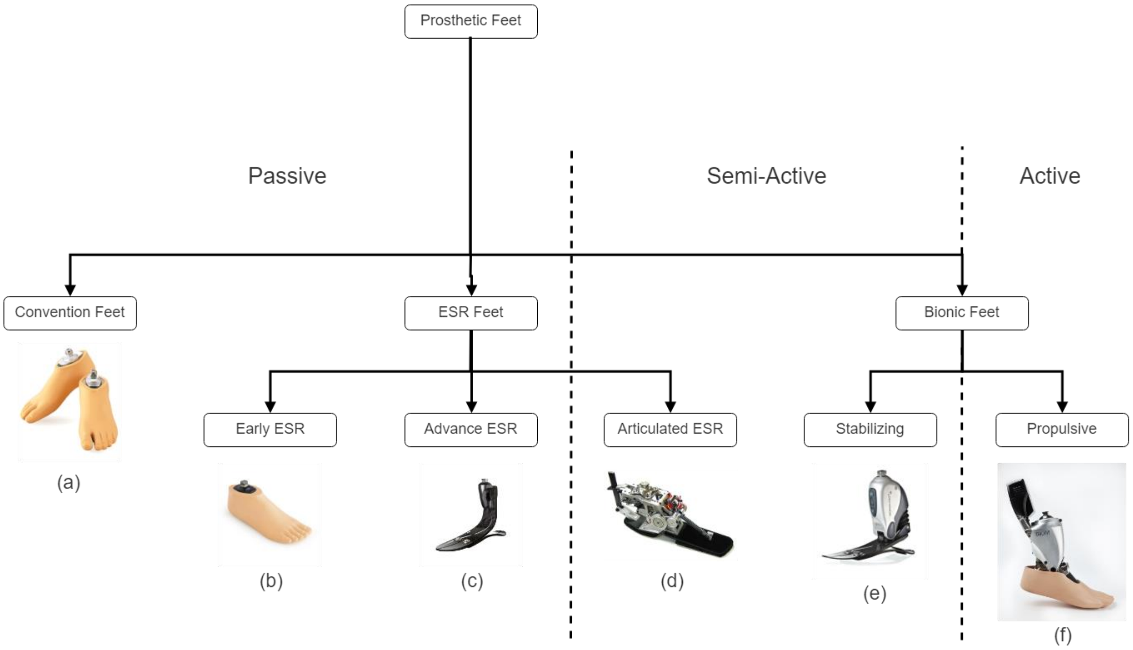

Figure 8: Categorization of prosthetic feet: (a) the SACH foot, (b) the SAFE foot, (c) ¨ Ossur's Flex-Foot, (d) the CESR foot , (e) ¨ Ossur's Proprio Foot, and (f) iWalk's Powerfoot BiOM -Adapted from (Cherelle *et al.*, 2014)

The articulated ESR feet typically utilizes small actuators and control electronics to engage and disengage locking mechanisms, to store elastic power when available and release it when necessary. Although these devices usually hold the store energy to release it during push-off, this type of actuation system does not fall on the propulsive category as it does not make use of an external mechanical power generation with the intent of providing the wearer with push-off power.

In the case of propulsion feet division, it can also be subdivided in stiff or compliant actuation (Figure 9), with the compliant actuators further divided into pneumatic actuators with pneumatic artificial muscles and electric actuators which encompass the series elastic actuators (SEA), the series elastic actuators with parallel springs (SEAPS), the variable stiffness (VSA) and the explosive elastic actuator (EEA).

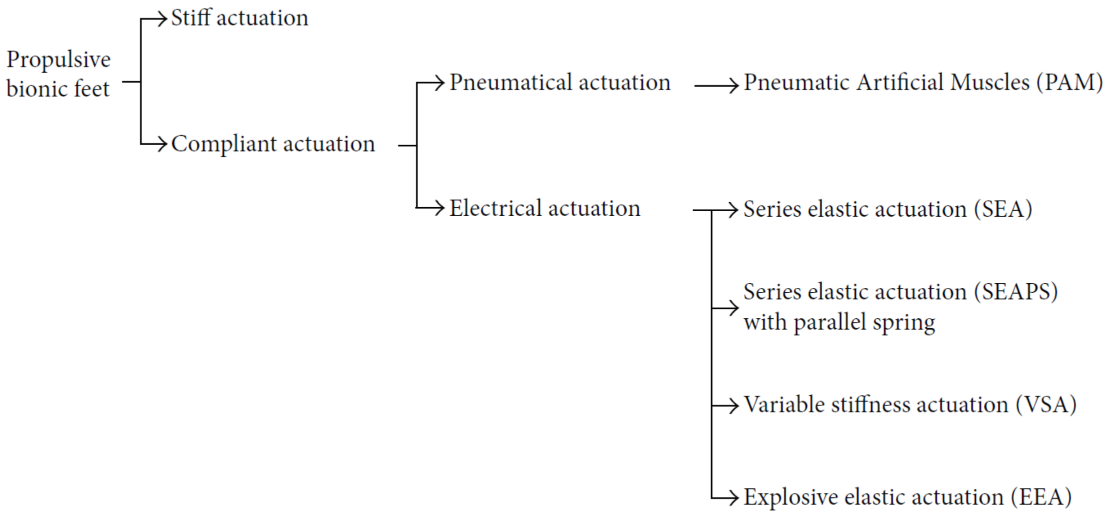
Propulsive bionic feet
Stiff actuation
Compliant actuation
Pneumatical actuation
Pneumatic Artificial Muscles (PAM)
Electrical actuation
Series elastic actuation (SEA)
Series elastic actuation (SEAPS) with parallel spring
Variable stiffness actuation (VSA)
Explosive elastic actuation (EEA)

Figure 9: Categorization of propulsive ankle-foot prostheses based on their actuation method - Adapted from(Cherelle *et al.*, 2014).

Stiff Actuators

In a prosthesis's context, an actuator is considered stiff if the prosthetic device is unable to store energy by means of elastic deformation. According to data from Winter's work (Winter *et al.*, 1990), considering a 75 Kg subject, a maximum torque output of approximately 120 Nm is needed. The ankle joint also needs to provide a peak power output of approximately 280 W, with a peak speed of 250 deg/s. When power losses are taken into account, from the gearboxes or the actuator itself, the minimum power rating for the actuator can increase to two times the peak power output. An example of a stiff actuator on a prosthesis is the prototype (Figure 10) from Carnegie Mellon University in Pittsburgh (United States) (Caputo and Collins, 2011). that was developed as an experimental tethered prosthesis testbed. It was created to conduct controlled experiments to understand the relationship between prostheses control parameters and prosthesis performance. The system has the capability to provide much more power and control than other prostheses to be able to test a wide variety of parameters and their consequent effect. By doing this, these experiments provided data to designers of future prostheses seeking optimal control strategies. The device has a single DOF and is actuated via a flexible Bowden-cable transmission that connects the 1.61 kW servomotor to the prosthesis.

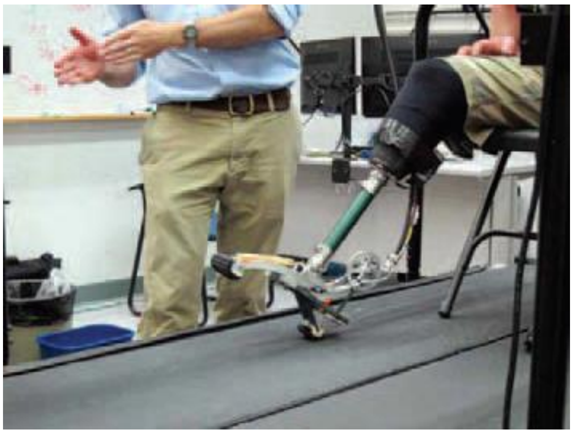

Figure 10: Tethered prosthesis testbed developed at Carnegie Mellon University, Pittsburgh, USA (Cherelle *et al.*, 2014).

Complaint Actuators

As opposed to the stiff actuators, complaint actuators will be able to store energy by elastic deformation. Its equilibrium position is defined as the position of the actuator where zero force or zero torque is generated.

The complaint actuators can be divided into pneumatic actuators and electric actuators. Some researchers choose pneumatic because of their design and setup closely resembles that of a human's musculoskeletal design and properties. This explains also why these actuators are generally called pneumatic artificial muscles (PAM). With the electrically driven stand-alone devices, the advantages are the reduced power requirements of the drive which results in a smaller, lighter and cheaper actuation setup.

Pneumatic Propulsive Actuation:

Pneumatic actuators are actuators with nonadaptable compliance and nonlinear force-displacement characteristics. To be able to control the compliance and equilibrium position of the prosthetic device, two pneumatic actuators are coupled antagonistically.

At the University of Washington (United States) Klute et al. (1999) designed an artificial muscle-tendon actuator to power a transtibial prosthetic device (Figure 11 (a)). The performance requirements were met by incorporating an artificial muscle consisting of two flexible pneumatic actuators in a parallel with a hydraulic damper and place in series with a bilinear, two-spring implantation of an artificial tendon.

Sup, Bohara and Goldfarb (2009) at Vanderbilt University (United States) developed a tethered powered actuator for both knee and ankle joint (Figure 11 (b)). The device is powered by two pneumatic cylinders, one for each joint. This prosthesis was designed to be a testbed for different control strategies, which further the development of an electrically powered version of the prosthesis.

Even though pneumatic systems have a better power to weight ration than electric ones, the high cost of pressurized air production and supply requirements create drawbacks for autonomy. Therefore, electric actuators are preferred when designing new prostheses.

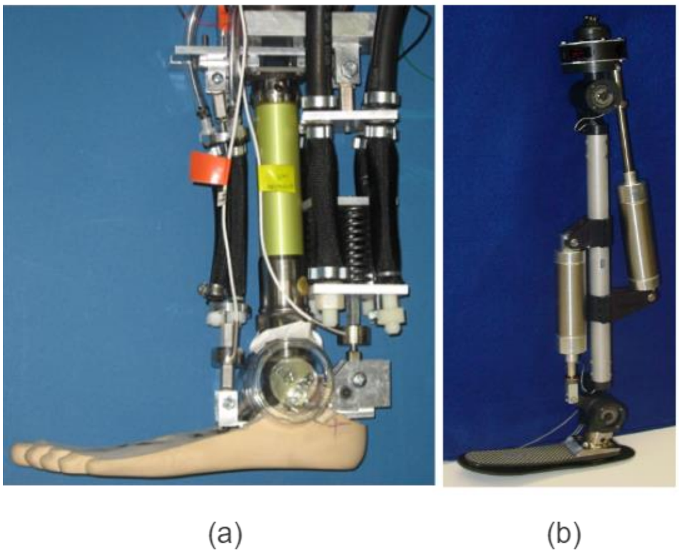

Figure 11: (a) Washington's variable stiffness prosthetic ankle; (b) powered transfemoral prosthesis from Vanderbilt University - From (Cherelle *et al.*, 2014)

Series Elastic Actuators (SEA)

A SEA consists of a motor in series with a spring. Since in a SEA the motor is still in series with the load, the required motor torque is still equal to the healthy reference data. The SEA is, however able to lower the motor speed when comparing to a stiff actuator, and by doing so lower the required power.

The SPARKy (Spring Ankle with Regenerative Kinetics) project, developed at the Arizona State University (United States), uses a robotic tendon actuator, which includes a 150 W Brushed DC motor to provide the entirety of the required push-off power for walking while maintaining intact gait kinematics. The first prototype, SPARKy 1 was shown storing and releasing approximately 16 J of energy per step, while a healthy ankle of an 80 Kg subject at 0.8 Hz walking rate needs approximately 36J. the second version, SPARKy 2, was built with a lighter and more powerful roller crew transmission and brushless DC motor. The working principles of both iteration of the project, rely on a SEA attached between the heel and the leg. A third prototype, SPARKy 3, was designed to actively control the two DOFs of the ankle. The version does not seem to have been built yet (Bellman, Holgate and Sugar, 2008) (Figure 12 (a)).

At the Marquette University in Milwaukee (United States) a powered ankle prosthesis, which utilizes a four-bar mechanism in conjunction with a spring and motor was developed (Figure 12 (b)). The proof-of-concept prototype (Mathias *et al.*, 2010) was design, optimized, fabricated and tested with the purpose of demonstrating its ability to match crucial ankle moments during the stance phase of the gait. The prototype was powered by a 200 W and its results from bench testing were relatively in accordance with expected values.

Zhu et al. (Zhu, Wang and Wang, 2014) at Peking University (China), developed the transtibial prosthesis PANTOE (Figure 12 (c)). This prosthesis, unlike most others, actively controls its toe joint. It does this by using two SEA, one powered by an 83 W motor for the ankle joint and the other powered by a 30 W motor for the actuation of the toe joint. The prosthesis's experimental results showed an improvement in walking performance when compared with commercial passive ones.

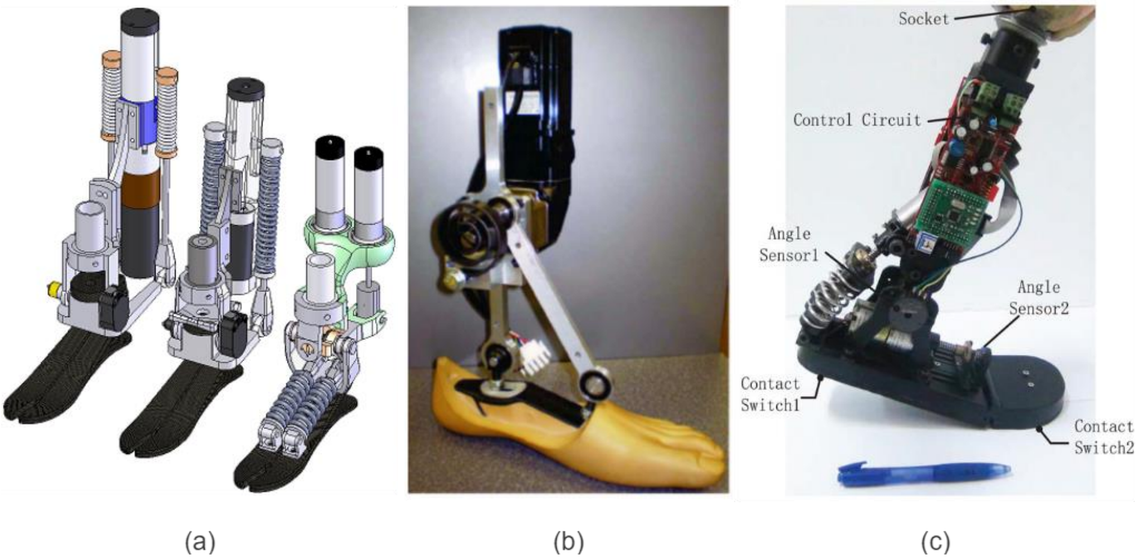

Figure 12: (a)The three versions of the CAD representations of SPARKy (SPARKy 1, 2, 3 from left to right) – from (Bellman, Holgate and Sugar, 2008)*; (b) Marquette University's Prosthesis – from* (Mathias *et al.*, 2010)*; (c) PANTOE – from* (Zhu, Wang and Wang, 2014)

Series Elastic Actuation with Parallel Spring (SEAPS)

The use of a spring in series in an actuation scheme has the potential to reduce the motor's required speed, but not the required torque. The torque reduction, however, can be achieved by the addition of a parallel spring to the actuator.

At the Massachusetts Institute of Technology- MIT (United States), Au et al. (2006; 2008) conducted research on powered prosthetic feet with electric actuators. One of the prototypes powered foot prosthesis that was designed, was compose by a high-power DC motor, a transmission, a series spring a unidirectional parallel spring and a carbon composite prosthetic foot, with the first three combining to form a rotary SEA. This device was intended to focus on control design (Figure 13 (a)).

Following their previous work on pneumatic transfemoral prostheses, Sup et al, at the Vanderbilt University (United States), designed a self-contained electrically driven device (Sup *et al.*, 2010) (Figure 13 (b)). Capable of accommodating to slop walking (Sup, Varol and Goldfarb, 2011) the device was designed for an 85 Kg user walking at a cadence of 80 steps/min and stair climbing. The device has two motor-driven ball screw assemblies that drive the knee and ankle through a crank-slider mechanism. The ankle unit includes an additional steel compression spring in parallel with the ball screw to supplement power during the ankle push off.

In Au and Herr (2006), (2008), the powered foot prosthesis, was also developed using a combination of a spring and a high-power SEA (Figure 13 (c)). During the controlled dorsiflexion phase, the spring was loaded and releases its stored energy during peak power moment, in conjunction with the SEA. This combination resulted in a peak power torque of 140 Nm and a power output of 350 W. The prosthetic device showed an improvement on the metabolic economy of walking individuals with transtibial amputation of about 7 to 20 % on average when compared to conventional prostheses (Au *et al.*, 2007; Au, Weber and Herr, 2009).

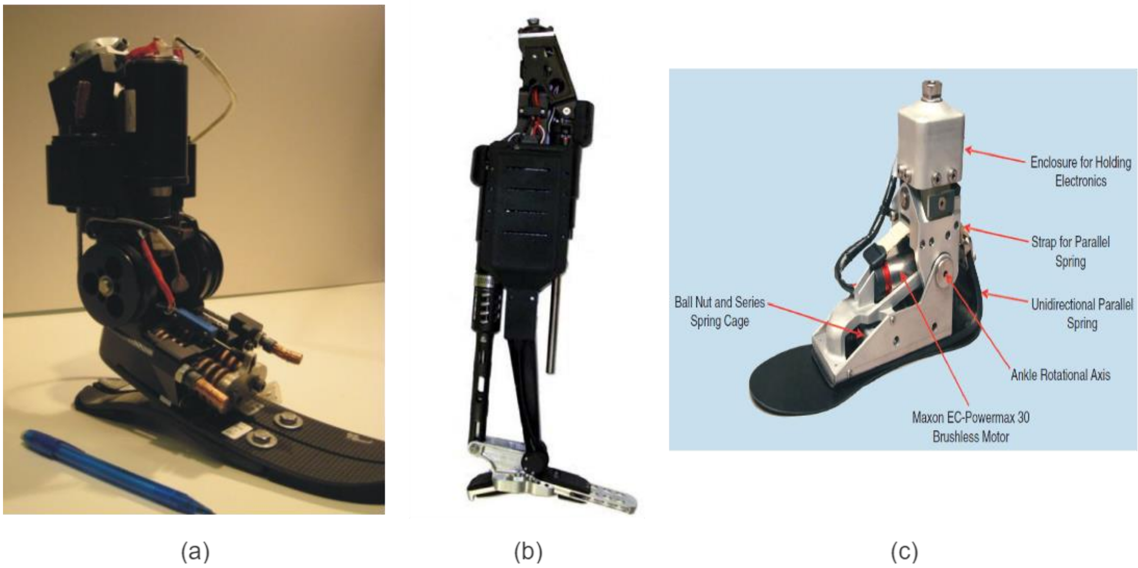
Enclosure for Holding Electronics
Strap for Parallel Spring
Unidirectional Parallel Spring
Ball Nut and Series Spring Cage
Ankle Rotational Axis
Maxon EC-Powermax 30 Brushless Motor

(a) (b) (c)

Figure 13: (a) MIT's Prosthesis prototype – from (Au, Berniker and Herr, 2008)*; (b) Vanderbilt University transfemoral prosthesis – from* (Sup, Varol and Goldfarb, 2011)*; (c) Prosthesis –from* (Au and Herr, 2008).

Variable Stiffness Actuation (VSA)

The CYBERLEG project, from the Vrije Universiteit Brussel (Belgium), consists of a robotic system constituted of a cognitive artificial leg to replace an amputated limb, as well as a wearable active orthosis, for the assistance of the contralateral sound limb. The first prototype, the CYBERLEG α prototype (Figure 14) (Geeroms *et al.*, 2013), was designed for transfemoral amputees and consists of a variable stiffness MACCEPA-type actuator, with a 200 W DC motor (Van Ham *et al.*, 2007), that is able to provide 100% of the push-off power properties at the ankle combined with a passive knee joint. The knee joint consists of locking and unlocking mechanisms which fix springs in place to allow the joint to imitate the knee joint torque-angle characteristics. Complex mechanisms of the knee joint were incorporated to enable energy transfer between the knee and the ankle in the late stance phase of walking. While this type of actuator offers some advantages such as the possibility to optimize for different step lengths, walking speeds and terrain adaptation, the actuator adds a significant increase in both complexity and weight to the system. To reduce the extra weight in the CYBERLEG ankle module, a very small motor combined with a very high reduction ratio was selected to vary the stiffness of the joint. This reduces the speed of the stiffness change, which instead of taking one stride, it would require a series of steps, thereby providing slow adaptation to different gaits

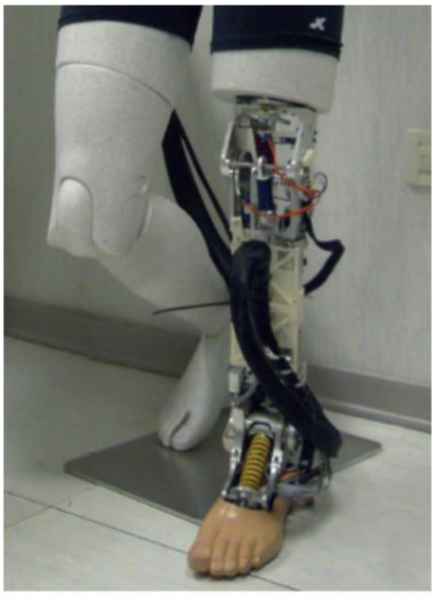

Figure 14: CYBERLEG – from (Geeroms *et al.*, 2013).

Explosive Elastic Actuation (EEA)

In general, an explosive elastic actuator (EEA) is comprised of a spring behind a locking mechanism and in series with a SEA. This mechanism releases the stored energy in a catapult-like manner, to hurl the payload with an energetic explosion, without the use of an explosive. This kind of explosive motion is the base of motion like jumping, kicking and punching. The torque requirement of an EEA is the same as a SEA, however, due to the locking mechanism, the motor can work for a longer period of time (typically 3 times for a prostatic ankle) and therefore reduce by the same amount its actuator speed and power.

The ROBOTIC & Multibody Mechanics Research Group at the Vrije Universiteit Brussel (Belgium) has developed the AMP-Foot prototypes. The second version of prototypes AMP-Foot 2 (Cherelle *et al.*, 2012) is an energy efficient powered ankle-foot prosthesis based on a principle off optimal power distribution (Figure 15 (a)). The prototype works similarly to devices using SEA, Except for the fact that the actuator works during the complete stance phase. The actuator provides a peak torque of 130 Nm and a peak power output of 250 W to 350, by utilizing a 60 W DC motor coupled to the ankle joint with a series spring assembly and a walking mechanism. The locking mechanism is ensured by a four-bar linkage mechanism moving in and out of its singular position. By doing so, the actuator can be loaded without affecting the kinematics or dynamics of the system. A second spring, located in the foot and called the plantarflexion spring, exists to make the device behave like an ESR, which permits the prosthetic device to act as an energy - storing - and - returning foot.

A third version of the AMP-Foot (Figure 15 (b)) was also developed (Cherelle *et al.*, 2016). This version was designed to act similarly to the AMP-Foot 2 except that the AMP-Foot 3 has an extra locking mechanism to enable the change in the rest position of the robotic ankle after foot-flat is achieved. The extra locking mechanism allows for more energy storing and for a natural adaptation to different walking speeds and slopes. The extra energy storage permitted a reduction of the motor power from 60 W to 50 W without the loss of overall power. The third version was validated on an amputee at about 4.7 Km/h of self-selected speed, up from 3.5 Km/h from the initial test with the subject owned passive prosthesis. The results also showed that approximately 13 J is stored in the spring assembly during early stance and that about 26 J of energy is delivered at push-off, which corresponds to the requirements of a sound ankle.

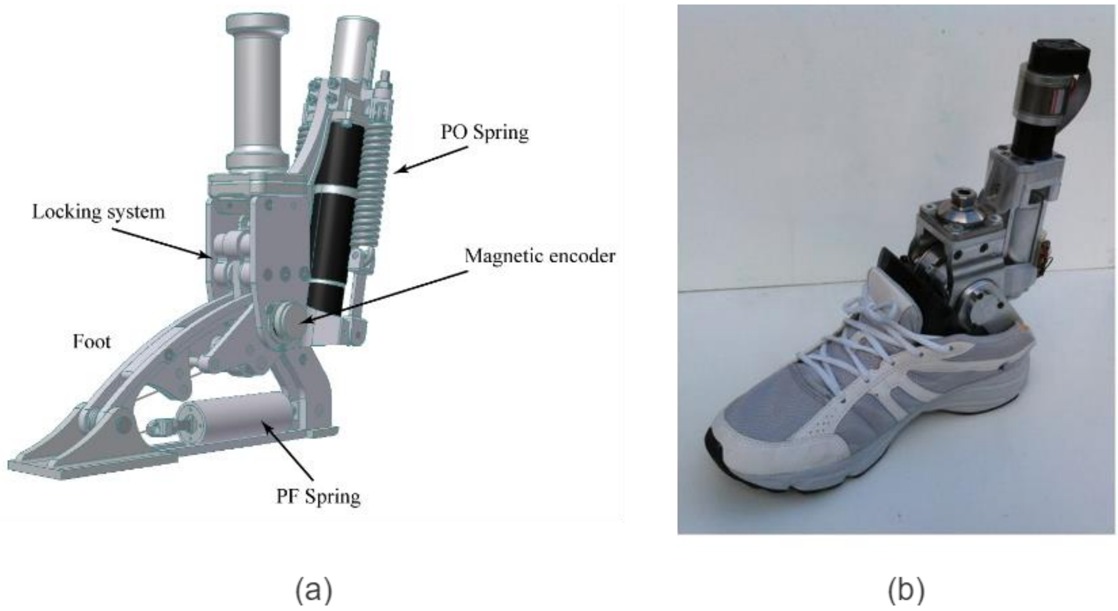

Figure 15: (a) CAD from AMP-Foot 2 – from (Cherelle *et al.*, 2012)*; (b) AMP-Foot 3 – from* (Cherelle *et al.*, 2016).

2.3.2 Control Strategies

The same way there are different types of designs for an ankle prosthesis, there are also different types of controllers. From Ferreira, Reis and Santos (2016)the control approaches of powered active prostheses, found within the literature, can be separated into four categories: echo control, finite impedance control, electromyography and Central pattern generators.

Echo Control

This type of control method can be traced back to the initial development of active lower limb prostheses is in the 70s. Here, the prostatic leg would be controlled by mimicking the kinematics of the previous cycle of the sound leg. This allows for an individualized control since the amputee's sound leg would supply the control signals for the prosthesis. Changes in locomotion can be dealt with as long as the sound leg supplied the proper trajectory. However, this method forces cross-limb symmetry causing problems with asymmetric stance/swing temporal ratios. The controller also assumes that the sound leg is providing the correct trajectory, which is not always the case. These problems combined with a delay of a minimum of a half - step led to the use of other controllers in new prosthesis designs (Grimes, 1979).

Finite State Impedance Control

Finite State Impedance (FSI) control have been the control approach most commonly used when designing intelligent prosthesis control. In this kind of controllers, the step cycle is divided into different states (states in a finite state machine) and, in each gait state, a different joint impedance is modeled using virtual spring-damper systems.

Before impedance control, most works relied on position control where the knee and/or ankle angle were provided to the actuator. In the same way as the echo control, position control is based on data taken from healthy individuals and therefore may not adapt to different environmental situations. Positioning tracking also requires high output impedance, forcing the amputee to react to the device instead of interacting with it. Impedance control, on the other hand, generates joint torques, providing a lower output impedance and a more adaptive motion.

Sup, Bohara and Goldfarb (2009) showed a tethered transfemoral prosthesis with pneumatic actuators. The prosthesis uses a four-state finite machine, separating stance, pressing, swing flexion and swing extension, with each state having its own set of stiffness and damping parameters. Transitions between states are determined in a cyclic fashion using data from the ankle angle, ankle torque, knee velocity and the axial load from the heel strike. With this approach, the prosthesis is guaranteed to stabilize around the equilibrium points associated to each of the gait states and to produce net work only when switching states.

Sup et al (2010) would later present a similar prosthesis to their previous pneumatic one. This new however was an electrically actuated powered transfemoral prosthesis. The control method for this device is divided into three levels. The high level is responsible for the recognition of the user's intention such as walking, standing or sitting. This information is then relayed to the middle level which switches the finite state machine to the one corresponding to the activity received. The middle level generates the torque reference and provided them to the low-level. The low-level is a closed -loop joint torque controller with transmission dynamics compensation to allow for a higher bandwidth and accuracy. The work showed that this prosthesis was capable of enabling amputees to exhibit biomechanics and power similar to that of a healthy human. However, the prosthesis would have to be tested with multiple amputees' subjects.

Another transfemoral prosthesis with a finite state impedance controller is Martinez – Villalpando and Herr (2009). Their prosthesis incorporated two SEAs in an agonistic-antagonistic disposition. This hardware disposition helps produce a more efficient prosthesis in terms of electrical energy cost, without compromising the capability of accurately mimicking the knee biomechanics of a human.

Eilenberg et al. (2010) also presented an FSI controller on a transtibial prosthesis. The controller architecture is composed by a finite state machine, a neuromuscular model and a low-level torque controller. The neuromuscular model is composed by a dorsiflexor model and a plantar flexor model acting as two virtual actuators. the dorsiflexor is implemented as a rotary spring -damper while the plantar flexor is implemented as a Hill-type muscle. Results showed the prosthesis capable of mimicking the human's ankle behavior in level-ground walking, with the neuromuscular controller being able to intrinsically adapt to the ground slope.

Lawson et al. (2013) presented the second version of the prosthesis known as Vanderbilt Leg. The prosthesis controller is based on a finite state machine, having two distinct machines, one for ascending stairs and one for descending stairs. The controller was tested with an amputee, in both scenarios, with stairs kinematics being more similar to a healthy joint for both knee and ankle. In stair descending, only the ankle kinematics of the powered prosthesis were closer to a healthy one, when compared to a passive prosthetic device.

In Liu et al (2014), a more robust FSI controller for transfemoral prostheses was presented. To achieve an increase in robustness, the authors used the Dempster-Shafter theory (DST) to improve the design of the transition rules. The use of the DST can improve some aspects of the controller like the transition rules to ensure the reliable transition between subjects, reduce control errors and a simplified tuning process with a shortened training time. These advantages make the prosthesis more practical for daily living.

EMG-based Control

With surface electromyography (EMG) based control, electrodes are placed on the skin of the residual limb (non-evasive technique) to record electrical activity produced by muscles.

Huang et al (2011) used surface EMG signals on their implementation of a user locomotion mode classifier and pattern recognition system. The system was tested with EMG data from two transfemoral amputees and eight healthy subjects and was shown to be capable of recognizing seven locomotion modes: level-ground walking, stepping over obstacles, climbing stairs, descending stairs, contralateral turning, ipsilateral turning and standing still.

A proportional EMG-based controller for an active transfemoral prosthesis was presented in Wu et al (2011), which enable the wearer to use his or her muscles to control the prosthesis. The EMG signals are used to calculate the control inputs for the implemented active-reactive controller. The system also incorporated a virtual agonist-antagonist structure that combined with the linear muscle model, calculates the torque to be applied to the knee joint.

In Wang, Kannape and Herr (2013), Wang et al. also presented a proportional EMG-based controller but in this case for a transtibial prosthesis. The implemented controller can be divided into three modules, the finite state machine, the plantar flexor model and the EMG module. The state machine is tasked with keeping the prosthesis synchronized with the gait cycle, the plantar flexor model, with generating the adequate torque within each phase and finally the EMG module is used to modulate the gain parameters of the torque generator allowing for a direct influence from the EMG signals on the torque generation.

CPG-based Control

Even though the FSI control approach is the most utilized control method, when designing a prosthesis controller, it is not without problems. Other than the need for detail sensor information from the device, which requires sensors and increases power consumption and cost, the control method is staged and not continuous (Nandi, Ijspeert and Nandi, 2008). This type of control is different from the control found in humans (Torrealba *et al.*, 2012).

Central Pattern Generators (CPGs) are biological neural networks, regulated by simple inputs and with the ability to produce coordinated cyclical patterns such as walking, running, swimming or flying (Kimura, Fukuoka and Cohen, 2007; Geyer and Herr, 2010; Torrealba *et al.*, 2012).

CPG-based control strategies offer several useful properties when considered for lower limb prosthesis control. These properties are the intrinsic rhythmic behavior, limit cycle stability, smooth online trajectory modulation by parameters change, low computational cost, easy feedback integration, robustness and coupling/synchronization and entrainment phenomena when coupled to mechanical systems (Torrealba *et al.*, 2012). All of these factors have led several researchers to explore the use of CPGs when designing active power prostheses.

Ryu et al. (2009) developed a CPG-based controller for a transfemoral prosthesis implemented in a simulated humanoid robot (HOAP-3). The CPG was implemented by a frequency-adaptive Matsuoka neural oscillators and had two functions come to generate prosthesis trajectory's and to coordinate both limbs. The prosthetic limb was also equipped with a spring-damper component between the hip and foot to provide compliant behavior.

In Torrealba *et al* (2010), Torrealba et al presented a biomechatronic knee prosthesis and two control strategies, a bio-inspired controller and an adaptive proportional controller. The bio-inspired controller was composed of three modules: an Accelerometry-based Event Detection Algorithm (AEDA), an Amplitude Controlled Phase Oscillators (ACPOs) and a Knee Angle Generator (KAG). The CPG was comprised of an ACPO, to track the gait cycle phase of the prosthesis and a KAG, to generate the knee angle reference. The adaptive proportional controller was only active during extension and consisted of a control action proportional to the measure knee angle. Tests with able bodies and amputees led the authors to conclude that, in their prosthesis, the adaptive proportional controller fitted better since the device did not have the optimal architecture to deal with the CPG control.

Torrealba et al (2012) would later propose an improvement on their previous work (Torrealba *et al.*, 2010) by adding a second ACPO in the CPG control. The second ACPO allowed for a smooth and continuous response during the walking gait, accomplishing the goal of having a continuous control of a prosthetic knee. The authors reasoned that applying a finite state control (non-continuous control) is wasting part of the capability of controllable actuators to module the prothesis response to the gait.

Other Control Schemes

Within the literature, one can also find lower limb prosthesis controllers that do not fall within the controller categories mentioned. These controllers can be radically different or offer enough differences to warrant a different categorization than the other controllers mentioned.

Au et al. (2007) presented a powered transtibial prosthesis with a SEA and a unidirectional parallel spring. This prosthesis was shown to have improved an amputee metabolic economy from 7% to 20 % on average when compared to a passive-elastic prosthesis. A finite state comptroller Was designed to implement 2 different control strategies. When the device was in the stance phase, the controller would provide torque commands, however, when it was in the swing phase, the device would generate position commands.

Gregg and Sensinger (2014) presented in their work, a novel control strategy for a powered transtibial prosthesis, testing it on a planar 6-link biped model. The control method relies on the Center of Pressure (COP), it being defined as the point of the foot where the resultant ground reaction force is transmitted, as it is independent over walking speeds, heel height and body weight. The authors used this invariant shape to control the knee and ankle angles. The control strategy shows an advantage as it did only require the tuning of a few parameters, increasing the possible clinical viability of the power device.

In Varol and Goldfarb (2007), an active-passive torque decomposition method for an active knee-ankle prosthesis is presented. This method describes the total torque at each joint has the sum of a passive and an active component. The passive component is represented as a spring-damper element and it is assumed you be a passive mapping of the angular displacement and velocity of the joint. The active component is represented as a function of the force acting on the prothesis's socket and it is assumed to be the user's input. The controller then uses a finite state machine to reconstruct the control torque as the sum of the passive and active components. This method effectiveness was demonstrated using experimental data from the knee joint at different walking speeds.

To summarize what was mentioned before, to have mechanical interaction, mechanical coupling with the environment is necessary, and therefore the manipulator in question should not be treated as an isolated system. This problem has been a fundamental problem of robotics and the subject of considerable research. Several methods were proposed over the years to overcome this problem, some of them mentioned in the previous chapter. These methods range from just overwhelming the interactions to adding springs to absorb the impacts generated by the interactions. For this work, the Impedance Controller, developed by Hogan (1985) was selected, to test its effectiveness with the control of a robotic arm, and later, in this paper, on a prosthetic ankle joint for the robot Darwin, that replaces the ankle and foot joints of the Darwin-OP.

In this chapter, a theoretical foundation of the Impedance Controller and a model of a two-link planar manipulator is first provided, being followed by an implementation of the impedance controller in MATLAB and an implementation in Webots, for a more accurate assessment of its performance. In the Webots implementation, a comparison between a controller with and without a dynamic model of the arm will be provided, and the advantages, as well as the disadvantages, derived from the use of the model, will be mentioned.

3.1 Implementation of Hogan's Impedance Control

An Impedance Controller differs from a conventional approach to manipulator control by attempting to implement a dynamic relation between manipulator variables such as end-point position and force rather than just trying to control these variables alone, resulting in the simplification of the control problem.

Following the work of previously published papers on the implementation of a planned end effector cartesian path, widely used for the development of industrial manipulators, Hogan's team (1985) investigated ways of presenting the environment with a dynamic behavior, which is simple if the workspace coordinates are expressed by, for example, Cartesian Coordinates.

The lowest order term in any impedance is the linear relation between output force (F) and input displacement (X), also known as stiffness.

$$F = K * X \tag{3.1}$$

Assuming that the actuator can be controlled by generating commanded forces (or torques), the existence of sensors capable of observing actuator position (or angle), θ, and a purely kinematic relation (i.e. no structural elastic effects) between actuator position and end-point position, $X = L(\theta)$ with L being the forward kinematics model for the manipulator, the design of a feedback control law becomes straightforward. Considering, F_{int} as force, X as position and X_0 as the desired equilibrium position for the end-point, in the absence of environmental forces, a general form for the desired force-position relation is:

$$F_{int} = K[X_0 - X] \tag{3.2}$$

By first computing the Jacobian, $J(\theta)$:

$$dX = J(\theta)\, d\theta \tag{3.3}$$

The actuation torque T_{act} can be determined by:

$$T_{act} = J^T(\theta)F_{int} \tag{3.4}$$

We can, therefore, obtain the require relation with the actuator coordinates:

$$T_{act} = J^T(\theta)K[X_0 - L(\theta)] \tag{3.5}$$

This relation is achieved without any restriction on linearity being imposed in $K[X_0 - L(\theta)]$, and the difference of X from X_0, does not need to be small. This is due to the fact that, in this equation, the inverse Jacobian is not required.

An advantage of this approach can be observed when trying to produce a desired time-history of the end-point positions, which has been one of the most difficult problems in robot control (Paul, 1981). When creating a desired time-history of the end-point, the determination of the time-history of the actuator (joint) position is required, which in turn needs the inverted kinematics equations. For some manipulators (e.g., those with nonintersecting wrist joints axes), the inverse calculation, may not have a possible explicit algebraic solution. However, if $K[X_0 - L(\theta)]$ is chosen so as to make the end-point sufficiently stiff, then a Cartesian end-point position controller will be accomplished, completely eliminating the “inverse kinematics problem”. To ensure that the behaviour was compatible with the fundamental mechanics of manipulation and that it is was expressed as an impedance, special care was taken to ensure that it would only be necessary to compute the manipulator’s forward kinematic equations.

Another important term in the manipulator impedance in the relation between force and velocity. Once more, considering the assumptions made previously with the relation for the desired force-position, it becomes straightforward to define a feedback law to implement in actuator coordinates a desired relation between end-point force and the end-point velocity as:

$$F_{int} = B[V_0 - V] \tag{3.6}$$

From the manipulator kinematics:

$$V = J(\theta)\omega \tag{3.7}$$

By using 3.1 and 3.2 in 3.4, the required relation in actuator coordinates can be written as:

$$T_{act} = J^T(\theta)B[V_0 - J(\theta)\omega] \tag{3.8}$$

Again, note that the relation $B[V_0 - V]$ does not need to be linear and that the inversion of the Jacobian is not required.

By adding the two terms together, we have the “Simple Impedance Controller”, which only takes the actuator position as an input and outputs the torque necessary to be applied to the actuator T_{act}:

$$T_{act} = J^T(\theta)K[X_0 - L(\theta)] + J^T(\theta)B[V_0 - J(\theta)\omega] \tag{3.9}$$

This controller, despite its simplicity, is adequate for some applications. By just adjusting the K and B values, to give the manipulator a stiffer and more accurate end-point position, or less accurate end-point position but a manipulator that does offers less resistance to the environment, it is able to achieve the desired behaviour. This, however, does not occur in most cases, requiring additional complexity to compensate.

The dynamic behavior to be imposed on the manipulator, by the foregoing equations, takes no account of the inertial, frictional or the gravitational dynamics of said manipulator. This simplification may be reasonable in some circumstances, but in many situations, these effects cannot be neglected. To ensure dynamic feasibility, the choice of the impedance that will be imposed should be based on the dominant dynamic behavior of the manipulator. In the end, and like most other controllers, the choice becomes a trade-off between keeping the complexity of the controller within manageable limits while ensuring that the imposed behavior adequately reflects the real dynamic behavior of the controlled system. This choice ends up depending in both the manipulator itself and on the environment in which it operates.

To improve the controller’s performance, the model of the manipulator may be added, to address the missing dynamics, a consequence of the simplification.

The kinematics, inertial, gravitational and frictional effects provide an acceptable model of the manipulator dynamics as follows:

$$I(\theta)\frac{\partial\omega}{\partial t} + C(\theta,\omega) + V(\omega) + S(\theta) = T_{act} + T_{int} \tag{3.10}$$

With $I(\theta)$ as the configuration – dependent inertia, ω as the actuator velocity, $C(\theta,\omega)$ as the inertial coupling torques, $V(\omega)$ as the velocity – dependent torques and $S(\theta)$ as the position – dependent torques, such as gravity. Assuming the desired end-point behaviour to be imposed T_{int}:

$$T_{int} = M\frac{dv}{dt} - B[V_0 - V] - K[X_0 - X] \tag{3.11}$$

The expression for the required actuator as a function of the actuator position and velocity, as well as the end-point force, can be derived by straightforward substitution:

$$\begin{gathered} T_{act} = I(\theta)J^{-1}M^{-1}K[X_0 - L(\theta)] + S(\theta) \\ +I(\theta)J^{-1}M^{-1}B[V_0 - J(\theta)\omega] + V(\omega) \\ +I(\theta)J^{-1}M^{-1}F_{int} - J^T(\theta)F_{int} \\ - I(\theta)J^{-1}G(\theta,w) + C(\theta,\omega) \end{gathered} \tag{3.12}$$

With $G(\theta, w)$ being an accelerative coupling term.

The M matrix is the desired inertia in the end-point coordinates. In an ideal situation, when the manipulator is decoupled from its environment, the effects from the environment should disappear, and in principle, the manipulator would exhibit a no mass-like behaviour. In practise, this does not verify, as the uncoupled manipulator still has nonlinear and configuration-dependent inertia. Being that there is no physically realisable strategy that can eliminate the inertia effects of the manipulator, Hogan's team set out to try and modify the apparent inertia seen at the end-effector. The approach taken was to "mask" the true nonlinear inertia manipulator behaviour and imposed simpler dynamics of a rigid body. Hogan gave, as an example, the inertia tensor of a rigid body such as that of a cube of uniform density, M , shown below, which eliminates the angular velocity products terms in the Euler equations for the motion of a rigid body.

$$M = \begin{bmatrix} m & 0 & 0 & 0 & 0 & 0 \\ 0 & m & 0 & 0 & 0 & 0 \\ 0 & 0 & m & 0 & 0 & 0 \\ 0 & 0 & 0 & I & 0 & 0 \\ 0 & 0 & 0 & 0 & I & 0 \\ 0 & 0 & 0 & 0 & 0 & I \end{bmatrix} \tag{3.13}$$

This matrix was the result of the simplification when the end-point inertia behavior remains invariant under translation and rotation of the coordinates axes. The matrix M is usually chosen to be small, however making it too small will result in instability. An interesting choice for the impedance inertia is to set it equal the actual end-point inertia of the manipulator, by having $M = J^T \, I(\theta) \, J^{-1}$. This choice of inertia assures that the stability constraints are met (Bonitz and Hsia, 1996).

3.2 Dynamic Model

The first term in equation (3.10) is the dynamic model of the manipulator. This model is the result of the dynamic analysis, which in turn are the description of a robot's response to the robot's actuator force (Murray, Li and Sastry, 1994). These forces can be provided by an electric, hydraulic or pneumatic actuator. It can be even a combination of the three of them.

The dynamic studies study the forces required to cause motion, by creating a mathematical model (i.e. differential equations) capable of describing the preferred trajectory of the mechanism. In terms of forces applied by the actuator and the external forces applied to the mechanism (Craig, 2004).

These differential equations (equations of motion) govern the dynamic response of the mechanical linkage to input joint torques. There are many methods of generating the dynamic equations of a mechanical system, including the Newton-Euler formulation and the Euler-Lagrange formulation. The Newton-Euler formulation is derived from the direct interpretation of Newton's Second Law, which describes dynamic systems in terms of force and momentum.

On the other hand, the Euler-Lagrange formulation relies on the energy properties, requiring only the kinetic and potential energies of the system and, using generalized coordinates, to compute the equations of motion.

In this chapter, the Euler-Lagrange approach was used to describe the dynamic equations from the manipulator mechanism.

3.2.1 Euler-Lagrange approach

As mentioned, the Euler-Lagrange derivation of dynamics technique has the advantage of requiring only the kinetic and potential energies of the system, also it can be seen as the best approach for the study of forward dynamic properties and analysis of control schemes, is the method most used in the literature for robotic mechanisms, such as in the biomedical field, namely researches from Au and Herr (2008); Richter et al. (2015); Hong-Liu et al. (2010); R Thavai and N Kadam (2016); Shorter et al. (2012).

The Euler-Lagrange equations of motion are a general set of differential equations that describe the time evolution of mechanical systems subjected to holonomic constraints - constraints in system configuration - when the constraint forces satisfy the principle of virtual work (Spong *et al.*, 2006).

To write the equations of motion, we first defined the Lagrangian L, in equation (3.14) as the difference between the kinetic K and potential P energy of the system written using the generalized coordinates (Murray, Li and Sastry, 1994).

$$L(q,\dot{q}) = K(q,\dot{q}) + P(q) \tag{3.14}$$

The q's are called a set of generalized coordinates ($q \in \mathbb{R}$) for the system. For a robot manipulator or a mechanism composed of links, these generalized coordinates are almost always chosen to be the angles of the joints.

The equations of motion for a mechanical system using the generalized coordinates (q_i) and the Lagrangian L, can be determined by:

$$\frac{d}{dt}\frac{\partial L}{\partial \dot{q}_i} - \frac{\partial L}{\partial q_i} = \tau_i \tag{3.15}$$

Where $i = 1, \dots, n$, corresponding to the number of system links and τ_i to the external generalized forces.

Considering that the model (3.10) can be written in the following matrix form:

$$I(q)\frac{d\dot{q}}{dt}+V(\dot{q},q)\frac{dq}{dt}+S(q)=\tau \tag{3.16}$$

With $I(q)$ as the inertia matrix, $V(\dot{q},q)$ the velocity term containing the Coriolis and Centrifugal Terms and $S(q)$ being the gravity vector, the model matrices can be determined, using the Euler-Lagrange approach, thusly:

To determine the inertia matrix, we first use the total kinetic energy ($K(q,\dot{q})$). This is a function of the vector $\dot{q}$, and is given by the sum of the n rigid bodies kinetic energies:

$$K(\dot{q})=\sum_{i=1}^{n}K_i(\dot{q}) \tag{3.17}$$

With

$$K_i(\dot{q})=\frac{1}{2}m_i v_i^T v_i+\frac{1}{2}\omega_i^T I_i\omega_i \tag{3.18}$$

Where m_i is the mass, v_i and $\omega_i$the linear and the angular velocity respectively and I_i the body inertia matrix, all corresponding to the i rigid body of the mechanism. It is important to note that the kinetic energy of the rigid body is the sum of the translational kinetic energy and the rotational kinetic energy. The equation (3.18) can also be written as:

$$K(\dot{q})=\frac{1}{2}\sum_{ij}^{n}d_{ij}(\dot{q})_i\dot{q}_j \tag{3.19}$$

Or considering the whole system as:

$$K(q,\dot{q})=\frac{1}{2}\dot{q}^T I(q)\dot{q} \tag{3.20}$$

With $I(q)$ being the inertia matrix for the model.

Considering that the linear and angular velocities of any link can be expressed in terms of the Jacobian matrix and the derivate of the joint's variables:

$$v_i=J_{vi}(q)\dot{q} \qquad \omega_i=J_{\omega_i}(q)\dot{q} \tag{3.21}$$

By substituting the (3.18) in (3.19), the expression (3.17) can now be rewritten as:

$$K=\frac{1}{2}\dot{q}^T\sum_{i=1}^{n}\left[m_iJ_{v_i}(q)^TJ_{v_i}(q)+J_{\omega_i}(q)^TI_iJ_{\omega i}(q)\right]\dot{q} \tag{3.22}$$

And the inertia matrix can now be calculated as:

$$I(q)=\sum_{i=1}^{n}\left[m_iJ_{v_i}(q)^TJ_{v_i}(q)+J_{\omega_i}(q)^TI_iJ_{\omega i}(q)\right] \tag{3.23}$$

Regarding the potential energy component, the expression for a rigid body i is written as follows:

$$P_i=g^Tr_{ci}m_i \tag{3.24}$$

With g as the gravity's direction vector, r_{ci} the coordinates of the centre of mass of the link i and m_i the mass of the same link. We can see that the energy potential is independent of the robot's joints velocity $\dot{q}$, depending only on its configuration q.

For the complete system, the potential energy is given by the sum of all n rigid bodies individual energy:

$$P = \sum_{i=1}^{n} P_i \tag{3.25}$$

The gravity vector can then be computed by:

$$S(q) = \begin{bmatrix} \frac{\partial P}{\partial q_1} \\ \vdots \\ \frac{\partial P}{\partial q_n} \end{bmatrix} \tag{3.26}$$

When replacing K and P in (3.14), we have:

$$L(q, \dot{q}) = \frac{1}{2} \sum_{ij}^{n} d_{ij}(\dot{q})_i \dot{q}_j - P(q) \tag{3.27}$$

Considering the equation (3.15), the first partial differential term of the Euler-Lagrange is given as follows (Prof. De Luca, 2016):

$$\frac{\partial L}{\partial \dot{q}_k} = \sum_j d_{kj} \dot{q}_j \tag{3.28}$$

$$\frac{d}{dt} \frac{\partial L}{\partial q_k} = \sum_j d_{kj} \ddot{q}_j + \sum_{ij} \frac{\partial d_{kj}}{\partial q_i} \dot{q}_i \dot{q}_j \tag{3.29}$$

As for the second partial differential term, it can be written as:

$$\frac{\partial L}{\partial q_k} = \frac{1}{2} \sum_{ij} \frac{\partial d_{ij}}{\partial q_k} \dot{q}_i \dot{q}_j - \frac{\partial P}{\partial q_k} \tag{3.30}$$

Then, grouping all the previous terms, it is possible to write the Euler-Lagrange equations as:

$$\sum_j d_{kj} \ddot{q}_j + \sum_{ij} \left\{ \frac{\partial d_{kj}}{\partial q_i} - \frac{1}{2} \frac{\partial d_{ij}}{\partial q_k} \right\} \dot{q}_i \dot{q}_j + \frac{\partial P}{\partial q_k} = \tau_k \tag{3.31}$$

By interchanging the order of summation and taking advantage of symmetry, it is shown that:

$$\sum_{ij} \left\{ \frac{\partial d_{kj}}{\partial q_i} \right\} \dot{q}_i \dot{q}_j = \frac{1}{2} \sum_{ij} \left\{ \frac{\partial d_{kj}}{\partial q_i} + \frac{\partial d_{ki}}{\partial q_j} \right\} \dot{q}_i \dot{q}_j \tag{3.32}$$

Hence:

$$\sum_{ij}\left\{\frac{\partial d_{kj}}{\partial q_i}-\frac{1}{2}\frac{\partial d_{ij}}{\partial q_k}\right\}\dot{q}_i\dot{q}_j=\frac{1}{2}\sum_{ij}\left\{\frac{\partial d_{kj}}{\partial q_i}+\frac{\partial d_{ki}}{\partial q_j}-\frac{\partial d_{ij}}{\partial q_k}\right\}\dot{q}_i\dot{q}_j \tag{3.33}$$

With the previous equation, is possible to calculate c_{ijk}, which are considered Christoffel Symbols of the first kind

$$c_{ijk}=\frac{1}{2}\left\{\frac{\partial d_{kj}}{\partial q_i}+\frac{\partial d_{ki}}{\partial q_j}-\frac{\partial d_{ij}}{\partial q_k}\right\} \tag{3.34}$$

By calculating the Christoffel Symbols, the elements of the matrix $C(\theta,\omega)$ can be derived, by having the $k$and j-th element of $C(\theta,\omega)$ defined as:

$$C_{k,j}=\sum_{i=1}^{n}C_{ijk}(q)\dot{q}_i \tag{3.35}$$

With this, we can rewrite the Euler-Lagrange equations as:

$$\sum_{i}d_{kj}(q)\ddot{q}_j+\sum_{ij}c_{ijk}\dot{q}_i\dot{q}_j+\frac{\partial P}{\partial q_k}=\tau_k,\quad k=1,\dots,n \tag{3.36}$$

Regarding equation (3.36), the first term involves the second derivative of the generalized coordinates, corresponding to the inertial terms. The second are quadratic terms in the first derivatives of q and reflect the inter-link dynamic interactions. These are classified into two types. Terms involving a product of the type ${\dot{q}_i}^2$ are called Centrifugal terms ($i=j$), while those involving a product of the type $\dot{q}_i\dot{q}_j$, where $i\neq j$, are called Coriolis terms. Moreover, these terms are present only when the multi-body inertia matrix is configuration dependent. In other words, the centrifugal and Coriolis terms are interpreted as nonlinear effects due to the configuration-dependent nature of the multi-body inertia matrix in the Lagrangian formulation. The third type of terms are those involving only q but not its derivatives. The latter arise, as seen before, from differentiating the potential energy (gravity terms).

3.2.2 Dynamic Model of a two-link manipulator

Following the Euler-Lagrange approach, and assuming that there is no friction force applied to the system ($V(\omega)=0$), the dynamic model of the manipulator (3.10) can be expressed using:

$$I(\theta)\frac{\partial\omega}{\partial t}+C(\theta,\omega)+S(\theta)=T_{act}+\ T_{int} \tag{3.37}$$

The two-link manipulator model used (Figure 16), is composed of two rigid body links with the mass of each rigid body focused on each center. For the links masses $m1$ and $m2$ were used, with $l1$ and $l2$ for their length, $lc1$ and $lc2$ for the mass centre position and $\theta1$ and $\theta2$ for the joints angles.

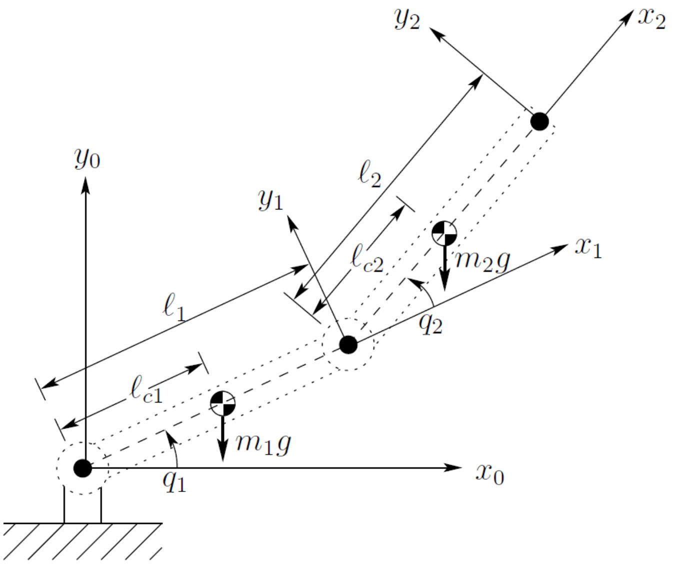

Figure 16: Two-link planar Manipulator model (Santos and Ferreira, 2016)

For the mass inertial matrix, $I(\theta)$, we use the total kinetic energy (3.23) to obtain:

$$I(\theta) = \begin{bmatrix} m_1 l_{c1}^2 + m_2(l_1^2 + l_{c2}^2 + 2l_1 l_2 \, cos \, \theta_2) + I_1 + I_2 & m_2 l_1 l_{c2} \, cos \, \theta_2 + m_2 l_{C2}^2 + I_2 \\ m_2 l_1 l_{c2} \, cos \, \theta_2 + m_2 l_{C2}^2 + I_2 & m_2 l_{C2}^2 + I_2 \end{bmatrix} \quad (3.38)$$

With I_x being equal to:

$$I_x = \frac{1}{12} m_x {l_x}^2 \quad , x = 1, \dots, n \quad (3.39)$$

Having calculated the mass inertial matrix, the Coriolis and Centrifugal matrix can be derived, with the definition for the Christoffel symbols of the first kind, using equation (3.35):

$$C(\theta, \dot{\theta}) = \begin{bmatrix} -l_1 l_{c2} m_2 sin \, \theta_2 \dot{\theta}_2 & -l_1 l_{c2} m_2 sin \, \theta_2 (\dot{\theta}_1 + \dot{\theta}_2) \\ l_1 l_{c2} m_2 sin \, \theta_2 \dot{\theta}_2 & 0 \end{bmatrix} \quad (3.40)$$

Lastly, we have the gravity vector. This term is easily obtained by differentiating the potential energy (3.26):

$$S(\theta) = \begin{bmatrix} m_1 g l_{c1} \cos \, \theta_2 + m_2 g (l_1 \cos \, \theta_1 + l_{c2} \cos(\theta_1 + \, \theta_2)) \\ m_2 g l_{c2} \cos(\theta_1 + \, \theta_2) \end{bmatrix} \quad (3.41)$$

3.3 Simulation Results

To test the impedance control, the controller was tested in two simulation settings. To check the matrices, the controller was implemented in MATLAB. The controller was then tested in a more realistic simulation using the physics simulation environment Webots. The tests focus on the stability of the manipulators and torques of each joint. In the Webots simulation, a comparison between a controller with and without a dynamic model is also presented.

3.3.1 MATLAB Implementation

The controller was first validated in a MATLAB simulation, so that we could ascertain the validity of the equations of motion determined, previously, through the Euler—Lagrange approach.

This implementation is accomplished with a mathematical simulation and not a torque-controlled device, therefore the controlled variable was substituted from the joint torque to the joint acceleration. In a regular controller, the joint torques necessary in order for the end-effector to reach a desired position, is what is determined, while in this controller, the joints accelerations caused by said torques are what is calculated. These accelerations are then integrated twice to determine the joint angles for the manipulator actuation.

For the MATLAB simulation, the code flow can be summed up as the initialization of the initial variables and the main controlled loop. In the initialization of initial variables, we have the initialization of variables such as the initial position and velocity, the lengths masses and inertial moments of each link as well as the gravity. On the other hand, the main controlled loop can be divided into the calculation of the matrices and the actuation of the manipulator. Before the matrices' calculations, there is a checking of the desired position, which can be changed at any time during the simulation (Figure 17).

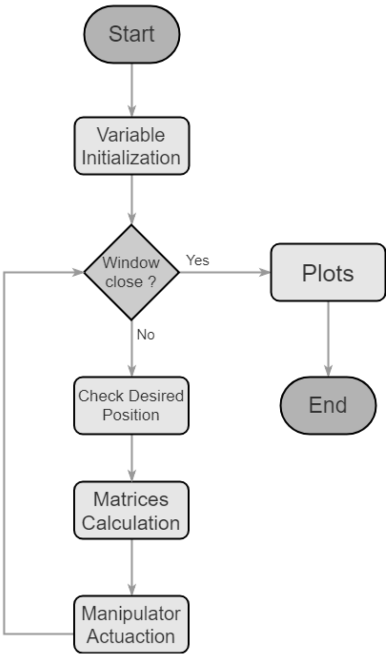

Figure 17: MATLAB controller flow chart

In the end, the model proved viable and functional, being able to lead the end-effector to the desired position. Is important to note that this model was made without regarding constraints and without taking into account friction of any kind.

In the Plots block, the visualization of the joints angles and the joints torques throughout the simulation is generated. In the following simulation graphs, we show the reaction of the two sets of variables (joint angles and torques), while changing the desired positions twice.

In figure 18, we see the representation of the two-link planar manipulator used for the test. We also see as a blue and a green ‘x’, representing the desired positions chosen for the test. The green position was the last chosen desired position and can be found under the red dot, representing the end-effector, while the blue position was the previously chosen desired position.

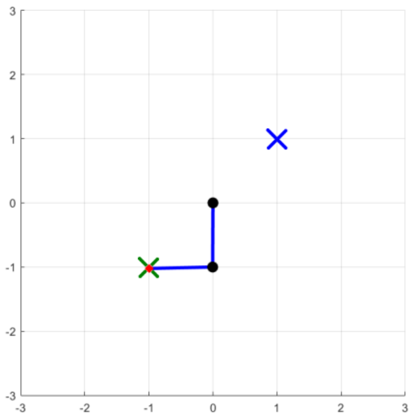

Figure 18: MATLAB arm representation.

TABLE I MATLAB CONTROLLER CHARACTERISTICS

Characteristic	Value
Link's length	1 meter
Link's weight	1 Kilogram
K	15
B	10
Initial Position	(2,0)

In figure 19, the evolution of the joints' angles, in blue, and the joints torques, in orange, are shown. In these graphs, it is easy to see the change of the desired position, since this change causes a sharp variation in both the joint angles and in the joint torques. These changes happen at four seconds and twelve and a half seconds and are the result of the T_{act} a term from (3.37). After the initial change of torques given by the controller, these tend to stabilize with the torque values necessary to maintain the end-effector position, given by the model.

This model could be further improved by including the velocity-dependent torques, $V(\omega)$, in (3.37), and by taking in consideration model constraints which were excluded from the simulation.

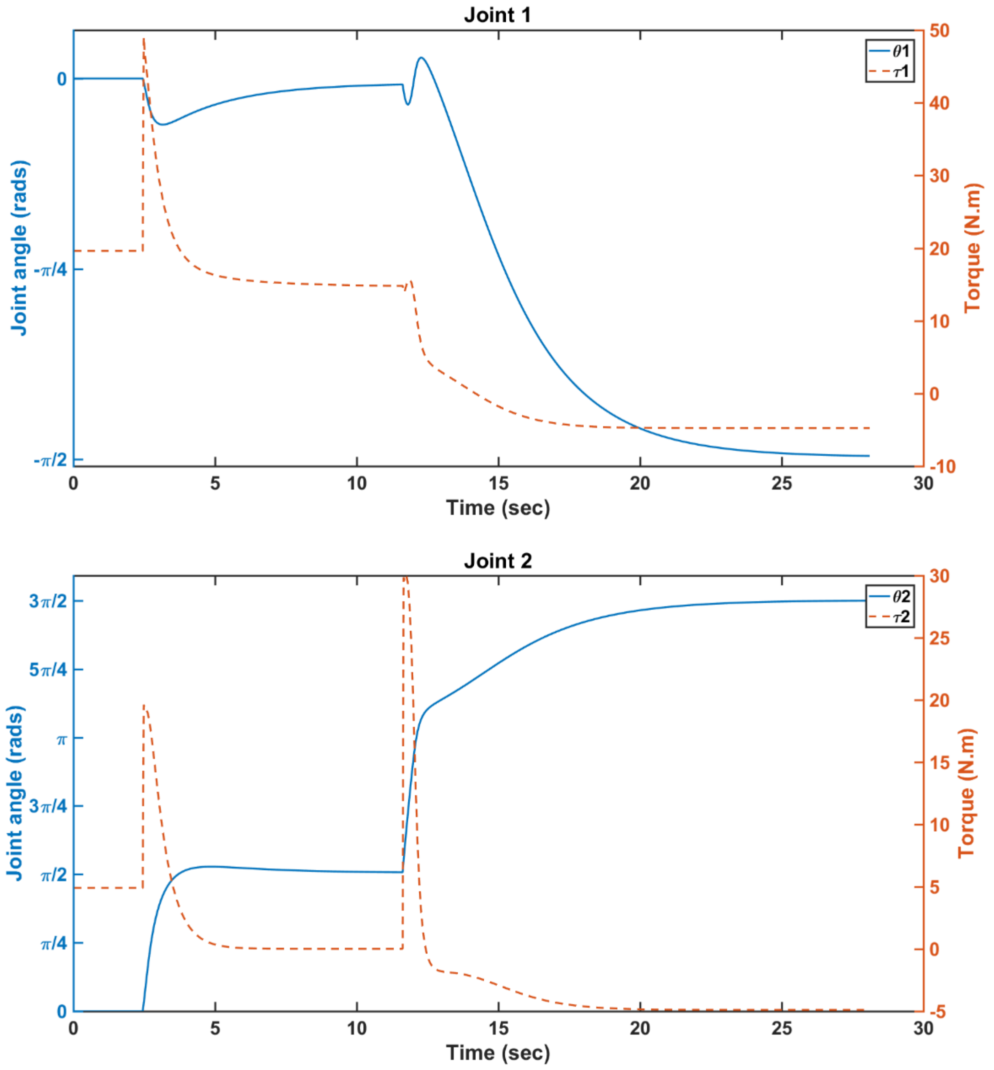

Figure 19: Joint and torque for both joints

3.3.2 Webot Implementation

After the validation of the model in MATLAB, the implementation of the impedance controller was started in Webots (Michel, 2004). With the Webots simulation environment, a more realistic simulation is achieved and, therefore, providing a better representation of the controller performance.

In this section, the main objective was to test the advantages and disadvantages arising from the use of a controller that takes into account the manipulator's model. Therefore, a comparison of the performance of the impedance controller with and without the manipulator model will be provided, in different situations.

For the Webots implementation, the two-link planar manipulator, used in the MATLAB test, needed to be constructed as a 3D model. For this, a simple rectangular prism was used for a link's body. The two prisms, comprising the two links of the manipulator, were then placed side-by-side connected by a rotational joint, or a Hingejoint in Webots. One of the links was then subject to the same procedure to connect it to the main body, which was fixed to the ground. To simplify the controller, the physical model of the manipulator was created without constraints. To accomplish this, the manipulator was raised from the ground high enough to give the ability for the manipulator to be completely extended towards the ground. There is also no possibility of contact between bodies, as they are placed in different planes so that a link can rotate 360 degrees. The complete model can be seen in Figure 20, with the controller characteristics shown in Table II.

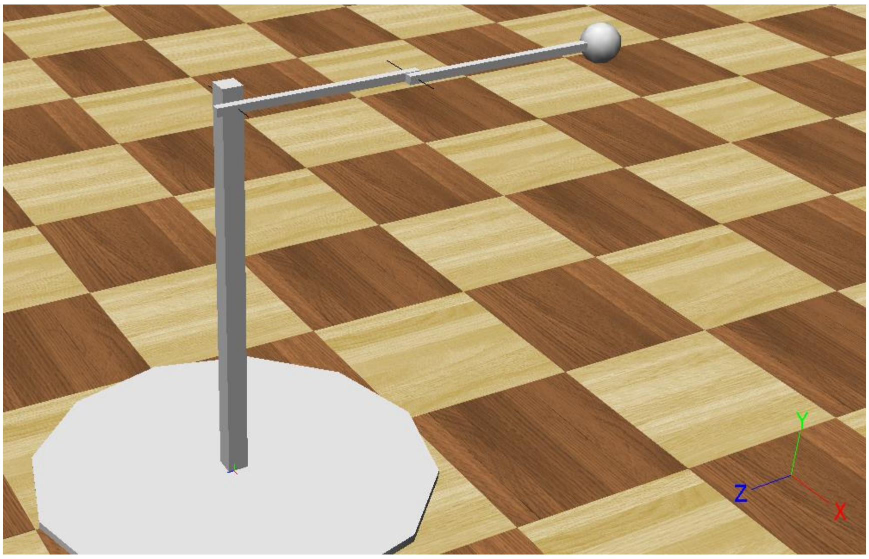

Figure 20: Webots arm model

TABLE II WEBOTS CONTROLLER CHARACTERISTICS

Characteristic	**Value**
Link's length	1.0 meter
Link's weight	1 Kilogram
K	15
B	10
Initial Position (X_i)	(0.0 , -2.0)
Motor Maximum Output	40 Nm

The tests on Webots are divided into the following subsections:

1) Controller without the dynamic model
2) Controller with the dynamic model
3) Controller without dynamic model with noise
4) Controller with the dynamic model with noise
5) Controller without dynamic model with perturbation
6) Controller with the dynamic model with perturbation

1) Controller without the dynamic model

The first controller tested, with the 3D model in Webots, was the impedance controller without the model, equation (3.9) (repeated here for convenience).

$$T_{act} = J^T(\theta)K[X_0 - L(\theta)] + J^T(\theta)B[V_0 - J(\theta)\omega] + S(\theta) \qquad (3.42)$$

A gravity compensation component, $S(\theta)$, was also added to the controller. The gravity term inclusion is due to the fact that its absence results in a large error of the end-effector. It can be excluded from the model, however, it is a simple way to decrease steady state error.

In Webots, the control of the manipulator is accomplished by simulating rotational motors. This allows for the torque control, that is required for a proper impedance controller, and the direct use for the controller output, T_{act}, unlike what was done with the MATLAB implementation, where the actuator torque was used to calculate the joints' accelerations. It can also be noted that the joint angles are measured in Webots, while in MATLAB the joint angle was assumed to be the angle obtained by integration of the joint acceleration.

For the tests with the controller without the model, the desired position was chosen and then the trajectory of the joints recorded. The tests involved the choice of four different desired positions, one on each of the four quadrants of operation. The desired positions were $X_0 = [1.0, 1.0]$, $[-1.0, 1.0]$, $[-1.0, -1.0]$ and $[1.0, -1.0]$,with 1.0 meters being the length of a link from the manipulator. For the values of the K and B gains, the ones used in the MATLAB section were used. The reason for an arbitrary value being chosen, was because the main goal of the test was to test the difference in response of the controller to different situations, such as the existence of noise in the actuation or the appearance of perturbations and not the determination of optimal gains for the manipulator. The control of the manipulator can be summarized by the figure 21

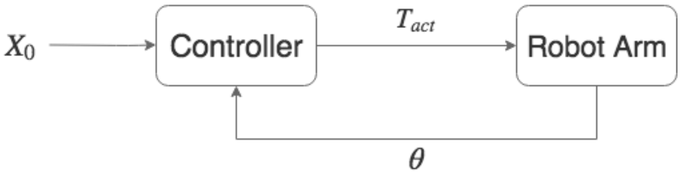

Figure 21: Controller Diagram

As it was expected, the controller response,(Figure 22), closely resembles a PD (proportional-derivative) controller. These oscillations and stabilization time can be reduced by optimizing the gains.

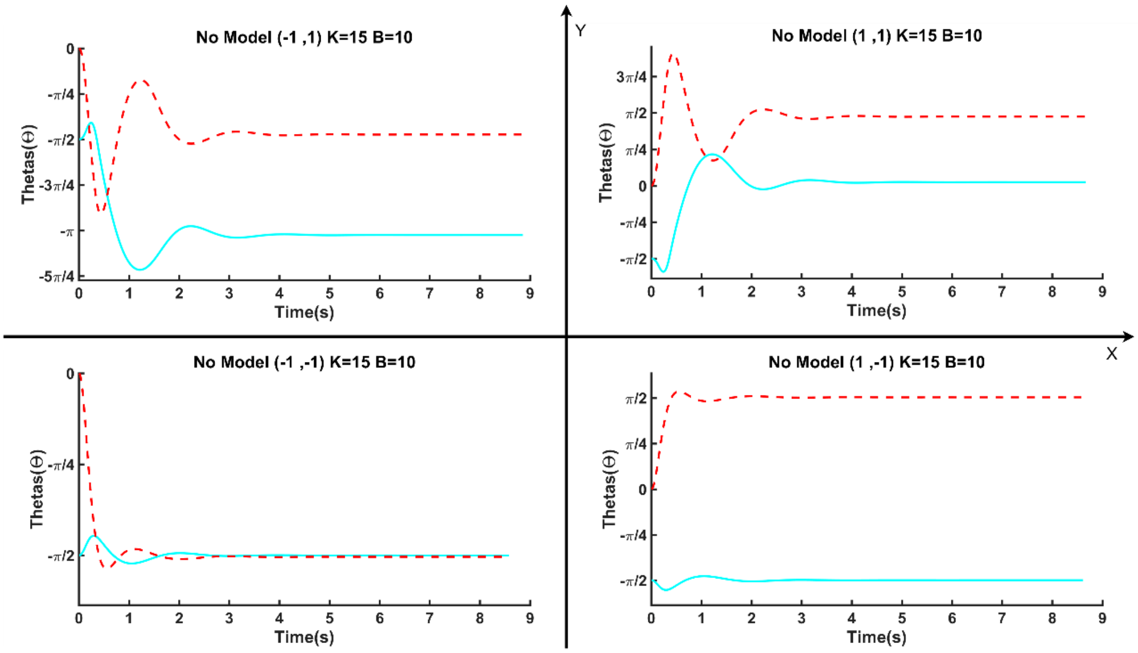

Figure 22: Controller without the dynamic model (Equation (3.40)*) (solid line – theta 1; dashed line – theta 2)*

2) Controller with the dynamic model

For the controller with the model, equation (3.10) (repeated here for convenience) is used.

$$\begin{aligned} T_{act} = {} & I(\theta)J^{-1}M^{-1}K[X_0 - L(\theta)] + S(\theta) \\ & + I(\theta)J^{-1}M^{-1}B[V_0 - J(\theta)\omega] + V(\omega) \\ & + I(\theta)J^{-1}M^{-1}F_{int} - J^T(\theta)F_{int} \\ & - I(\theta)J^{-1}G(\theta, w) + C(\theta, \omega) \end{aligned} \tag{3.43}$$

To simplify the model the velocity-dependent term $V(\omega)$ and the external forces F_{int} were not considered or in other words, were equal to 0.

The addition of the model to the controller results in the manipulator's stabilization time and oscillations being reduced as the figure 23 shows

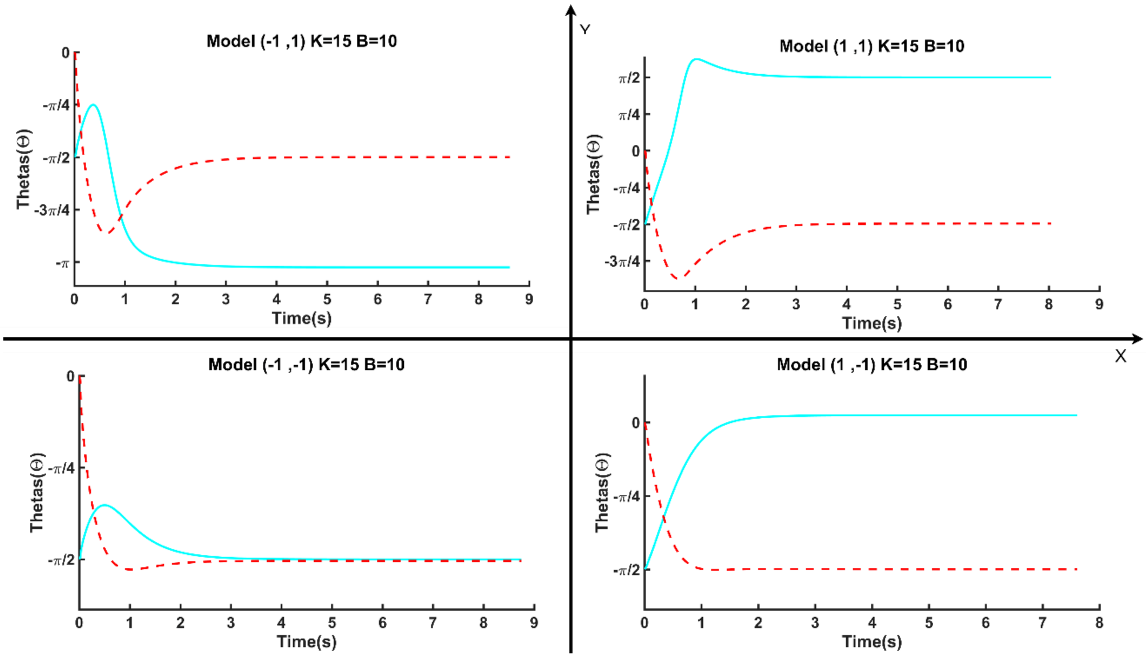

Figure 23: Controller with the dynamic model (Equation (3.41)*) (solid line – theta 1; dashed line – theta 2)*

The figure shows the motion stabilizing in less time than the tests without the model, demonstrating an improvement on the controller's response. The test also shows that, while the manipulator's end position is the same as the tests without the model, the manipulator's configuration (i.e. the manipulator's links physical position) and the path taken can be different.

In the four tests perform, the Model (-1, 1) and the Model (-1, -1) have the same end configuration and took the same path to it, while the Model (1, 1) and Model (1, -1) have different end configuration and therefore took different paths when compared to the tests without the model. The impedance control approach does not restrict the path to the desired position and so the motion the end-effector takes and its final configuration, can be different.

3) Controller without dynamic model with noise

To test the influence the addition of noise has on the system, the manipulator was exposed to four different amounts of noise (Figure 24). These were 0.05 Nm, 2.5 Nm, 5 Nm and 10 Nm. The noise component was a random value, between the noise values shown, and was added to the controller output T_{act}. The 0.05 Nm and the 2.5 Nm noise tests show a small amount of movement in the link joints. Only after 5 Nm, does the noise's influence is noticeable on the joints' angles.

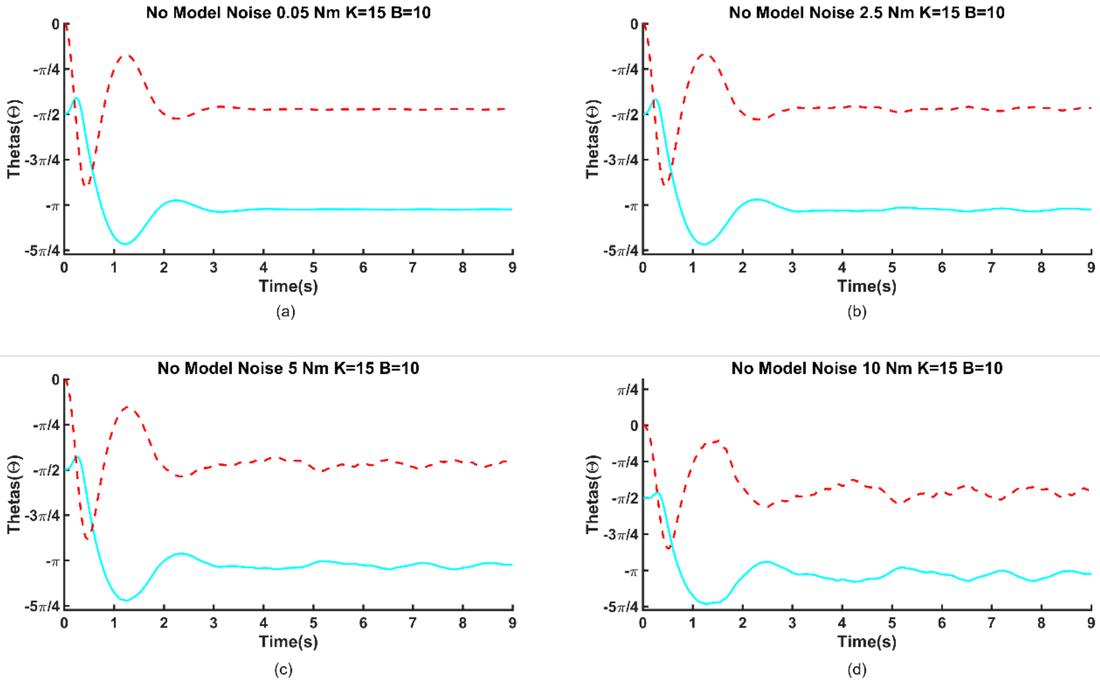

(a)

(b)

(c)

(d)

Figure 24: Controller without the dynamic model and with noise (solid line – theta 1; dashed line – theta 2)

4) Controller with the dynamic model with noise

The noise affects primarily the steady state, preventing a total convergence of the end-effector when the model is not present. For the controller with the dynamic model, the manipulator’s response (Figure 25) does not variate substantially from the response without the noise, being able to maintain the end-effector position more stable. Only with the 10 Nm noise, does the controller start to have difficulty maintaining the joint angles.

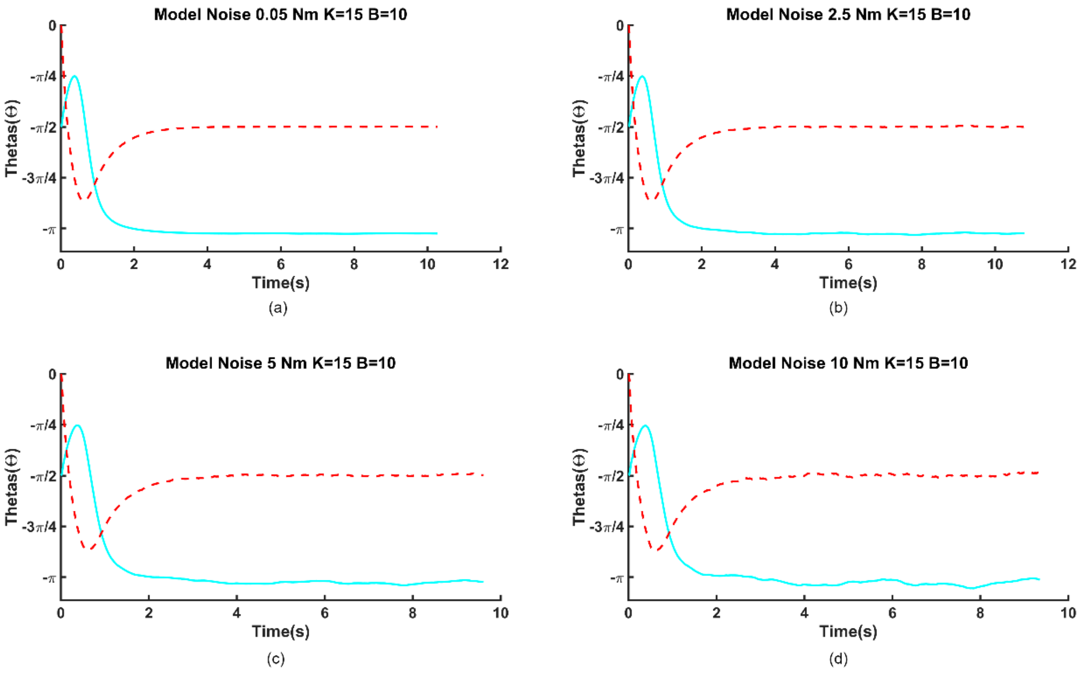

(a)

(b)

(c)

(d)

Figure 25: Controller with the dynamic model and with noise (solid line – theta 1; dashed line – theta 2)

5) Controller without the dynamic model with perturbation

The benefits of the model can also be seen when a perturbation is encountered. To test this, eight tests were devised, four to test the response to different perturbations strengths and four to test the response to different perturbation directions. These perturbations were created with the help of a plugin that was added to the Webots simulation and work by applying a constant force on the end-effector. For the strength tests, a force was applied on the Z axis and it was started after the end-effector stabilized, with a duration of a few seconds. The strength of the perturbation tested were 2.5 N, 5 N, 10 N and 20 N. For the direction tests, a force of 5 N was applied to end-effector in the positive Z axis, the negative Z axis, the positive yy axis and the negative yy axis. Figure 26 shows a perturbation as a red line, pointing toward the desired direction of the positive Z axis.

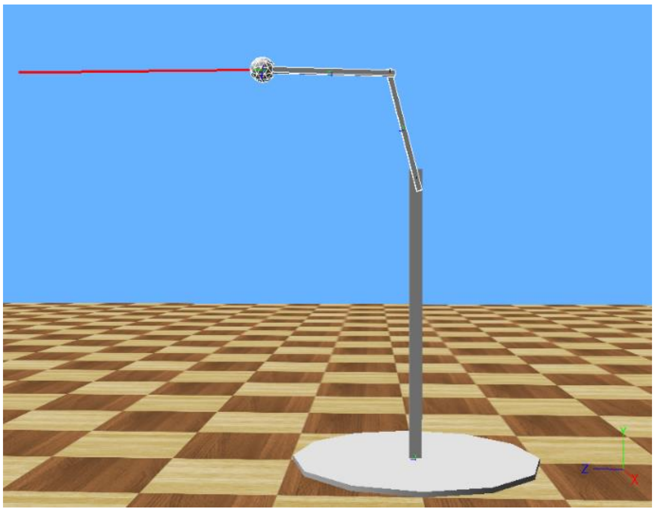

Figure 26: Perturbation representation on the Webots arm model

In the controller without the model, the perturbations cause some oscillations while the end-effector stabilizes with the new equilibrium point. The different force strengths affect the position of the equilibrium point and the forces the manipulator has to output to counter the perturbation. Figure 27 shows the joints response to the four perturbations, while figure 28 shows the torque from each test. From these figures, only the figure 27(c), shows a significant difference from the rest, since the manipulator’s configuration, after the encountering the perturbation, was not the same from the prior to the perturbation.

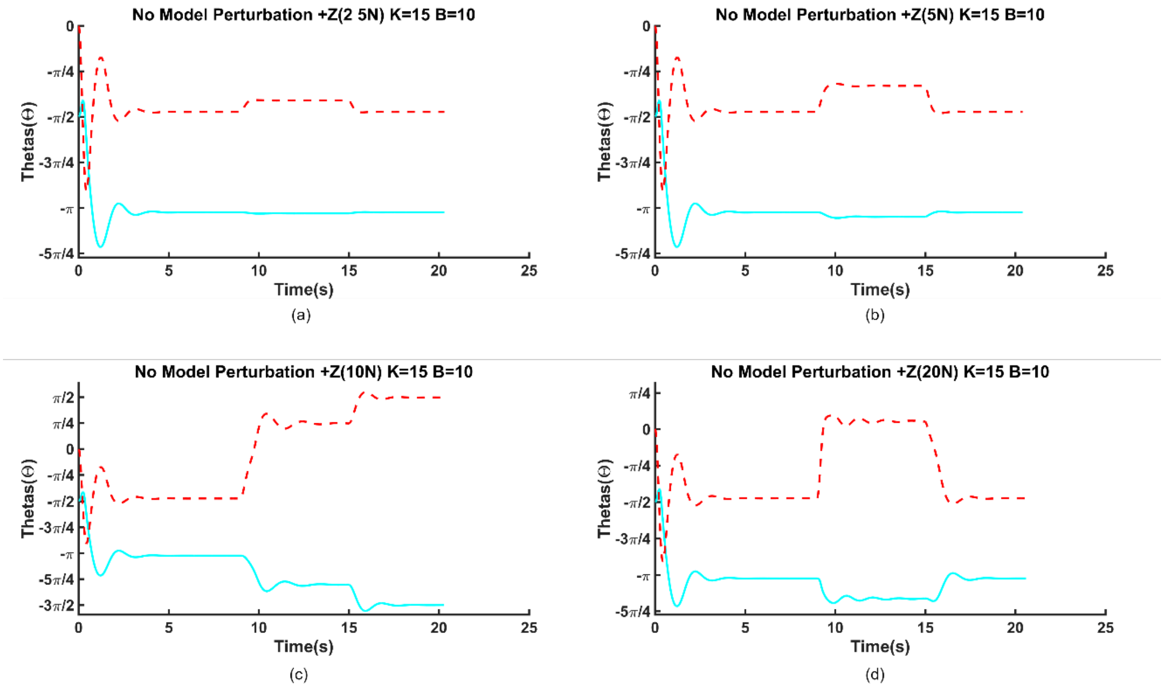

(a) (b) (c) (d)

Figure 27: Controller without the dynamic model and different strength perturbations (Joint angles) (solid line – theta 1; dashed line – theta 2)

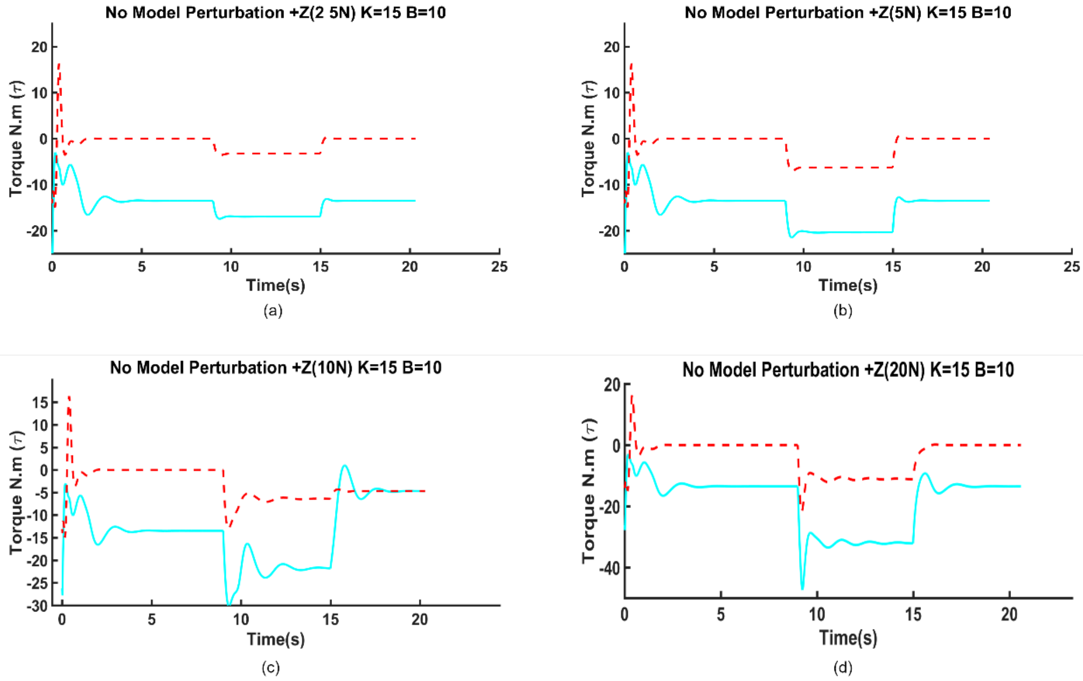

(a) (b) (c) (d)

Figure 28: Controller without the dynamic model and different strength perturbations (torque) (solid line – torque 1; dashed line – torque 2)

The different direction perturbations do not seem to have a significant change in how the perturbation is dealt with since the only difference is the direction the joints 'angles and the motors' torque change. The figures 29 and 30 show the response from the joint angles and the motor torques respectively.

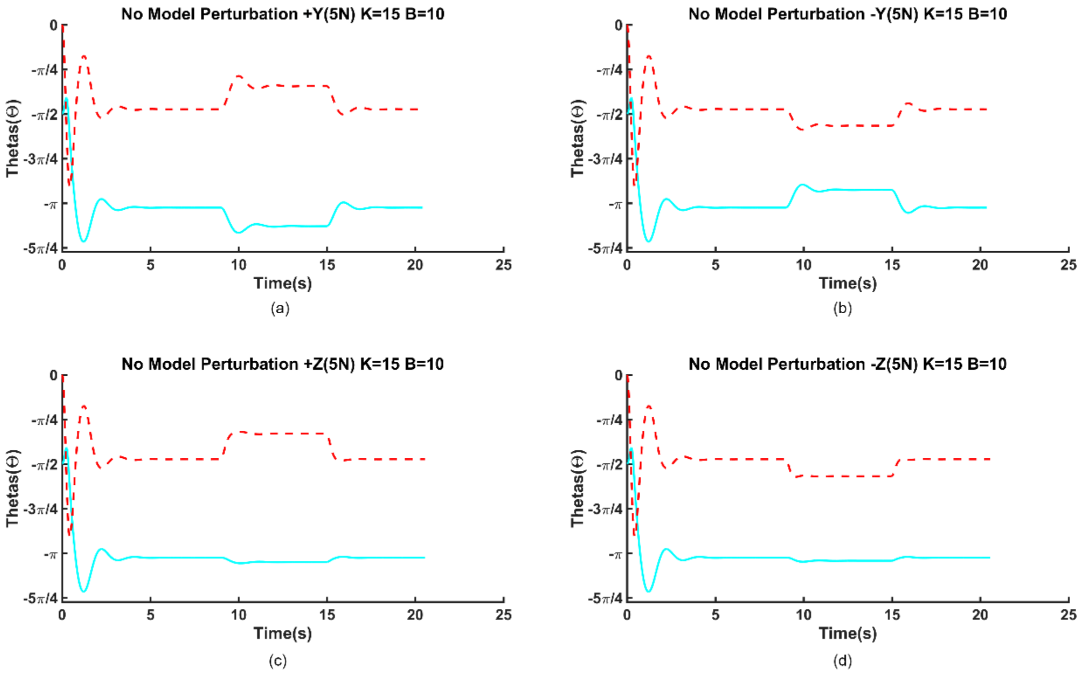

(a)

(b)

(c)

(d)

Figure 29: Controller without the dynamic model and different direction perturbations (Joint angles) (solid line – theta 1; dashed line – theta 2

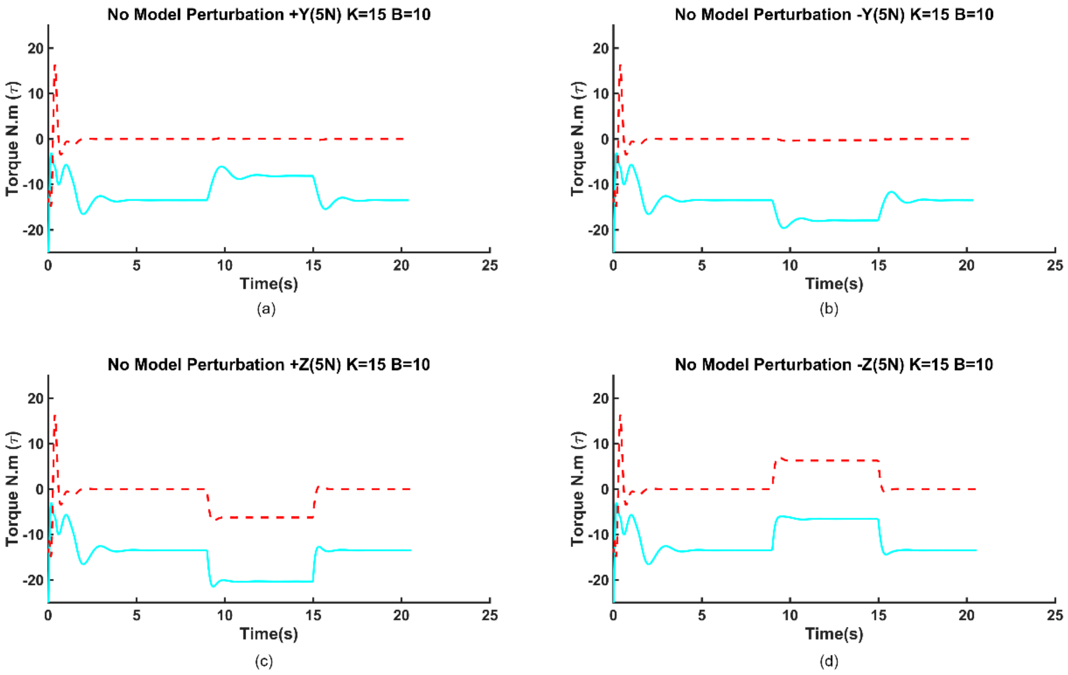

Figure 30: Controller without the dynamic model and different direction perturbations (torque) (solid line – torque 1; dashed line – torque 2)

6) *Controller with the dynamic model with perturbation*

The addition of the model to the different strength perturbation test has the same advantages that were pointed out in the noise tests. The model aids the manipulator, by reducing the oscillations and the time it takes to reach the steady state. Figure 31 and the figure 32 show that, with the model, the perturbation causes fewer oscillations and the manipulator is able to reach a stable position in the time the perturbation force is present. The joint torques are also smaller than those on the manipulator without the model. The model, however, is not without problems. When the perturbation force is high enough, to force the joint 2's angle to 0 or 180 degrees, the manipulator will be in a singularity which will cause a sharp increase of the joint speed. While the perturbation is present, the manipulator will be forced to the singularity which in turn the causes instability. This can be observed in figure 32(d), where the torques tend to infinity, only to stabilize after the perturbation is no longer present. It is also possible to see the same high values at 0 seconds caused by the same problem since the initial position of the manipulator is a singularity $X_i = [0, -2.0]$.

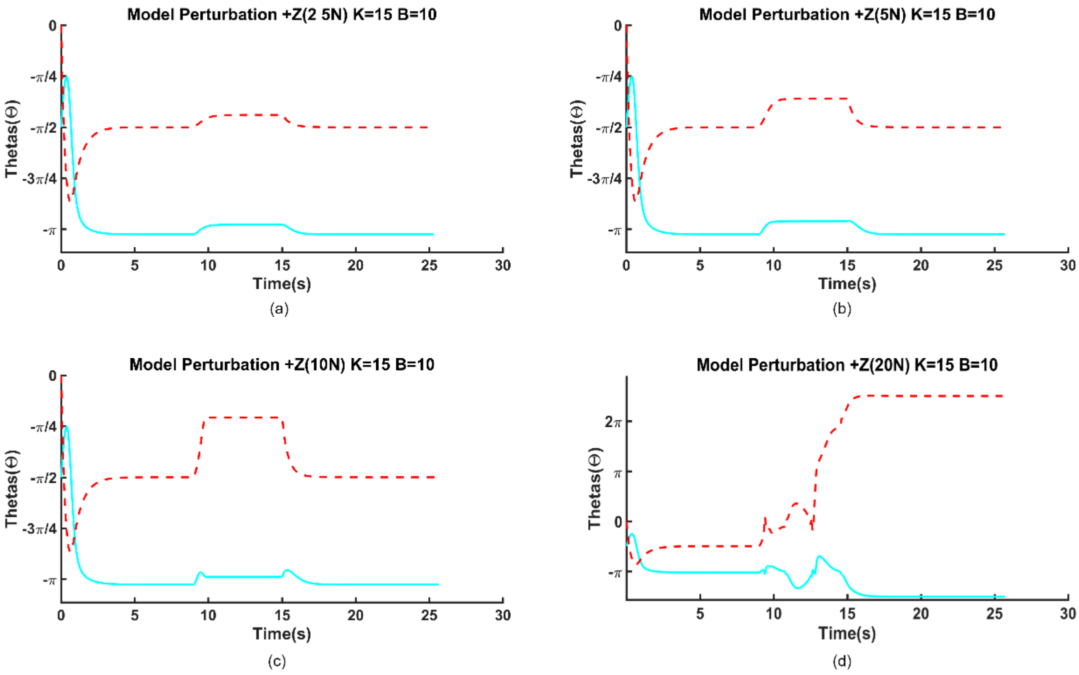

(a) (b) (c) (d)

Figure 31 Controller with the dynamic model and different strength perturbations (Joint angles) (solid line – theta 1; dashed line – theta 2

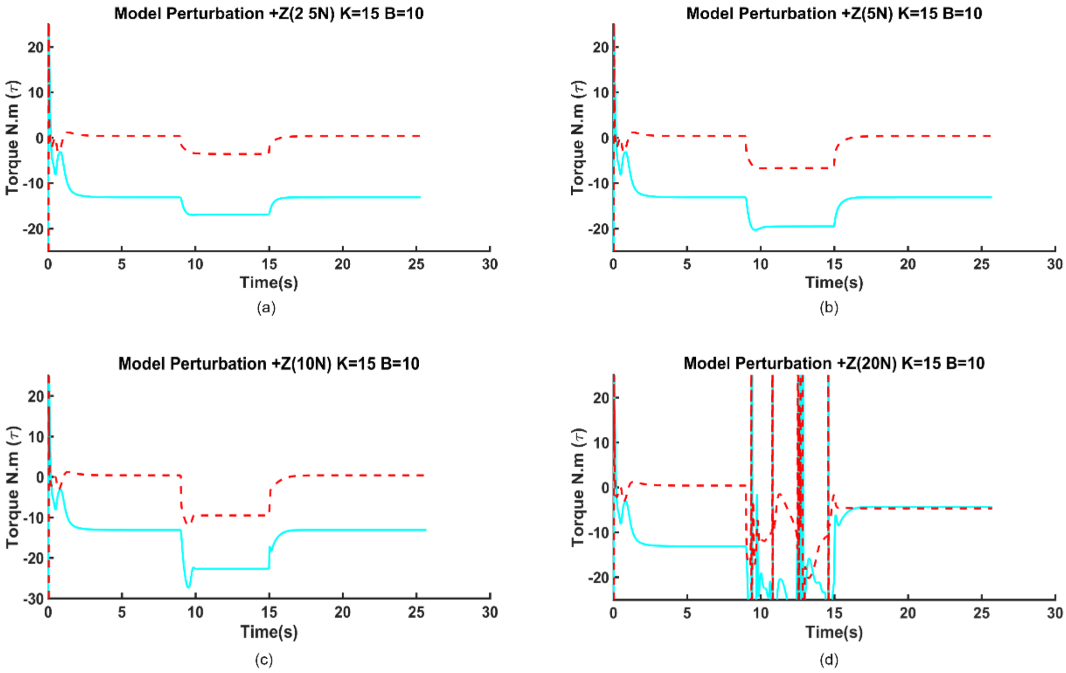

(a) (b) (c) (d)

Figure 32: Controller with the dynamic model and different strength perturbations (torque) (solid line – torque 1; dashed line – torque 2)

The response of the model to perturbations from different directions is shown in the figures 33 and 34. The model decreases the steady state error of the end-effector and therefore when in contact with a perturbation, the joints need to be corrected by a larger amount. This can be seen in the figure figures 33(b) wherein the test without the model, the joint 1 did not move significantly and with the model it did. The torque, on the other hand, shows little to no oscillations when compare to the tests without the model.

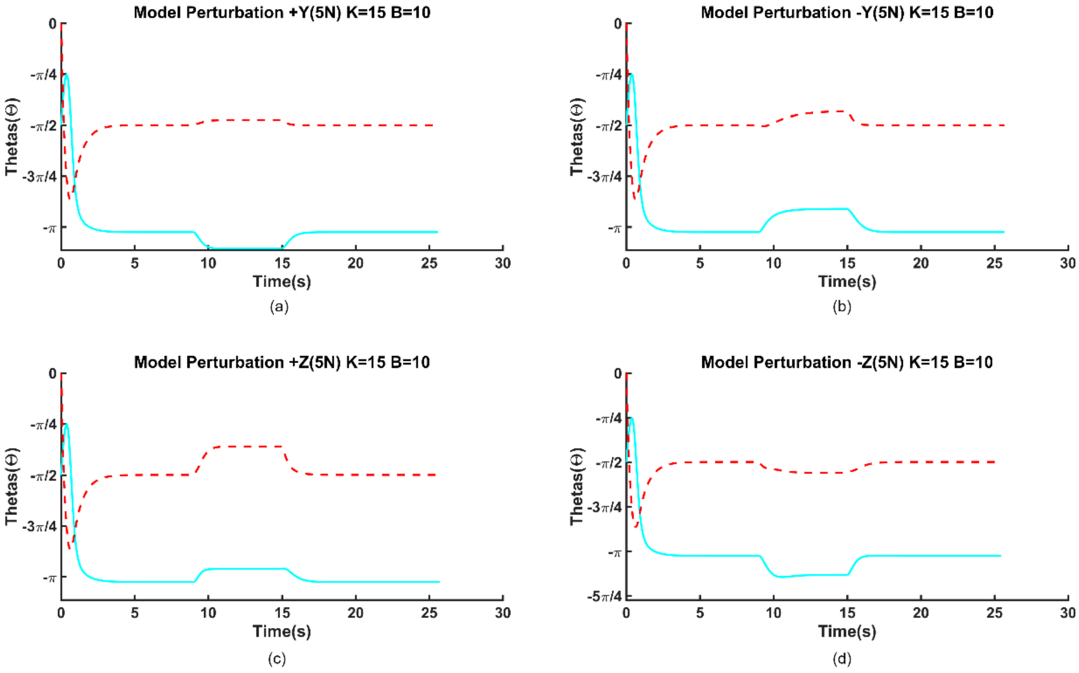

(a) (b) (c) (d)

Figure 33: Controller with the dynamic model and different direction perturbations (Joint angles) (solid line – theta 1; dashed line – theta 2

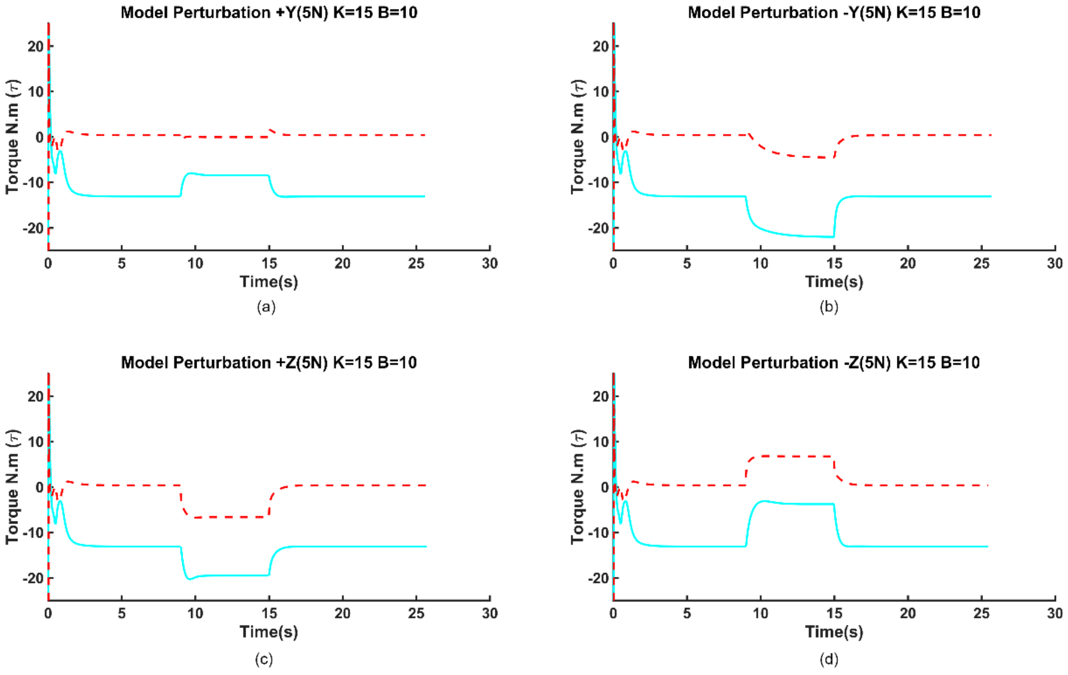

Figure 34: Controller without the dynamic model and different direction perturbations (torque) (solid line – torque 1; dashed line – torque 2)

3.4 Chapter Conclusions

In this chapter, a theoretical foundation of the Impedance Controller and a model of a two-link planar manipulator was first provided, being followed by an implementation of the impedance controller in MATLAB and an implementation in Webots, for a more accurate assessment of its performance. In the Webots implementation, a comparison between a controller with and without a dynamic model of the arm was also provided in conjunction with the advantages as well as the disadvantages, derived from the use of the model mentioned.

The MATLAB implementation proves the validity of the of the controller and the model derived in the theoretical foundation section of the chapter. In this implementation, the end-effector was able to reach the desired position successfully.

From the Webots implementation, a comparison of the controller with and without the dynamic model was tested in a more realistic environment. The controller without the model had the gravity term from the model on all the tests. In these Webots tests, it is clearly shown that the model improves the performance of the controller. With the model, the controller is able to reach a smaller steady state error, in a smaller time period and with less overall oscillations. The advantages, arising from the use of a manipulator model, that were mentioned allow for a lower controller stiffness while keeping the response fast and stable. By lowering the stiffness, a less restrictive and more adaptable manipulator is achieved, and this results in a lower amount of force present in the interaction points. This, on the other hand, results in a safer manipulator, for both the manipulator and the environment.

The main disadvantage for the use of the model in the controller is the difficulty in its determination when involving more complex manipulators. The increased number of links, degrees of freedom, constraints, the use of more complex joints and more complicated environments such as the movement in liquids, all increase the complexity of the manipulator model and, therefore, decreases its usability in said situations.

The fact that determining a dynamic model may be a difficult task, is not the only problem with relying on the model. Using an incorrect model may also lead to high forces involved and even instability. The model also introduces singularities to the controller, which are not present in the controller without the model.

CHAPTER 4 HUMAN LOCOMOTION GENERATION

In the previous chapter, it is shown an implementation of Hogan's Impedance Control, in the control of a robotic two link planar arm. The tests focused on the evaluation of the advantages and disadvantages in using the impedance control, with and without a dynamic model of the manipulator. They showed that the introduction of a dynamic model greatly improves the performance of said controller, in respect to speed and accuracy of the actuator, reaching the desired end-effector position faster and with less steady state error. The model also helps in reducing the impact of noise on the system. However, although the addition of a dynamic model improved the performance of the controller, it was not used in the controller of the prosthetic device. The choice of not using the model, when it seems that the controller would benefit from it, was because the model tested, in a real environment, resulted in an erratic movement, with high joints torques. This can be attributed to an inaccurate model, that didn't take into account the frictional drags and more complex inertial moments. The development of a more accurate model might resolve these problems, but it would require the full dynamics analysis of the prosthesis. As such, and as it is recommended, the controller used is the "Simple Impedance controller" pair with a low internal impedance robot.

In this chapter, the tools used to generate the locomotion for the Darwin-OP robot are presented. The chapter starts with the explanation of the controller used to generate the talking motion. The controller utilized was a control pattern generator or CPG controller. This specific implementation was proposed, by Vitor Matos in (2014) where the controller was designed to rely on the dynamical system approach for its implementation, especially on the use of the nonlinear oscillators and the exploitation of their properties. Matos also proposed feedback mechanisms for the regulation of the timing of the step phases

To determine all the necessary parameters, for the state machine, the impedance controller and the CPG controller parameters necessary for it to work in conjunction with the prosthesis, a stage genetic algorithm optimization was used, which is explained further in the chapter.

4.1 CPG Controller

CPGs Overview

The concept of Central Pattern Generators has gained widespread attention in the robotics community as inspiration for the design of mid-level motor control. This type of controller was developed under the scope of bio-inspired robotic movements, in which knowledge from biological studies is applied to real-world engineering. The applications can be found in biosensing, bio actuation and biomaterials and may take the form of a simple application of biological concepts to full biomimicry. In robotics, bio-inspiration has long been used to design robots which mimic an animal's method of locomotion, from flying, snake and fish like, biped, quadruped and multi-legged robots (Maki, 2007).

The general, accepted definition of a Central Pattern Generators is as a functional group of neural networks in the central nervous system, which can generate and regulate the rhythmic motor processes in the body, such as those involved in respiration, swallowing, chewing, digestion, flying, walking, running and swimming, as well as other rhythmic movements (Arshavsky, Deliagina and Orlovsky, 1997).

Locomotor CPGs are not a recent discovery, being first found by Brown in 1911 (Brown, 1911). In his studies, Brown suggested that locomotor behaviors are the result of central rhythmic mechanisms in a cat. This was later followed by research in both invertebrates (Marder *et al.*, 2005) and vertebrate animals (Orlovskii, Deliagina and Grillner, 1999; Kiehn, 2006). There is definite evidence on the existence of CPGs for locomotion in vertebrates like the cat, dog and rabbit, but there is only indirect evidence indicating the existence of CPGs for locomotion in humans. (Orlovskii, Deliagina and Grillner, 1999; R., YURI and M., 2006).

Research indicates that complex walking behavior is accomplished primarily by the locomotor CPG, which retain a repertoire of motor programs used in locomotion (Grillner *et al.*, 2008). In the complete absence of rhythmic inputs, the CPG produces the rhythmic motor patterns necessary for the locomotion. These patterns are solely commanded through stimulation on the supraspinal regions, which are capable of generating complex rhythmic movements and controlling their level of activity

Equally important is the integration of sensory information and feedback mechanisms, able to govern and shape the generated patterns. When trying to adapt and correct the walking environment accordingly to the current environment and behavior context, these feedback mechanism and sensory information become a very important component of the controller. The sensory information is obtained from signals stemming from the supraspinal, spinal and other peripheral structures, and are continuously integrated by the CPG for the proper expression and short-term adaptation of locomotion. The sensory information is then used to select the rhythmic pattern, modulate the amplitude of muscle burst and pattern frequency. They can also regulate the structure and transition between step phases, assist whit foot positioning and correct movements when obstacles appear (Rossignol, Dubuc and Gossard, 2006). This short-term adaptability provides a large degree of versatility to an otherwise fixed set of motor patterns in the CPG repertoire, by dynamically adapting the movements to the environment.

In regard to the organization of a mammalian's CPG, it has been suggested that the CPG can be divided into two distinct layers, the rhythmic generation layer and the pattern generation layer. Whereas the rhythmic generation layer is responsible for the rhythmic coordination within the CPG and the coordination between CPGs, the pattern generation layer is responsible for generating the patterns of locomotion (Lafreniere-Roula and McCrea, 2005; McCrea and Rybak, 2008).

This proposed organization provides the advantages of independent influence onto each layer. This means that changes acting on the motor patterns do not directly influence the rhythmic activity, and, in the same way, the rhythmic changes will not directly affect the motor patterns.

Throughout the years, CPG based controllers have been successfully employed in multi-legged robots. Due to their distributed characteristics, this type of controllers can be found, applied to robots with little as two legs such as humanoid robots, up to robots with six, eight or more legs. When considering biped walking, an increased level of difficulty arises, due to the loss of stability provided by the extra number of legs. However, CPG has also been applied successfully and in different kinds of bipedal robots. From servo actuated tethered bipeds constrained to the sagittal plane (Taga, 1998; Nakanishi *et al.*, 2004) to full-sized humanoid robots (Hyon, Morimoto and Cheng, 2008; Morimoto *et al.*, 2008) including compliant actuated humanoids (Hyon, Morimoto and Kawato, 2010) and football playing robots (Behnke, 2006).

An extensive number of works apply CPGs in simulated bipeds, many of which aim to demonstrate the feasibility of CPG based controllers and their integration with feedback mechanisms, or to achieve an easier system analysis (Taga, Yamaguchi and Shimizu, 1991; Aoi and Tsuchiya, 2006).

Bipedal CPG approach

The CPG based controller, proposed by Vítor Matos (2014), to tackle the biped walking problem, can be divided into two layers. A distributed rhythmic generator or temporal reference and a pattern generation layer or spatial reference. The distributed generation layer is implemented as a phase oscillator with a unit for each leg, producing the coordinated base rhythmic signal that drives the pattern generation layer. As for the pattern generation layer, it is using a pattern generator based in a set of forcing terms in attractor dynamical systems, which define motion primitives.

The phase oscillators produce an intrinsic rhythmic generation which, then allows for easy coupling and synchronization. For the production of coordinated movements in the biped solution, a coordinated set of motions primitives are utilized, while being dependent on the timing of the shared phased oscillators.

The proposed solution allows for easy modulation of the produced motor patterns by means of parameter manipulation resulting in straightforward and meaningful changes in the final motor behavior. These changes result in smooth modulation for the desired trajectories, even if an abrupt parameter alteration occurs. Moreover, by having the motor pattern behavior controlled by parameter manipulation, it is possible to map the changes from the control parameters to a higher-level command, abstracting the control.

These systems produce stable rhythmic patterns in regard to their limit cycle behavior, returning to the normal stable state after small transient perturbations. This intrinsic robustness of the dynamical system allows for easy integration with a sensory feedback mechanism, which temporarily influences the system state.

It can be also mentioned that, due to its parameterizable and modular approach, it is possible to use optimization and other learning algorithms to extend the robot's motor abilities.

The proposed locomotion system has two CPGs, one for each leg, which control all of the leg's DOFs by outputting an angular position reference. As previously stated, this CPG is modeled on a two-layer organization, by having a rhythmic generation layer produce the temporal reference and a pattern generation layer produce the spatial reference in accordance with the temporal drive. A group of motion patterns generators, each responsible for a single joint, are driven by a shared rhythmic generator.

This approach tries to emulate the generation of motor generation output, in a vertebrate motor system. Other works (Flash and Hochner, 2005; Bizzi *et al.*, 2008) have hypothesized that a vertebrate motor system is accomplished by a combination of units of motor output. Small functional units in the spinal cord generate specific patterns of muscle activation, also denominated by synergies, as discrete building blocks which, when combined, result in the production of a variety of different movements. This method for the problem of motor control allows the CNS to handle a large collection of solutions, simplifying the low-level activation of the muscles by handling only the activations of the synergies, instead of the individual's muscles involved in the movement (Schaal and Schweighofer, 2005). This way is possible to easily accomplish coordination among a large number of DOFs for a determined behavior in low-level control. The problem of motor control comes down to a role in selecting, appropriately activating pre-existing motor primitives or even transforming and deriving from the existing primitives limited number of store primitives.

In the proposed approach, similar to other approaches, motion primitives are encoded as a set of non-linear dynamical equations with well-defined attractor dynamics. These motion primitives are them able to be smoothly and easily modulated regarding their amplitudes, frequencies and pattern offsets.

The starting repertoire of primitives should be able to achieve a, while basic, capable walking behavior. This repertoire is created manually through a progressive increment of motion primitives, using sinusoidal and bell-shape trajectories to describe the general motions observe from biped walking. A sinusoidal is a good candidate for a primitive since complex signals can be generated from the sums of these elements.

Rhythm Generator

Similarly, as other CPG implementations, the rhythm generator layer is implemented as a coupled phase oscillator and is given by:

$$\dot{\phi}_i = \omega + k\,sin(\phi_i - \phi_o + \pi) \tag{4.1}$$

Where ϕ_i (rad) is the phase CPG i and ϕ_o (rad) is the place of CPG o. the phase increases monotonically and linearly with the rate of ω (rad s^{-1}), bounded in the range [-π, π]. The rhythmic output ϕ_i can be then employed as a time keeping clock, used in the generation of timely and coordinated motor trajectories.

The included coupling term $k\,sin(\phi_i - \phi_o + \pi)$ maintains a desired phase relationship of π between the oscillator $i$and o, with a coupling strength of k. An oscillator will then anchor each motion primitive into a specific phase value, where an oscillator period corresponds to a step cycle period, guaranteeing the coordination between all motion within a leg.

Motion Pattern Generator

Each CPG is composed of six motion pattern generators driven by the shared phase oscillator, which addresses all the joints of a leg for the humanoid Darwin-OP. a single motion pattern generator produces the trajectories in real-time for each joint within a leg, and its final periodic output is used as a reference of the angular position of a joint, in the low-level PID controller present on the Darwin-OP robot. The produced periodic trajectory by each motion pattern generator is the overall result from the sum of several motion primitives, f.

In the proposed implementation, each motion pattern generator is based on a set of non-linear dynamical equations, defining the attractor dynamics. Joint position $z_{j,i}$ is generated according to the current phase ϕ_i of the CPG,

$$\dot{z}_{j,i} = -\alpha\left(O_{j,i} - z_{j,i}\right) + \Sigma f\left(z_{j,i}, \phi_i, \dot{\phi}_i\right) \tag{4.2}$$

With $O_{j,i}$ specifying the offset attractor for the final generated rhythmic pattern, and α its time constant.

In the equation (4.2), while the subscript i defines the leg, right or left, the subscript j defines the motion pattern generator of a single joint from the Darwin-OP legs: hip roll (hRoll), hip yaw (hYaw), hip pitch (hPitch), knee (kPitch), ankle roll (aRoll) and ankle pitch (aPitch). A single motion primitive is defined by the function $f_j^{motion}\left(z_{j,i}, \phi_i, \dot{\phi}_i\right)$ and maps the current joint position and the phase of the step cycle to a force that influences the system's final output. The final generated trajectory $z_{j,i}$ is obtained by adding all the forcing functions for that joint. Without any forcing terms f_j, the system converges asymptotically towards the goal O, and no rhythmic activity exists. The system must then be subject to periodic influences through the forcing terms and the phase oscillator output, producing the final rhythmic trajectory.

In terms of stability, the system is guaranteed to converge to the attractor O in the absence of forcing terms if an appropriate α is chosen (α > 0). Furthermore, the magnitudes of the forcing terms employed are limited and bounded by design, thus the system is BIBO (Bounded-Input, Bounded-Output) stable, producing a solution around O given that the rhythmic forcing terms are limited in amplitude.

In this formulation, a single motion primitive is defined as a set of forcing functions assigned to the pattern generators among the required joints. The set of forcing functions defines a rhythmic motor behavior, coordinating all the recruited DOFs, used as a building block for the final motor behavior.

Biped locomotion requires the same motions to be produced for both legs in an alternate fashion, therefore, when a motion primitive is defined, it is used for both legs. To simplify the design of the motion primitives and the general walking behavior, it was assumed that the feet should be maintained parallel to the ground during the entirety of the step cycle. To accomplish this, symmetric motion primitives from the hip pitch and ankle pitch are assigned to the joint ankles.

For the motion primitives, two motion profiles were used. A sinusoidal profile, which is useful to in the recreation of symmetric motions, that repeat a maximum excursion one or more times during a step cycle. This profile can be described by:

$$f_j^{motion} = -A_{j,motion}\dot{\phi}_i \sin(\phi_i + \psi_{motion}) \tag{4.3}$$

With amplitude A_{motion} and phase shift ψ_{motion} for the joint j in leg i.

The other motion profile used is the bell-shaped profile. This profile is more appropriately utilized to describe motion which happens once per step cycle, with a defined duration within said step cycle. The bell-shaped profile can be described as:

$$f_j^{motion} = -\frac{A_{j,motion}\dot{\phi}_i(\phi_i + \Psi_{motion})}{\sigma^2} e^{\left(-\frac{(\phi_i+\Psi_{motion})^2}{2\sigma^2}\right)} \tag{4.4}$$

Where A_{motion} defines the amplitude and σ the width of the bell curve, with Ψ_{motion} its phase shift.

Motion Primitives

By resorting only to the sinusoidal and bell-shaped profiles one can put together a set of coarse motion primitives that should be able to compose a basic locomotion. The walking motion is derived from own familiarity with human walking, observations and kinematical descriptions from the literature.

It has been verified that by using a minimum of four motion primitives it is possible to achieve capable biped locomotion. The four motions needed are: the balancing motion, the flexion motion, the compass motion and the turning motion. Other motion primitives can be considered, either for expanding the locomotor abilities, e.g. pelvis rotation motion, or to add detail to the walk, e.g. yielding motion.

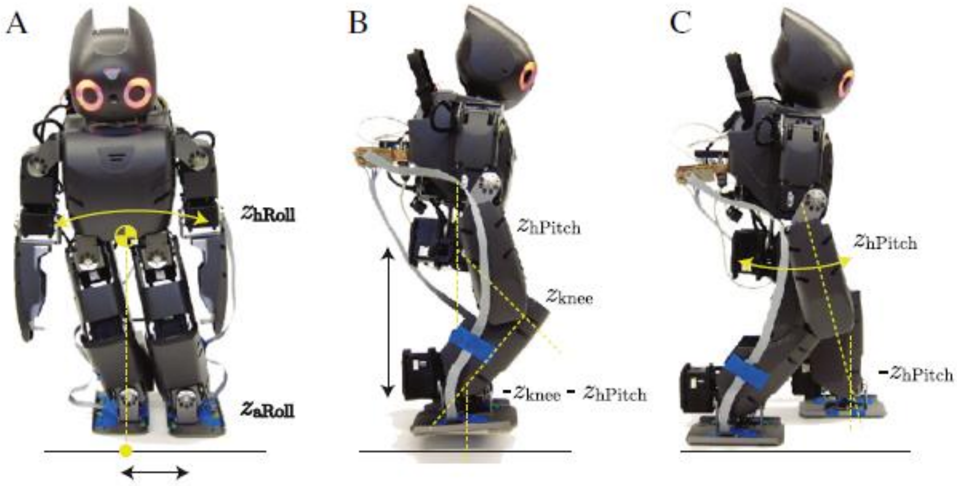

Figure 35: 3 motion primitives. (A) Balancing motion; (B) Flexion motion; (C) Compass motion- From (Matos and Santos, 2014)

Balancing Motion

The balancing motion is one of the crucial motions for bipedal walking, as it tries to provide stability during the step. As the robot steps alternately, it goes through moments of single foot support, requiring the entire weight of the robot to be supported by a single foot, and double feet support, where both feet are on the ground. During the single foot support, the robot's body needs to shift over the supporting foot, while unloading the other foot, for it to start its swing motion. Failing to perform this motion in a correct and timely manner would lead to a fall.

The balancing motion acts on the hip roll (hRoll) and the ankle roll (aRoll) and can be described as a sinusoidal trajectory that makes the robot oscillate laterally. This motion can be defined as:

$$f_{hRoll,i}^{balancing} = -A_{balancing}\dot{\phi}_i \, sin(\phi_i) \tag{4.5}$$

$$f_{aRoll,i}^{balancing} = -f_{hRoll,i}^{balancing} \tag{4.6}$$

Where $A_{balancing}$ specifies the lateral displacement motion, disabling the motion when set to 0.

Flexion Motion

Flexion motion is also an important motion, as it is meant to achieve vertical clearance for the feet. After the displacement of the weight, the swinging foot is unloaded, and the flexion motion changes the foot's height by actuating and the three pitch joints: hip, knee, and ankle.

This motion is described at the joint level as having a bell-shaped curve, and the three primitives can be described as:

$$f_{hPitch,i}^{flex} = \frac{A_{hip}\dot{\phi}_i\phi_i}{\sigma^2}e^{\left(-\frac{\phi_i^2}{2\sigma^2}\right)} \tag{4.7}$$

$$f_{kPitch,i}^{flex} = \frac{A_{knee}\dot{\phi}_i\phi_i}{\sigma^2}e^{\left(-\frac{\phi_i^2}{2\sigma^2}\right)} \tag{4.8}$$

$$f_{aPitch,i}^{flex} = -\left(f_{hPitch,i}^{flex} + f_{kPitch,i}^{flex}\right) \tag{4.9}$$

The amplitude of the flexion motion is specified by the amplitude for the hip, A_{hip}, and the amplitude for the knee, A_{knee}. By having the motion primitive of the ankle equal to the symmetric sum of the hip and the knee, the feet can stay parallel to the ground.

Compass Motion

The compass motion is the one responsible for producing the propulsion of the body during locomotion. This motion moves the legs in the sagittal plane, alternately moving the contralateral legs forward and backward. It generates the forward steps in coordination with all the other motions, resulting in forward walking. This motion is described as sinusoidal profiles at the hip pitch and ankle pitch joints, as such:

$$f_{hPitch,i}^{compass} = -A_{compass}\dot{\phi}_i\, sin\left(\phi_i + \frac{\pi}{2}\right) \tag{4.10}$$

$$f_{aPitch,i}^{compass} = -f_{hPitch,i}^{compass} \tag{4.11}$$

With amplitude $A_{compass}$ and $\frac{\pi}{2}$ phase shift.

Turning Motion

After achieving forward walking, it is easy to obtain a turning motion while walking. During the single support phase of the step cycle, if the robot twists by its vertical axis, the placement of the next stance foot will be pointing towards the direction of the turn. The turning motion is generated by applying a sinusoidal to the yaw joints of the robot, as:

$$f_{hYaw,i}^{turn} = -A_{turn}\dot{\phi}_i\, sin\left(\phi_i + \frac{\pi}{2}\right) \tag{4.12}$$

By having the same phase shift as the compass motion, the turning motion will be synchronized with the compass motion.

Knee Yielding Motion

A characteristic of legged locomotion is the yield that occurs in the knee joint when the leg starts the stance phase and the body’s weight is shifted onto it. With this yield, it is possible to flatten the COM vertical trajectory while walking, which is beneficial to the humanoid robot being used.

This motion is added to the knee and ankle joint as a sinusoidal profile, and they can be described as:

$$f_{hPitch,i}^{yield} = A_{yield}\dot{\phi}_i \, sin(\phi_i + \pi) \tag{4.13}$$

$$f_{kPitch,i}^{yield} = -2A_{yield}\dot{\phi}_i \, sin(\phi_i + \pi) \tag{4.14}$$

$$f_{aPitch,i}^{yield} = -f_{hPitch,i}^{yield} \tag{4.15}$$

Pelvis Rotation Motion

This motion can be seen employed in human walking and it is used to help flatten the vertical COM, as well as, smooth the inflections that occur when changing the vertical directions of the COM. However, this motion is employed here, for its ability to increase the step length by twisting the body, placing the swinging foot further in front. This pelvic rotation can also be described as a sinusoidal trajectory and it is performed at the hip yaw joints as:

$$f_{hYaw,i}^{rotation} = -A_{rotation}\dot{\phi}_i \, sin\left(\phi_i + \frac{\pi}{2}\right) \tag{4.16}$$

Motion Summary

In this approach, the repertoire that was compiled is composed by four strictly required motion primitives: balancing, flexion, compass and turning motion. To these four, two others were added to further add new features, pelvis rotation motion, or just to fine-tune the performance, knee yielding motion.

The proposed CPG could then be constructed with these motion primitives, thus obtaining the following:

$$\dot{\phi}_i = \omega + k \, sin(\phi_i - \phi_o + \pi) \tag{4.17}$$

$$\dot{z}_{hRoll,i} = \ -\alpha\big(z_{hRoll,i} + O_{hRoll}\big) + \ f_{hRoll}^{balancing} \tag{4.18}$$

$$\dot{z}_{aRoll,i} = -\alpha\big(z_{aRoll,i} + O_{aRoll}\big) + \ f_{aRoll}^{balancing} \tag{4.19}$$

$$\dot{z}_{hYaw,i} = -\alpha\big(z_{hYaw,i} + O_{hYaw}\big) + f_{hYaw}^{rotation} + f_{hYaw}^{turn} \tag{4.20}$$

$$\dot{z}_{hPitch,i} = -\alpha\big(z_{hPitch,i} + O_{hPitch}\big) + f_{hPitch}^{flex} + f_{hPitch}^{yield} + f_{hPitch}^{compass} \tag{4.21}$$

$$\dot{z}_{kPitch,i} = -\alpha\big(z_{kPitch,i} + O_{kPitch}\big) + f_{kPitch}^{flex} + f_{kPitch}^{yield} \tag{4.22}$$

$$\dot{z}_{aPitch,i} = -\alpha\big(z_{aPitch,i} + O_{aPitch}\big) + f_{aPitch}^{flex} + f_{aPitch}^{yield} + f_{aPitch}^{compass} \tag{4.23}$$

With the motion primitives determined, the tuning of the parameters was performed in order to achieve bipedal walking. This parametrization is performed by sequentially and incrementally tuning and adding each motion primitive in sequence by trial-and-error. In the end, these were the parameters obtained:

TABLE III ORIGINAL CPG PARAMETERS

Amplitude	(°)	Offset	(°)
$A_{balancing}$	14	O_{hYaw}	0
A_{hip}	15	O_{hRoll}	1.5
A_{knee}	30	O_{hPitch}	-25
A_{yield}	0	O_{kPitch}	40
$A_{compass}$	11	O_{aRoll}	-1.5
$A_{rotation}$	0	O_{aPitch}	20
ω $(rad\ s^{-1})$	4.9	k	7

Sensory Feedbacks

The CPG locomotion described previously is easily degradable when considering, even the minimal amount of noise at a joint level. Due to its open-loop nature, the impact of each movement has an environment will not be considered when computing gait dynamics, resulting in a lack of stability with the possibility of a fall. Besides, one could theorize that locomotion that adapts in response to the interaction with the environment and body changes, would have a better performance than one that does not adapt. It is, therefore, important when considering a CPG-based control of legged locomotion, to be able to incorporate reactive behavior into the controller.

In the controller used, the idea described in Ferreira and Santos (2015) and André, Santos and Costa (2016) is applied to the biped humanoid robot to generate highly adaptative behavior proportional to the foot contact with the ground. For this task, a simple implementation of a sensory-driven feedback loop is adapted, whereby using sensory information from the force sensors located in the feet, the oscillator phase can be adjusted in a quantitative way. The implementation is as follows:

$$\dot{\phi}_i = \omega + k\, sin(\phi_i - \phi_o + \pi) + \sigma GRF_i \sin(\phi_i) \tag{4.24}$$

With σ as the feedback strength and GRF_i the Ground Reaction Force, of the i^{th} leg, which corresponds to the sum of the values measured by the four force sensors on each foot.

This feedback mechanism is designed to slow down the leg oscillator proportionally to the GRF during the stance phase and speed up in a similar way during the swing phase. It is based on the assumption that higher GRF values during stance imply that the robot's weight is primarily distributed on a single leg, thus meaning that the opposite leg is still in swing.

To further improve the robustness of the controller, three other feedback mechanisms were also introduced to the controller. These were previously used in other works such as (Macedo, 2014) This feedback mechanisms are designed to act upon the ankle pitch, ankle roll and hip yaw.

The first of these three mechanisms is the ankle pitch correction. As it was stated before, for this humanoid robot, the robot's feet must be parallel to the ground, when they make contact. This parallelism and an equal distribution of the weight of the robot, along the front and the back of the foot plant, help achieve a better support and balance, for an overall more stable walking motion using the force sensors distributed in each corner of each foot, a mechanism to correct the ankle pitch angle can be established as the following:

$$F_{pitch} = \eta_{pitch}\begin{pmatrix}(FSR_{left,left,front} + FSR_{left,right,front} + FSR_{right,left,front} + FSR_{right,right,front})\\ -(FSR_{left,left,back} + FSR_{left,right,back} + FSR_{right,left,back} + FSR_{right,right,back})\end{pmatrix} \quad (4.25)$$

$$\dot{z}_{aPitch,i} = -\alpha(z_{aPitch,i} + O_{aPitch}) + f_{aPitch}^{flex} + f_{aPitch}^{yield} + f_{aPitch}^{compass} + F_{pitch} \quad (4.26)$$

Where $FSR_{i,j,k}$ is the output of an FSR sensor in the i leg in the position (j,k) and η_{pitch} controls the strength of the applied correction.

This correction increases or decreases $\dot{z}_{aPitch,i}$ according to the difference of the measure force sensors. For example, if the sum of the forces in the back sensors is greater than the sum of the sensors in the front, F_{pitch} will be negative, having the effect illustrated in the figure 36.

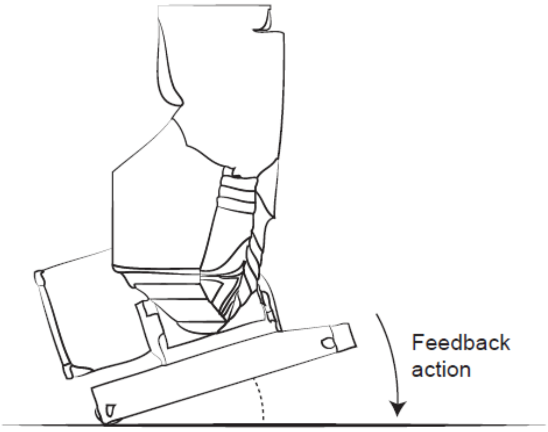

Figure 36: Effect of the ankle pitch correction feedback – From (Macedo, 2014)

The next feedback mechanism is the ankle roll correction. This mechanism acts in an analogous manner to the pitch correction, but regarding the balance between the forces measured in the left and right sensors in each foot plant figure 37. It can be applied by:

$$F_{roll} = \eta_{roll}\begin{pmatrix}(FSR_{left,left,front} + FSR_{left,left,back} + FSR_{right,left,front} + FSR_{right,left,back})\\ -(FSR_{left,right,front} + FSR_{left,right,back} + FSR_{right,right,front} + FSR_{right,right,back})\end{pmatrix} \quad (4.27)$$

$$\dot{z}_{aRoll,i} = -\alpha(z_{aRoll,i} + O_{aRoll}) + f_{aRoll}^{balancing} + F_{roll} \quad (4.28)$$

Where η_{roll} controls the strength of the applied correction.

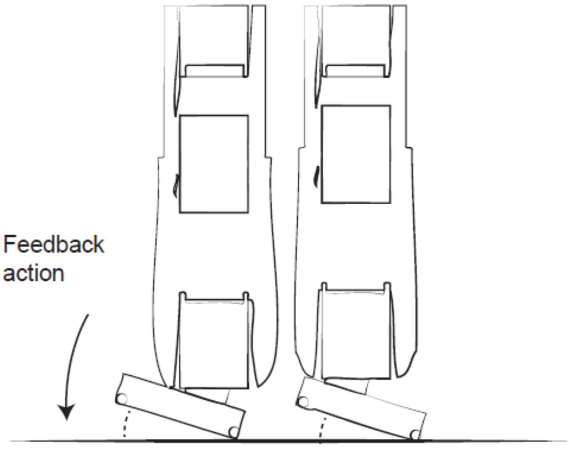

Figure 37: Effect of the ankle roll correction feedback – From (Macedo, 2014)

The last of the feedback mechanisms is the turn or direction correction. Without constant correction of the direction, a deviation rate will always force the robot's facing direction to slowly and steadily change. This phenomenon can also be observed in humans, whereby closing one's eyes, it turns the of moving in a straight line into an almost impossible one. In robots, this problem is aggravated when the surface on which the robot is walking is inclined.

In order to suppress this deviation, a feedback mechanism that changes A_{turn} is used, which perturbs the hip yaw trajectory, causing the robot to turn. This can be achieved by adding the following dynamical system:

$$A_{turn} = \eta_{a,Direction}\left(\eta_{\beta,Direction}\left(\theta_{goal} - \theta\right) - \dot{\theta}\right) \tag{4.29}$$

An advantage of this dynamical system is that changing the θ_{goal} value, does not cause the sudden change of the hip yaw angle. This allows using this mechanism to not only correct the direction of the robot but also give the ability to change it (Figure 38).

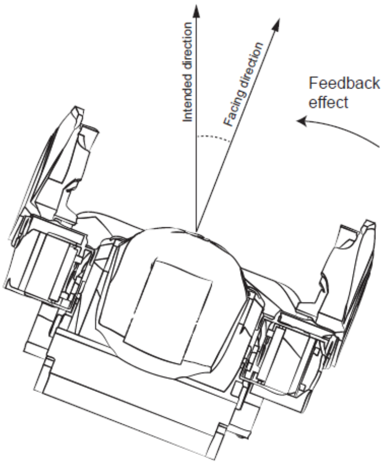

Figure 38: Effect of the direction correction feedback – From (Macedo, 2014)

4.2 Optimization Method

The proposed work involves the use of an impedance controlled prosthetic device, substituting the foot of a CPG controlled humanoid robot. The impedance controller for the prosthesis uses a finite state machine, switching between two states, Stance and Swing when a transitioning event happens. Each state provides the required parameters to the impedance controller.

Each of the controllers has their one set of parameters that need to be set for the desired behavior. The CPG controller generates different movements by changing the values of the amplitudes and offsets of the controller's motion primitives. The CPG controller's motion for each joint is controlled by the motion primitives and the respective offset.

The parameters involved in the control of each joint and their corresponding variables are shown in Table VI. The feedback mechanism included in the CPG controller is shown in Table V. this represents a total of twenty-one CPG parameters that need to be tuned. The prosthesis controller also has parameters which need to be tuned to have the desired behavior. This can be divided into those from the finite state machine and those from the impedance controller.

Concerning the finite state machine, the parameters are those that define the gait events are provided in Table VI. In Table VI, the parameters for the impedance control are also provided. The prosthesis controller also allows for the tuning of the passive prosthetic ankle joint parameters. The passive ankle roll joint parameters that were optimized were the stiffness and damping, as the equilibrium point for the passive ankle roll was fixed to zero.

In the overall, there is a total of thirty-six parameters that need to be tuned and optimized to achieve the desired behavior.

TABLE IV CPG CONTROLLER PARAMETERS

Joint	**Related Parameters**			
	Amplitudes		**Offset**	
Hip Roll	Balancing Hip Roll	$-A_{balancing}$	Hip Roll	O_{hRoll}
Hip Yaw	Pelvis Rotation	$-A_{rotation}$	Hip Yaw	O_{hYaw}
Hip Pitch	Flexion Hip Compass Hip	A_{hip} $-A_{compass}$	Hip Pitch	O_{hPitch}
Knee Pitch	Flexion Knee Stance Flexion Knee	A_{knee} $-A_{yield}$	Knee Pitch	O_{kPitch}
Ankle Pitch	Flexion Ankle H Flexion Ankle K Stance Flexion Ankle Ankle Compass	A_{hip} A_{knee} $-A_{yield}$ $A_{compass}$	Ankle Pitch	O_{aRoll}
Ankle Roll	Ankle Roll	$A_{balancing}$	Ankle Roll	O_{aPitch}

TABLE V CPG CONTROLLER FEEDBACK MECHANISMS PARAMETERS

Variable	
FSR Feedback Weight	σ
Ankle Pitch Correction Strength	η_{pitch}
Ankle Roll Correction Strength	η_{roll}
Turn Correction	$\eta_{a,Direction}$

TABLE VI PROSTHESIS CONTROLLER PARAMETERS

Finite State Machine	
FSR Total Sum	FSR_total
Pre-Swing Upper Counter	pr_swing_UC
Pre-Swing Lower Counter	pr_swing_LC
Pre-Stance Upper Counter	pr_stance_UC
Pre-Stance Lower Counter	pr_stance_LC
Upper Gyroscope Threshold	gyro_UT
Lower Gyroscope Threshold	gyro_LT
Threshold for the FSR sum	FSR_t

Impedance Controller		
Stance	Stiffness	K_0
	Damping	B_0
	Desired Equilibrium Point	θ_{d0}
Swing	Stiffness	K_1
	Damping	B_1
	Desired Equilibrium Point	θ_{d1}
Passive Joint Impedance Controller		
	Stiffness	
	Damping	

Due to the number of parameters that need to be tuned, finding the values through trial and error is not feasible. Therefore, an optimization method was needed to tackle this problem. There are several different methods which could have been chosen. Some of these methods include the simulated annealing (Kirkpatrick, Gelatt and Vecchi, 1983), particle swarm optimization (Shi, 2015), ant colony optimization (Al Salami and Salami, 2009) and evolutionary algorithms (Zitzler and Thiele, 1999), which are representations of natural process found in nature and have shown remarkable success in the optimization of natural phenomena.

In this work, the optimization method selected was the genetic algorithm. The genetic algorithm optimization method and the previously mentioned methods, work by generating new points (i.e. attempts at a solution to the problem) by applying operators to the previous points and statistically moving towards more optimal solutional in the search space. The methods mainly differ in the operators used to generate the new points.

The genetic algorithm (GA) is an optimization and search technique based on the principles of genetics and natural selection. A GA allows a population composed of many individuals to evolve under specified selection rules to a state that maximizes the fitness. Develop by John Holland in 1975 (Holland, 1975) and popularized by David Goldberg, when he was able to solve a difficult problem involving the control of gas -pipeline transmission in 1989 (Goldberg, 1989), the genetic algorithm has seen many different versions and implementations with varying degrees of success. Some of the advantages of the GA are the fact that:

- Optimizes with continuous or discrete variables;
- Does not require derivative information;
- Simultaneously searches from a wide sampling of the cost surface;
- Deals with a large number of variables;
- Is well suited for parallel computers
- Optimizes variables with extremely complex cost surfaces (they can jump out of a local minimum);
- Provides a list of optimum variables, not just a single solution;
- May encode the variables so that the optimization is done with the encoded variables;
- Works with numerically generated data, experimental data, or analytical functions;

In GA, the genetic operators available to generate a new population are the reproduction, crossover and mutation. These genetic operators try to simulate the ones found in nature, introducing variations to the population gene pool and thus adapt in nature or finds the optimal solution for a problem.

With the reproduction individuals are chosen from the population, to be the parents for the new generation. There are several methods to choose the parents. This GA utilizes a tournament system where two individuals are randomly chosen from the population and the one with better fitness is selected to be a parent. This is repeated until a desired number of parents is achieved. With the parent pool created, a pair of children can be generated by selecting two parents randomly.

After creating the children, the crossover operator is used to add gene variation from the parents. In the reproduction phase, good genes are probabilistically assigned to a large number of individuals in a population, since individuals with said genes are more likely the ones that will be able to procreate. However, no new combination of genes is created this way. Using crossover, new combinations can be created, by swapping genes from the parents. To accomplish the crossover the SBX (Simulated Binary Crossover) (Deb and Bhushan Agrawal, 1995) was implemented. The use of this method is due to the continuous nature of the parameters of the optimization, instead of discrete parameters.

To further increase variations to the gene pool, mutation is also included. Although always present, the mutation operator does not influence in a significant manner, during the first iterations of the GA. In the beginning, the individuals' genes are very different from one another, caused by the first generation being composed of random parameters, therefore, the small mutations changes to the genes are negligible. During this time of the optimization, the crossover operator can cause the greatest impact on the fitness of the individuals. However, towards the end of the optimization, the crossover's influence on the fitness of the individual starts to decrease, due to the fact that by this point on the optimization, the population gene pool has already converged towards a better individual. In this situation, the mutation operator forces an individual's genes to change or mutate, which will further improve the fitness of an individual.

Fitness is a concept in optimization, which is used to rank the individuals in a generation. In algorithm implemented, the fitness is a single value variable which is calculated using the chosen metrics derived from the Darwin-OP during a run of an individual. This metrics can be the forward displacement the robot accomplish, the time it took or a more complex value such as a representation of balance.

The Genetic Algorithm can be summed up to the following pseudo-code:

```
/*GA Pseudo Code*/
for each individual in the population do
        generate random individual
end for
while the end criteria are not met do
        for each individual in the population do
                calculate the fitness
        end for
        generate parent pool by a two individuals' tournament
        while the number of individuals in the new population is less than the population number established do
                select two random parents
                generate two children by means of crossover and mutation
        end while
        check end criteria
end while
```

In this project, the fitness is characterized by more than one objective. This means that the optimal individual must be able to accomplish different objectives to achieve a good fitness. In this work, the objectives used were the displacement of the humanoid robot, its foot clearance and the number of times the gait event detector was able to correctly determine the gait state the robot was in. The calculation of this type of fitness using a single variable fitness can be accomplished by a weighted sum:

$$fitness = w_1 * objective_1 + w_2 * objective_2 + \cdots + \ w_n * objective_n$$

Although being simple to implement, it requires determining the required weights, which is normally done through trial and error. This method requires a few generations to be calculated, to check the validity of the weights being used, which can take time, this being exacerbated if the calculation of an individual's fitness is long and/or the number of individuals per generation is high. To overcome this problem one could use a stage fitness calculation.

The stage fitness calculation works by optimizing a single objective at the time, switching to the next one when some desired condition is fulfilled while maintaining the previous objectives conditions met. To limit the influence of each objective in the overall fitness and prevent an objective's fitness from interfering with the previous objectives' fitness, the objective that is being optimized in that moment is passed through a sigmoid function limiting its fitness to a range of -1 to 1. The calculation of the fitness is shown in figure 39.

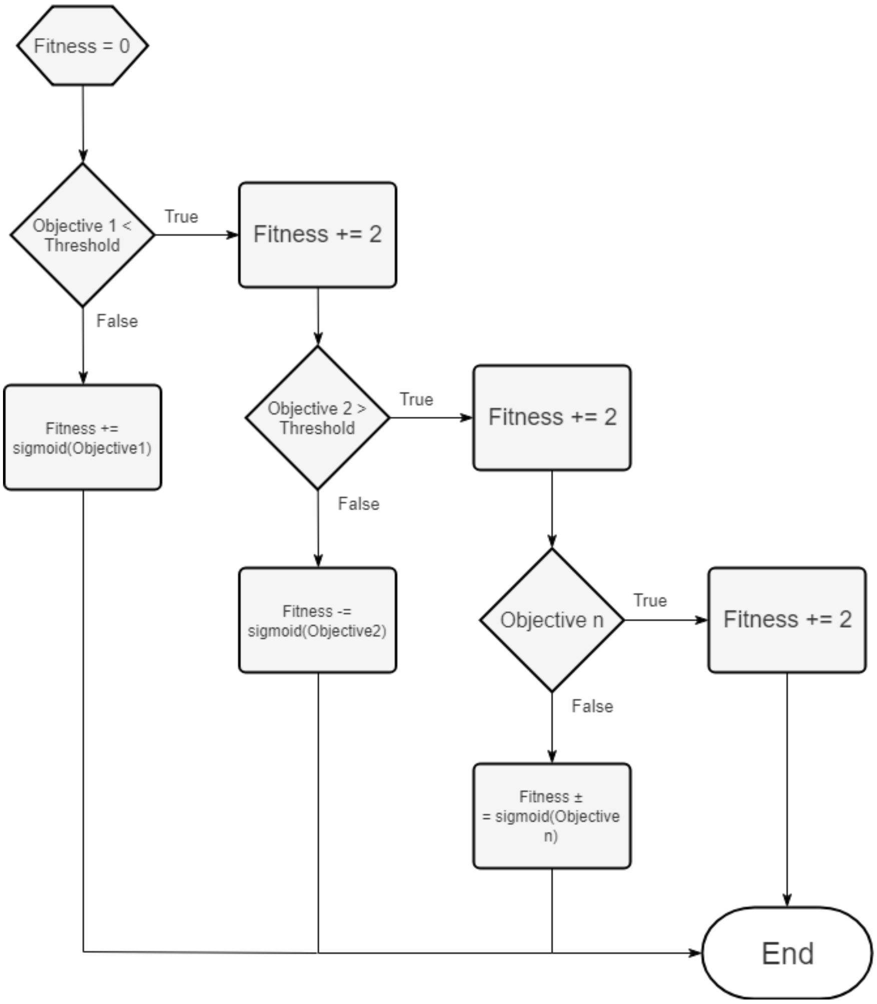

Figure 39: Staged Fitness

By using the stage GA, the optimization of the 36 parameters required for the CPG controller and the prosthesis controller was performed. This GA also incorporates in its generations an elite population, comprised of the 10 % of the generation individuals with the highest fitness. This 10 % is kept for the next generation, therefore the elite population is the best 10 % of individuals, of the optimization, until that point. Figure 40 shows the fitness mean (solid blue line), the elite fitness mean (dotted yellow line) and the fitness of the best individual (dashed red line) throughout the optimization.

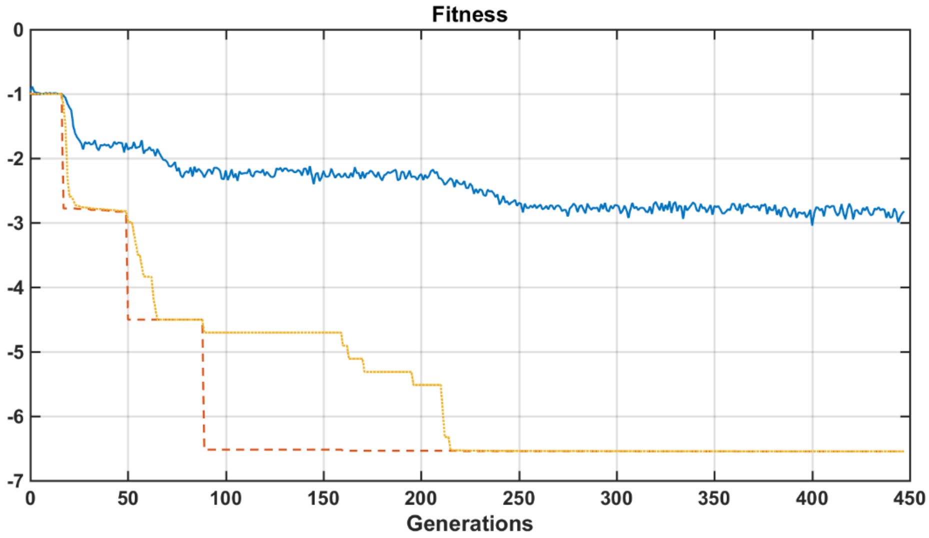

Figure 40: Fitness throughout the optimization (Solid blue line - Generation Mean; Dotted yellow line – Elite Population Mean; Dashed red line – Best Individual)

Due to the number of parameters the optimization was performed with a high maximum limit on the number of generations. The optimization, however, would be stopped if the best individual did not improve, restarting the optimization again with new random individuals. As expected throughout the optimization, the fitness (full solid blue line) would improve as the generations number keep increasing. However, since the sensibility of the humanoid controller is high (i.e. small differences on the parameters can result in big difference in the final result) and the mutation percentage of the optimization was set higher than normal, the fitness mean of the population is significantly smaller than the mean of the elite population (yellow dotted line).

Figure 41 shows the mean of the displacement from the individuals of each generation, as well as the mean displacement of the elite population and the displacement of the best individual. In this run, the chosen stage objectives were first the simulation time (time in seconds until the robot falls or reaches the max of 40.1 seconds); then the displacement (forward distance the robot has walked); followed by the foot clearance (maximum height of the prosthetic foot); and the gait event "accuracy" (number of iterations with a correct assessment of the gait phase) in the end. The stage GA optimizes one objective at a time, maintaining the previous objectives condition met and ignoring the future ones. So, in the first few generations when the specified simulation time was not yet being met, the displacement fluctuates since this objective is being ignored. When the simulation time is met, around the generation 25, the optimization of the displacement starts. This optimization (Figure 41) lasts until generation 60 when the stage GA swifts its focus to the foot clearance (Figure 42). As long as the condition set for the displacement, of 1.7 meters, is not broken, the displacement of the elite population will start to fluctuate again. The same can be observed in the other metrics' graphs shown below.

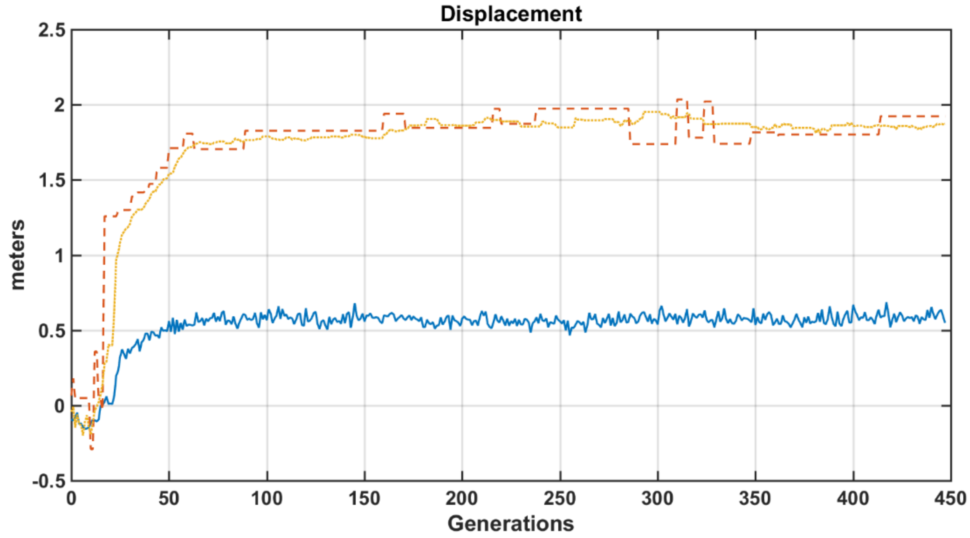

Figure 41: Displacement metric throughout the optimization (Solid blue line - Generation Mean; Dotted yellow line – Elite Population Mean; Dashed red line – Best Individual)

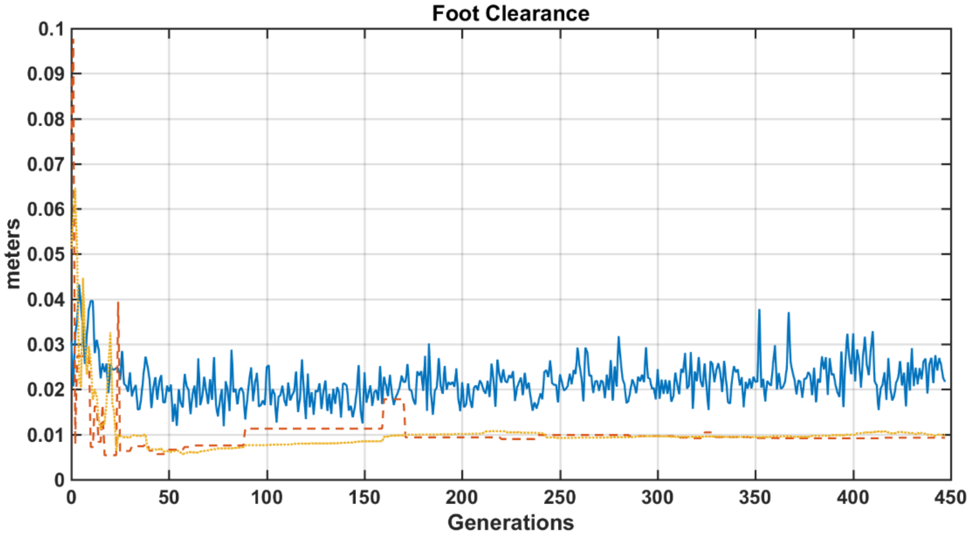

Figure 42: Foot Clearance metric throughout the optimization (Solid blue line - Generation Mean; Dotted yellow line – Elite Population Mean; Dashed red line – Best Individual)

In the foot clearance, this fluctuation is harder to see due to the nature of the of the variable being measured. The foot clearance measures the highest point reach by the prosthetic foot. During the first generations, when the simulation time is still being optimized, the robot will sometimes launch himself in the air, resulting in a high foot clearance. Similar situations occur during the next generations, as the robot falls almost immediately after starting with a high foot clearance. In this case, the condition for this objective is that the foot clearance must be higher than 0.009 meters. Since most of the individuals end up with a higher value than this, it becomes hard to see where the optimization of the foot clearance starts and finishes.

The gait event "accuracy" is the number of iterations the gait state from the prosthesis controller is correct. To classify the gait state as correct, the prosthesis controller state is compared to the state that the "healthy" individual would be in that moment. The healthy state was measured by detecting the transitions between stance and swing on a "healthy" individual with a passive right ankle roll joint. The transitions were manually detected and the corresponding value of the CPG controller' oscillator recorded. These values of the oscillators are what signals the transitions of the "healthy" individual which alters the current "healthy" gait phase. The current gait phase from the prosthesis is then compared to the current "healthy" gait phase, determining the "accuracy" of the prosthesis gait event detector. Figure 43 shows the gait event accuracy through the optimization.

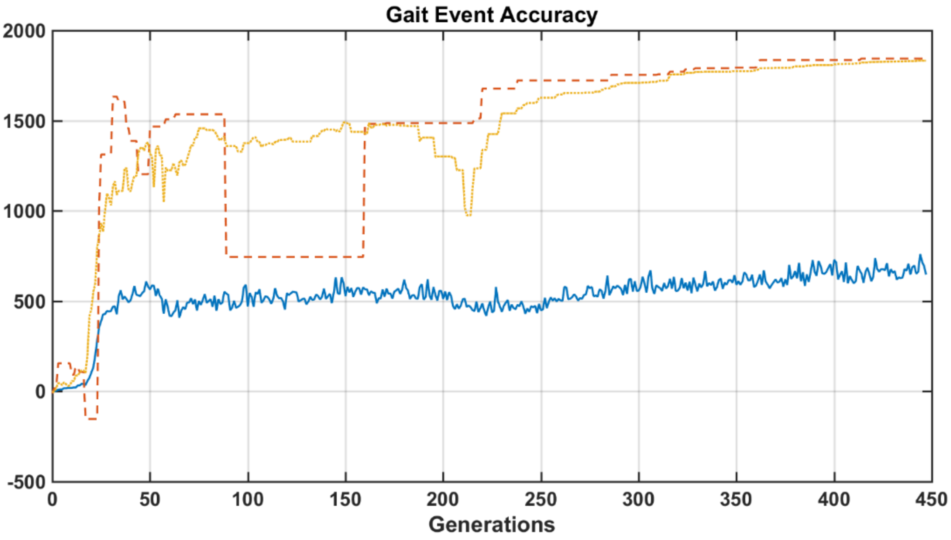

Figure 43: Gait Event Accuracy metric throughout the optimization (Solid blue line - Generation Mean; Dotted yellow line – Elite Population Mean; Dashed red line – Best Individual)

CHAPTER 5 IMPEDANCE CONTROL ON A PROSTHETIC DEVICE

The previous chapter explains the tools used to generate the human-like locomotion for the Darwin-OP robot. It also presents the optimization method employed to determine the parameters for the CPG controller and the prosthesis controller.

This chapter demonstrates the work done for the prosthetic device controller, for the simulated environment. This work involves the emulation of the prosthesis using the original Darwin-OP joints and the development of the "Simple Impedance Controller" in a state machine driven controller for the prosthetic device. For the gait motion of the robot (i.e. to control the other joints of the Darwin-OP), a CPG controller with sensor feedbacks was employed.

The chapter also includes the device model for the simulation and the hardware for the physical implementation. The chapter ends with the results and discussion of the results from the tests performed.

To test the prosthetic device, the Darwin-OP humanoid needs to be able to perform a walking motion, so that the performance of the prosthesis could be established in comparison with a "healthy" gait (i.e. a gait achieved with just a walking motion controller).

5.1 Prosthesis Controller

The overall system is composed of the humanoid robot and the prosthetic device and is controlled by two different controllers, a CPG based controller and an Impedance based controller. The CPG controller is used to provide the walking motion to the humanoid robot's joints, while the Impedance Controller, or the prosthesis controller, controls the actuation of the prosthetic device. The prosthesis controller was made to be to operate independently of the main controller, in this case, the CPG controller. The choice to make the prosthesis controller independent was made to enable an abstraction of the CPG controller in regard to the missing joints. This abstraction facilitates the yielding of control of the joints by just ignoring the controls for the same joints, from the original controller. In other words, the CPG controller will continue to calculate and provide the desired position for the joints controlled by the prosthesis, they will just be ignored.

The prosthesis controller is considered independent, meaning it does not require input or some other type of information, from the CPG controller, to operate. The CPG controller, however, requires the FSR data, originated from the prosthetic leg, for the feedback mechanisms. The FSR data from the feet is used to regulate the speed of the leg's oscillators, as well as to correct the robot's CPG controlled foot so that it can maintain a parallel orientation with the ground. To provide the necessary data to the CPG controller, in the physical prosthesis, a physical connection was established via a USB cable, from the prosthesis to the Darwin-OP humanoid robot.

In the simulation tests, the communication between the prosthesis ‘s controller and the Darwin’s controller is not needed since the prosthesis’s controller is embedded in the Darwin CPG controller.

The controller architecture designed for this prosthetic device can be divided into three different levels of control, all implemented in the same computing unit. These levels are:

- High-level : that is responsible for tracking the gait phase and providing the corresponding parameters;
- middle-level : which receives the parameters from the high level and calculates the desired torque
- low-level : that converts the desired torque to the motor control.

The low-level control, that was utilized in the simulated tests, is not the same as the low-level control present in the physical implementation of the prosthesis. The simulated tests were performed in the Webots™ simulated environment. This environment provides access to torque controlled rotational motors, which employ a PID (Proportional–Integral–Derivative) controller for the low-level control. In the physical prosthesis, simple DC (direct current) motors were used, which were in turn combined with a different low-level control.

All of the levels take in data from the prosthetic device. The high-level uses the gyroscopic values of the prosthetic foot as well as the FSR values to determine the current gait phase; the middle-level uses the ankle joint position to calculate the desired torque to be applied; and the low-level control, in the physical implementation, takes the ankle joint position and the motor position for the conversion from the desired torque to a PWM (Pulse Width Modulation) duty-cycle, for the motor control.

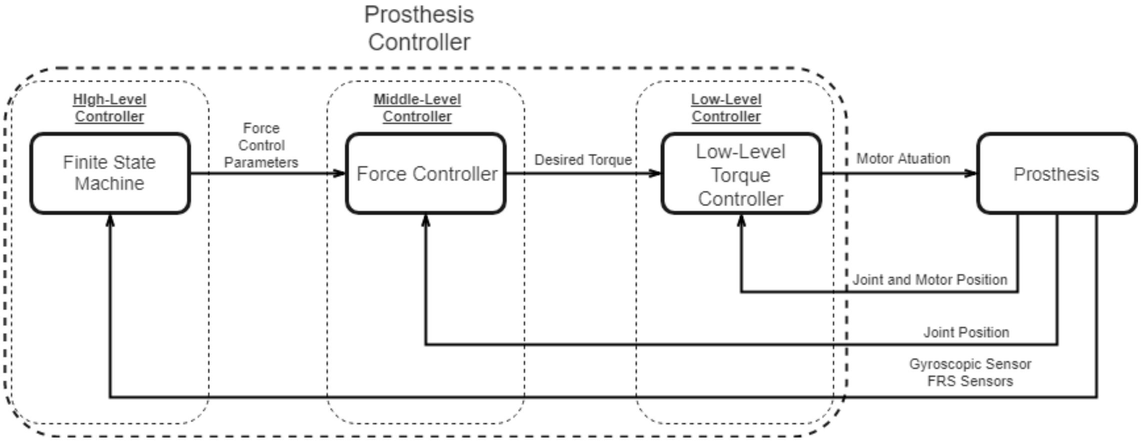

Figure 44: Control Architecture

High-Level Control

For both simulated and physical prosthesis controller, the high-level control is the same. The only difference between both systems is the values of the parameters used.

The main objective of the high-level control is to determine the phase of the gait, the humanoid robot currently is, and to pass the respective parameters to the middle-level control. To accomplish this, a finite state machine was utilized, which keeps track of the state the prosthetic foot is currently on.

In this work, the humanoid robot's feet are kept parallel to the ground during the entire gait motion. This means that, although similar, the robot's gait is different from the normal gait of humans. In a human's gait, each walking cycle can be divided into two major phases: the stance phase, when the foot is in contact with the floor, and the swing phase, when the foot is moving through the air, during the leg's forward motion. These two phases can then be further subdivided into gait sub-phases which are: load response, mid-stance, terminal stance, pre-swing, initial swing, mid-swing and terminal swing. Dividing these subdivisions are the gait events. On an average human, four gait events can be easily distinguished (Figueiredo *et al.*, 2016). This are:

- heel strike : an event that occurs with the first contact of the swinging leg the ground;
- foot-flat : when the plantar surface of the foot places on the ground so that the leading limb can take over the body weight;
- heel-off : is the moment at which the heel lifts from the ground and the push-off is initiated;
- toe-off : event corresponding to the instant of the time the foot leaves the ground, completing the stance phase and beginning the swing phase;

These phases of humans walking require the foot to constantly change its angle in relation to the ground. Since the humanoid robot's feet are kept parallel to the ground, the gait events mentioned cannot be replicated. However, even if the foot position, over the walking cycle, is not the same as a human's, the robot's feet will still experience the same main walking phases, stance and swing.

By using these two gait phases, a two-state finite machine can be designed with one state for each phase. By having just, the stance and swing phase, the gait events that are necessary to be able to detect are the foot contact, when the foot contacts the ground, starting the stance phase and the foot off when the foot leaves the ground and starts the swing phase. To detect the events, the FSR sensors and the gyroscope sensor can be used. For the detection of the contact of the foot with the ground, one could theorize that the usage of the FSR sensors would be sufficient, however, due to the foot bouncing, which occurs when the foot raises completely of the ground after starting a stance phase, relying solely on the FSRs is inadvisable. Keeping this problem in mind, to increase the reliability of the finite state machine, two intermediary states were added, one between the transition stance to swing and the other between the transition swing to stance. The two intermediary states help in decreasing the number of false positives when transitioning between stance and swing, by adding another condition with the other sensor to the transition (Figure 45).

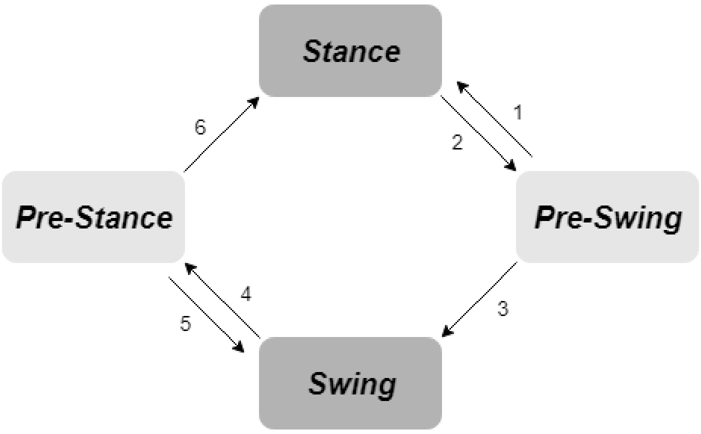

Figure 45: Finite State Machine's states

The separation of the sensors in different transitions could be ignored and just add all the transitions to a set of conditions between the main phases, stance and swing, removing the need for the two extra states. However, the existence of these states allows for easier tracking of false positives from stance and swing.

To detect the start of a swing or the beginning of stance, the gyroscope is used. Represented by the transition number 2 and 4 in figure 45, this condition checks the current foot pitch speed with a threshold. If the threshold is passed, the state changes to the Pre-Swing state or the Pre-Stance. In these states, the parameters that are passed to the middle-level control have not been yet updated. In the Pre-Swing and Pre-Stance states, the parameters from the previous state, Stance and Swing respectively, are kept. By not updating the parameters in these pre-states, they act as confirmation of the transition before changing to the other main state, through the transitions number 3 and 6. In the case of these transitions, the FSR sensors are the ones that confirm the transition by also checking a threshold. For this condition, the outputs of the four FSR sensors in the prosthetic foot are added. Using the sum of the FSR sensors for the condition, allows for an assurance of the full contact of the four sensors with the ground or no contact from any of them, therefore, confirming that the gait phase has truly changed.

In this finite state machine, the gyroscope was chosen for the main state trigger, which signals that a possible gait phase has happened, and the FSR sensors were chosen for the confirmation, which detects if the gait phase change really occurred. This confirmation can be questioned since, if the gait phases that are represented, are just stance and swing, why not just use the FSR sensors? To justify the use of this configuration, it was mentioned previously that the use of the gyroscope can help the reliability of the state machine, by helping to ignore the foot bouncing. In addition to this, during the optimization of the controller, the gyroscope in the current configuration provided a faster method for improvement of the robot's walking motion than just using the FSR sensors.

The following table, Table VII, shows the conditions present in the high-level control of the finite state machine, for each transition. The next table, Table VIII, describes the parameters involved in the transitions.

TABLE VII CONDITIONS TABLE

Number	Condition
1	GE_Counter > pr_swing_UC
2	Gyro_yy < gyro_LT
3	FSR_total < FSR_t && GE_Counter < pr_swing_LC
4	Gyro_yy > gyro_UT
5	GE_Counter > pr_stance_UC
6	FSR_total > FSR_t && GE_Counter < pr_stance_LC

TABLE VIII GAIT EVENT PARAMETERS

Variable	Description
GE_Counter	Number of cycles it's been on the current state
Gyro_yy	Foot Pitch speed
FSR_total	Sum of the 4 FSRs
pr_swing_UC	Upper Threshold for the Pre-Swing Counter
pr_swing_LC	Lower Threshold for the Pre-Swing Counter
gyro_UT	Upper Threshold for the gyroscope
gyro_LT	Lower Threshold for the gyroscope
FSR_t	Threshold for the FSR sum
pr_stance_UC	Upper Threshold for the Pre-Stance Counter
pr_stance_LC	Lower Threshold for the Pre-Stance Counter

Middle-Level Control

The same way as the high-level control, the middle-level control is the same in both simulated and real environments, differing only in the values of the parameters involved in each scenario.

For the middle-level control, the main objective is to utilize the parameters received from the high-level control and calculate the desired torque reference, which will then be given to the low-level control. To calculate the joint torque, the middle-level control implementation is based on the notion of impedance control proposed by Hogan. By having the joint torque of the prosthetic ankle described by a passive spring and damper with a fixed equilibrium point, the desired ankle torque could be given by:

$$\tau = K_i(\theta - \theta_{di}) + B_i\dot{\theta} \tag{5.1}$$

Where K_i, B_i and θ_{di} denote the linear stiffness, damping coefficient and equilibrium point, for the i^{th} state (Stance or Swing).

The impedance control shown here describes a passive spring and damper, however, the prosthetic device can still be considered active, as the prosthetic joint is able to provide mechanical energy to the humanoid robot. This energy comes from the switching between appropriate equilibrium points during the transitions between states. In this manner, the prosthesis is guaranteed to be passive within each state but is able to generate power during the switching of states.

The following tables showcase the values received from the high-level control and used by the middle-level control in the simulated environment and the real environment:

TABLE IX IMPEDANCE CONTROLLER PARAMETERS (SIMULATED ENVIRONMENT)

	K	$\boldsymbol{\theta_d}$	B
Stance	2.0415615	0.000985	-0.2347297
Swing	0.0	18.0396198	-0.3864996

Low-Level Control

The low-level control is the only portion of the overall prosthesis controller that is not the same, when regarding the simulated and the physical environments. The simulated tests were performed in the Webots™ simulation environment. In this environment, the prosthetic device, emulated by using the existing ankle and foot joints of the Darwin-OP robot, employed rotational motors that are controlled by torque. This way, the desired torque can be directly applied to the motor, which then employs a PID controller for the simulated low-level control. In the case of the physical environment, the motor is not torque controlled directly. The physical prosthesis uses regular DC motors with no additional hardware, meaning that the low-level needed to be implemented. For this implementation, the torque control used in the simulation tests was opted out, being replaced by motor velocity control. The substitution was made due to the fact that, series elastic actuators with a drive running in velocity mode typically have lower actuation impedance and smoother torque tracking with lower errors (Zhang, Chien Chern and Collins, 2016). The desired motor velocity can be calculated as:

$$\begin{aligned}\dot{\theta}_{m,des} &= \frac{1}{T} \cdot \Delta\theta_{m,des} \\ &= \frac{N}{T} \cdot \Delta\theta_{p,des}\end{aligned} \tag{5.2}$$

where $\dot{\theta}_{m,des}$ is the commanded motor velocity, T is a gain related to rise time, $\Delta\theta_{m,des}$ is desired change in motor position, N is the motor gear ratio, and $\Delta\theta_{p,des}$ is desired change in pulley position, determined by the low-level torque controllers described below. The value of T was tuned so as to minimize motor position rise time without causing oscillations during torque tracking.

The low-level torque control that handles the calculation of the desired motor position change is the proportional control with damping injection. This controller is analogous to the classical proportional-derivative control of torque, with pulley velocity taking the place of the derivative term and providing the damping injection. The controller can be expressed by:

$$\Delta\theta_{p,des} = -K_p \cdot e_\tau - K_d \cdot \dot{\theta}_p \tag{5.3}$$

Where K_p is a proportional gain, $e_\tau = \tau - \tau_{des}$ is torque error, τ is measured torque, τ_{des} is desired torque received from the middle-level control, K_d is a damping gain, and $\dot{\theta}_p$ is the measured velocity of the motor pulley.

The damping term is more effective than the term with the derivative of torque error in this controller since the measurement of the pulley position is less prone to errors as it is done by an encoder. The damping was also place on the motor pulley rather than the prosthetic joint due to the fact that it being less effective when using the prosthetic joint (Zhang, Chien Chern and Collins, 2016).

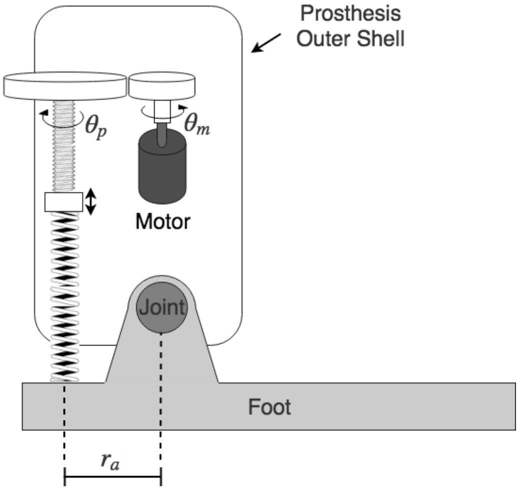

Figure 46: Prosthesis Actuator Diagram

On the low-level torque controller, the measurement of the torque that is being applied to the prosthetic joint is required. This measurement can be performed directly using torque sensors or indirectly measuring the variables related to the torque being applied. In this work, the method chosen for the measurement was to use encoders to measure the ankle joint and the motor positions and use them to estimate the torque on the joint. By using the following force-position relationship, one can estimate the force the springs are applying:

$$F = K_c\left(r_p\theta_p - r_a\theta_e\right) \tag{5.4}$$

In which K_c is the total effective stiffness of the springs and θ_p and θ_e are the pulley and the device joint relative to an initial position. While r_a is the distance from the actuation point, where the springs force is applied, to the joint and it is used to calculate the angular displacement, r_p is the pitch of the screw and it is used to calculate the linear displaced caused by the pulley rotation.

With the force-position relationship, the torque-angle relationship can be determined. Starting by the defining R as the gear ratio of the transmission and expressed by:

$$R = \frac{r_a}{r_p} \tag{5.5}$$

The torque applied by the device can be written as:

$$\begin{aligned} \tau &= F \cdot r_a \\ &= r_a \cdot r_p \cdot K_c \left(\theta p - \frac{r_a}{r_p} \theta_e \right) \\ &= K_t \left(\theta p - \frac{r_a}{r_p} \theta_e \right) \end{aligned} \tag{5.6}$$

With the transmission stiffness K_t defined as:

$$K_t = r_a \cdot r_p \cdot K_c \tag{5.7}$$

Relating the torque being applied to the angles of the angles of the motor pulley and the device joint.

After obtaining the desired motor velocity to be, the input motor voltage V_a needs to be calculated. In (Zhang, Chien Chern and Collins, 2016)the relationship between inputs voltage and actual motor velocity was derived from the motor dynamics equations:

$$\begin{cases} K_a \cdot i_a(t) = I_e \cdot N \cdot \ddot{\theta}_p(t) + fe \cdot N \cdot \dot{\theta}_p(t) \cdot \dfrac{1}{N} \cdot \tau_0(t) \\ V_a(t) = R_a \cdot i_a(t) + K_b \cdot N \cdot \dot{\theta}_p(t) \end{cases} \tag{5.8}$$

in which K_a is the motor-torque constant, i_a is the armature current, I_e is the effective moment of inertia of the motor and gear referred to the motor shaft, $N = \frac{\dot{\theta}_m}{\dot{\theta}_p}$ is the gear ratio, θ_m is the angular position of the motor shaft, θ_p is the angular position of the gear output shaft, fe is the effective viscous friction coefficient of the combined motor and gear referred to the motor shaft, to is output torque at the gear output pulley, V_a is the armature voltage, R_a is the armature resistance, and K_b is the motor voltage constant.

From the motor dynamics equations, one has:

$$\begin{aligned} V_a &= \frac{R_a I_e N}{K_a} \ddot{\theta}_p + \left(\frac{R_a f_e N}{K_a} + K_b N \right) \dot{\theta}_p + \frac{R_a}{K_a} \tau_0 \\ &= \frac{R_a I_e}{K_a} \ddot{\theta}_m + \left(\frac{R_a f_e}{K_a} + K_b \right) \dot{\theta}_m + \frac{R_a}{K_a} \tau_0 \end{aligned} \tag{5.9}$$

When the angular acceleration is zero, this reduces to:

$$V_a = \left(\frac{R_a f_e}{K_a} + K_b \right) \dot{\theta}_m + \frac{R_a}{K_a} \tau_0 \tag{5.10}$$

At moderate torque and speeds, the contribution of the armature resistance to the voltage drop is negligible, ignoring this term:

$$V_a = \left(\frac{R_a f_e}{K_a} + K_b \right) \dot{\theta}_m \tag{5.11}$$

Which relates the motor input voltage with the motor velocity linearly at low torque and high speed.

5.2 Prosthesis Design

The previous section focused on the presentation of the controllers implemented in this work. It gave an overview of the CPG based controller used to generate the motions for the joints for the “healthy” individual and the joints not controlled by the prosthesis, for the individual using the prosthetic device. It also shows how the prosthesis controller is designed, indicating the different levels of control present and how they are connected. The previous chapter ends with the reason for the addition of the DOF provided by the ankle roll, that was added to the prosthesis and why it was made passive.

In this section, the simulated model for the robot that was used to test the prosthesis is showcased, in conjunction with an overview of the prosthesis develop by Joana Alves for the humanoid robot. This section indicates how the prosthesis is connected to the robot and the possible constraints that needed to be considered. This section is also where the implementation of the hardware which was developed for the physical prosthesis, is presented. In here, it is shown how the electronics are connected and how they interact with each other to achieve the desired behavior. The chapter ends with the test methodology for the prosthesis tests and the results for the manual tests on the prototype.

In this section, the simulated Darwin-OP model is presented first, followed by an overview of the develop prosthesis. The section continues with the implementation of the necessary hardware for the physical tests and ends with the section for the test methodology.

5.2.1 Simulated Darwin-OP Amputee Model

To test the prosthesis prototype, a humanoid robot that was able to perform a gait motion similar to a human’s, was necessary. For this purpose, the robot Darwin-OP was chosen. Develop and manufactured by Robotis, a Korean robot manufacturer, its main purpose is research and so, it is equipped with advanced computing power, sophisticated sensors, high payload capacity and dynamic motion abilities. The Darwin-OP has 20 DOFs, each controlled by a servo motor and able to be independently actuated. Of these 20 DOFs, 12 of them are for the legs, each having six. The six DOFs of each leg can be divided as such: three of them are for the hip (hip pitch, hip roll and hip yaw), one for the knee (knee pitch) and two for ankle or foot (ankle pitch and ankle roll).

The prosthetic device was designed to substitute the ankle pitch of a leg. As such the right foot was removed from the Darwin-OP robot, which removes the ankle pitch from its gait motion controller. Due to the location of the ankle roll joint, situated physically near the ankle pitch, and to avoid relocating the actuator to a different location on the robot, the ankle roll joint also had to be removed from the gait controller.

The figure 47 shows a representation of the prosthetic device mounted in the Darwin-OP, in the Webots simulated environment. The section of the leg under the knee joint was removed and replaced with the prosthesis model. This model, as it is the case for most prosthetic devices, was designed to perform, ideally, exactly the same way as the part of the body it replaces. As such, and to simplify the communication and the development of the controller for the prosthesis, this model was not used. The prosthesis was emulated, by just removing the control of the ankle pitch and ankle roll joint, from the CPG controller and control these joints using the impedance control from the prosthesis controller. The changes required to do this were made in software, without the need for any model wise changes to the simulated robot.

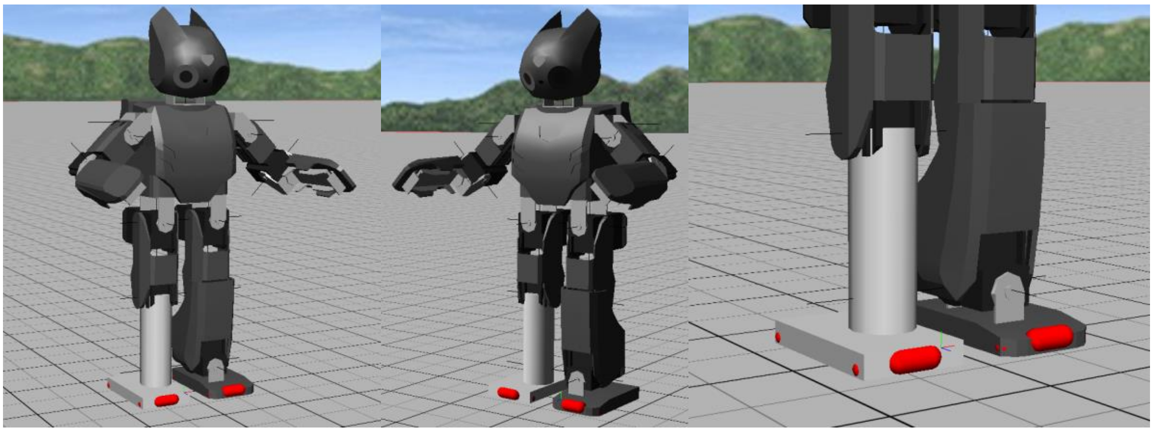

Figure 47: Simulated Amputee Model Representation

Figure 48 shows the model used in during the development and tests of the prosthesis. In the model, the green section of the robot is what is controlled by the prosthesis controller and it encompasses the ankle pitch and ankle roll for the right leg.

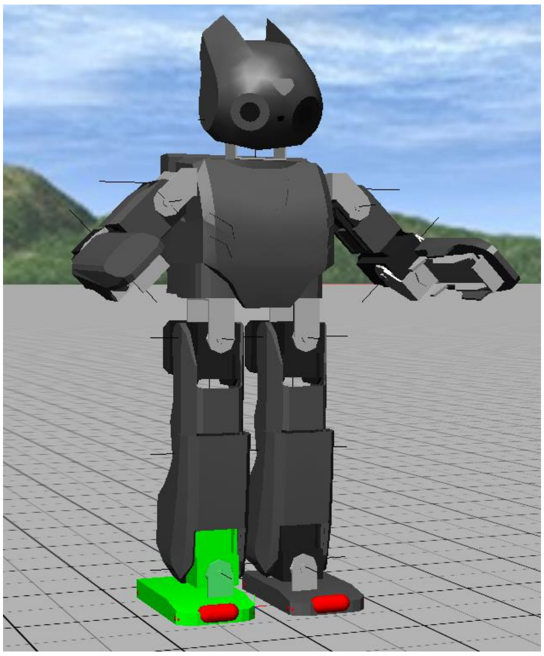

Figure 48: Simulated Amputee Model Used

5.2.2 Physical Prosthetic Device Overview

While in the simulation tests, the prosthesis was emulated using the Darwin-OP existing joints, for the physical tests, a prosthesis prototype was built and instrumented. The prosthetic device that was used in the tests with a humanoid robot was designed by Joana Alves in (Alves, 2017). In her work, Alves presented a design for a transtibial prosthetic device for a human user, as well as the reduced scale prosthesis model for a biped robot, employed in this work.

The human's prosthesis was based on a prosthesis developed by Herr (2012) at MIT (Massachusetts Institute of Technology). This ankle-foot prosthesis had one DOF and consisted of a lower foot structure, which was considered the passive component providing shock absorption, and the ankle joint mechanism, which was the active component. The prosthesis would then have an upper leg shank topped with a pyramid fixture for attaching the prosthetic device to the amputee's socket (Figure 49).

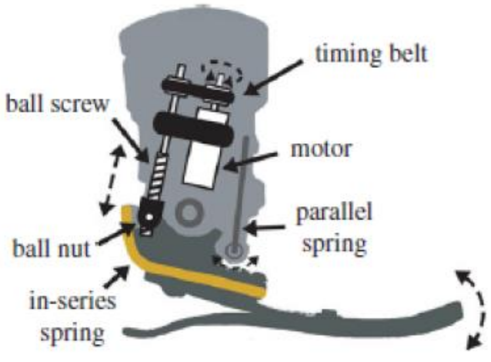

Figure 49: Diagram of the drive train (Herr and Grabowski, 2012)

Summing up, the mechanism for the ankle joint works the following way. The motion starts at the motor when this is activated by a control command. The motor's rotary motion is then converted into a linear motion through the drive train transmission (ball screw and belt drive) with a defined reduction ration. The consequent ball screw's rotary motion leads to the linear motion (up and down) of the ball nut, which in return causes the in-series spring to compress or extend, actuating the joint. With the design of the prosthesis from figure 49, Joana Alves designed the following prosthesis (Figure 50).

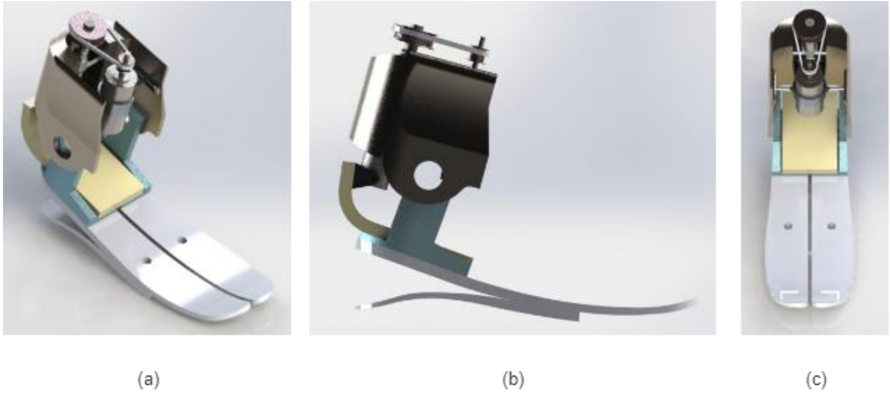

Figure 50: Prosthesis CAD Model from different angles (Alves, 2017)

Since the project is in an early stage, this prosthesis's tests could not be considered for a human amputee. Thus, the construction of the prosthesis on a smaller scale was necessary, in order to study the model without any constraints.

Developed specifically for the Darwin-OP robot, this smaller size prosthesis was designed to be about 30% of the scale of the one design to be worn by a human amputee. For the reduction, some modifications needed to be performed. These modifications were made to facilitate the connection with the robot's leg, facilitate the integration with the necessary sensors, mainly the encoders, and to modify the in-series spring to allow for a double spring system.

The initial design for the prosthesis for the humanoid robot, only foresaw minor changes to the original prosthesis design, as the figure 51 shows. These changes done were only those needed to accommodate the smaller size of the new prosthesis.

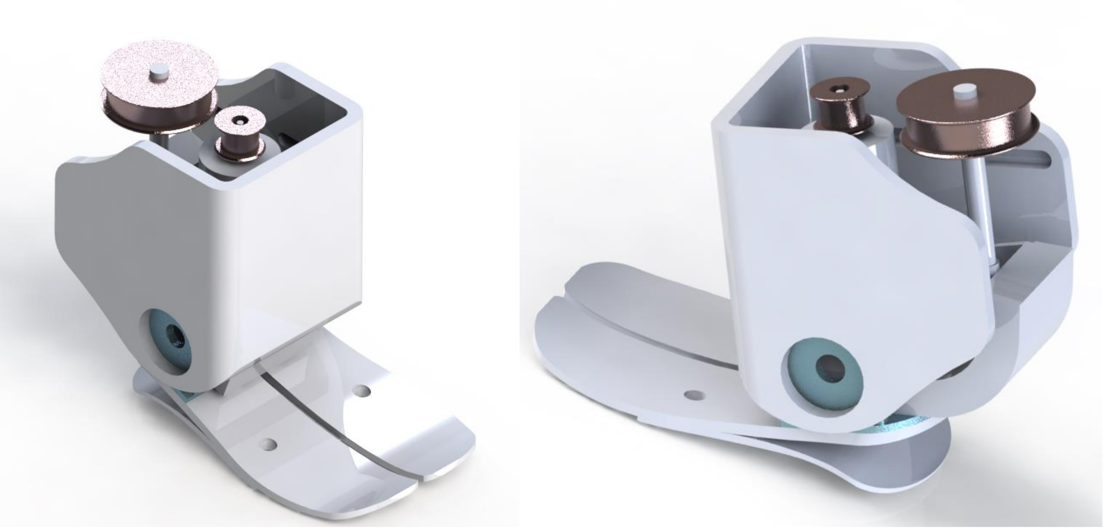

Figure 51: Darwin-OP Prosthesis CAD Model from different angles (Alves, 2017)

After the necessary modifications mentioned above, the prosthesis became:

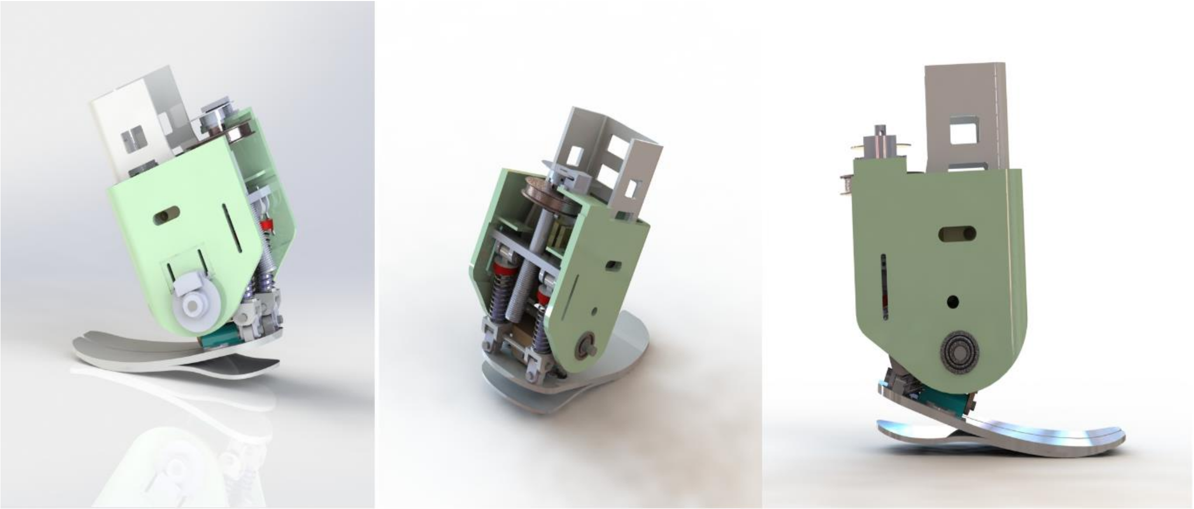

Figure 52: Darwin-OP Prosthesis CAD Model from different angles with the modification

5.2.3 Passive Ankle Roll

When using the prosthesis, the humanoid robot loses the control of two DOFs from a leg. This DOFs correspond to the robot's ankle pitch and foot roll joints. The prosthesis controller only handles the control of the ankle pitch, which leaves the foot roll DOF without control. To address this, in the first tests on the simulated prosthetic device, the foot roll joint was locked to the initial value of 0 degrees, from the "healthy" (i.e. robot fully CPG controlled) parameters, throughout the entire gait cycle. Through optimization, it became clear that the foot roll was necessary for a proper walking motion. To keep from increasing the complexity of the physical prosthesis, the foot roll DOF was turned into a passive joint. In the simulated tests, this passive joint was controlled with an impedance controller, equal to the one used for the prosthetic ankle pitch, with constant parameters through the entirety of the walking test. For the physical test, the prosthesis needs to first undergo modifications as it originally did not include the foot roll joint, and it is actuated with a spring

5.2.4 Hardware Implementation

With the prosthesis prototype designed and built, the attention switched to the electronic hardware. The prototype needed to be fitted with electronic components to operate the prosthesis. The electronic components required were the sensors to measure the foot force, foot angular speeds and angular position. It also required a motor for the actuator and a motor controller to power it. To control the sensors and actuate the motor, the prototype needed to use a microcontroller. An SD card Reader was also added to allow for the storage of the prosthesis data generated during the trials. For the acquisition, process and storage of information, as well as, the actuation of the prosthesis, the following hardware needed to be procured:

- 4 Small FSRs
- 1 IMU sensor
- 2 Encoders
- 1 Motor
- 1 Motor Driver Board
- 1 Microcontroller
- 1 SD Card Reader

For the IMU sensor, the MPU 6050 was chosen, for its cheap price and widespread use, which facilitates its use in the development. For the encoders, an Optical Incremental Encoder from BROADCOM was used, with 500 CPR (Count per Revolution), which allows for an accurate measurement of the motor and joint positions. The motor driver, L298N, was chosen due to it being a common PWM motor controller. The microcontroller needed to be small in size and be fast, computational wise, to be able to read all the sensors and calculate the necessary PWM to provide to the motor. With these requirements, the STM NUCLEO, STMF303K8, was selected, which provides a 72 MHz, 32 bits ARM processor and a variety of peripherals on a 50 by 18 millimeters package. From the peripherals, the prototype used the ADCs, some timers in Encoder Mode (uses the timer to keep track of the pulses and their order to increase or decrease the encoder count on a hardware level) and the SPI and I2C peripherals for communication with the card reader and the IMU, respectively. The selection of the motor required the necessary characteristics to be determined, first.

To start determining the desired motor properties, first, it is necessary to measure the output peak torque for the “healthy” individual, which is around 1.35 Nm. With the peak torque and knowing the moment arm of the screw (distance between the ankle joint and the transmission mechanism), the force applied by the screw can be calculated as follows:

$$F = \frac{T_a}{r_s}$$

Where T_a is the torque at the ankle joint and r_s the moment arm. If, as it is in this case, T_a is equal to 1.35 Nm, and r_s is 0.0295 m, F is equal to 45.76N.

The drive torque, for when rotation is converted into linear motion, can be calculated from the following formula:

$$T_d = \frac{Fl}{2\pi\eta} \times 10^{-3}$$

Where T_d represents the driving torque (Nm), F the axial load (N), l the screw lead (mm) and η the average efficiency for a worm screw. By using the calculated F value, l as 1mm and η as 90%, T_d is equal to 8.093 mN·m.

To determine the required peak torque of the motor, the transmission ratio, R, is used with T_d in:

$$T_{motor} = \frac{T_d R}{\eta_{timing\ belt}}$$

Using the transmission ration of $\frac{11.14}{30.54}$ and the timing belt efficiency of 90%, the required output peak torque for the motor is 3.28 mN·m.

To comply with the maximum dimensions, impose for the motor, which was derived by the design of the prosthesis, the motor chosen was the Canon Brushed DC Motor with 2.45 mN·m of peak torque and 6800 rpm of maximum velocity. As it is clear to see the motor torque is smaller than the peak torque calculated before. This is not a problem since the gait of the robot is slowed when it is using the prosthesis, reducing the maximum required speed and torque for the prosthesis.

Figure 53 showcases the hardware acquired for the implementation of the controller for the prosthesis.

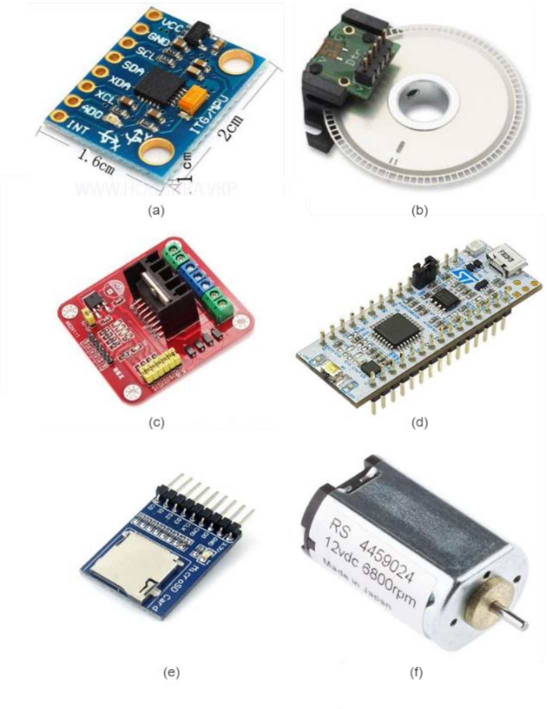

Figure 53: Required Hardware: (a) MPU 6050; (b) Incremental Encoder; (c) Motor Driver L298N; (d) STM32F303K8 Nucleo; (e) SD Card Reader; (f) Motor

With the components selected, the assembly of the prosthesis controller could begin. The same way as the simulated version, this prototype collects sensory data from four FSR sensors on the prosthetic foot, as well as a gyroscope also situated on the foot. The FSRs, the gyroscope and the encoder located at the joint comprise the sensors needed for the prosthesis controller to operate as in the simulated tests. The second encoder is used to measure the motor's angular position and, in conjunction with the joint's angular position, estimate the torque that is being applied at that moment. The torque estimation is used in the implementation of the low-level torque controller, as a replacement for a torque sensor. The sensory data provided by the sensors is then collected and processed by the microcontroller which, after calculating the torque to be applied, converts it to a PWM signal. This signal is supplied to the motor driver that is responsible for directly powering the actuator motor, and by doing so, altering the impedance of the prosthetic joint.

For the storage of the data from the sensors and the torque, estimations gather throughout the trial, the prosthesis controller employs an SD card reader, which stores the data on a micro SD card.

The prosthesis is also connected to the computer on the Darwin-OP robot, via a USB cable. This connection provided a mean for the controller to give the prosthetic foot FSR values to the Darwin-OP controller for its the feedback mechanisms. Although the prototype uses a USB cable, the communication between the two controllers is done using the UART (Universal Asynchronous Receiver/Transmitter) protocol.

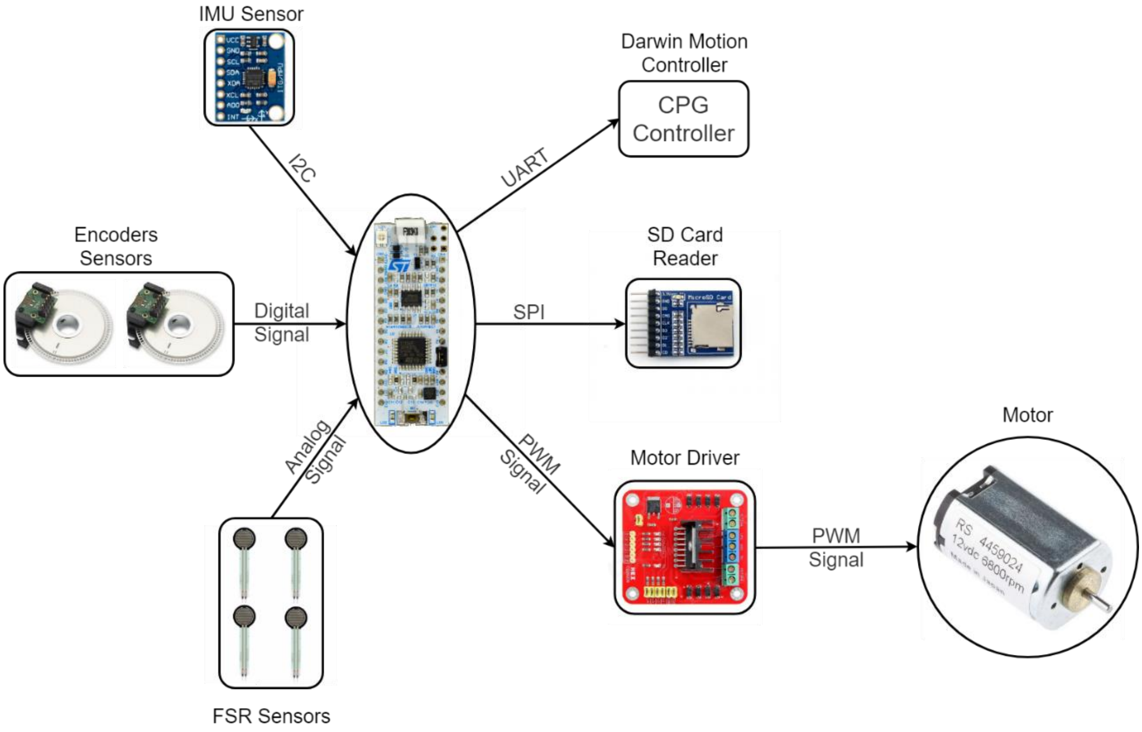

Figure 54: Communication Diagram

To properly connect all of the components, three different circuit boards were created. The choice for distributing the components connections between three boards instead of having one single board was to simplify the design of said boards. The design of a board which connects to a few sensors and another board is simpler and can be made more compact than one board responsible for handling all of the sensors and actuators.

Two of the boards that were designed and built, connect directly to the microcontroller and act as shields (Figure 55(a) and Figure 55(c)), while the other board handles the sensors of the prosthetic foot (Figure 55(b)), the FSRs and the gyroscope. From the two that connect directly to the microcontroller, one handles the encoders and the motor actuation, while the other is in charge of the SD Card Reader and the provide a, easier connection to the foot's circuit board. The circuitry of each board is shown in figure 55.

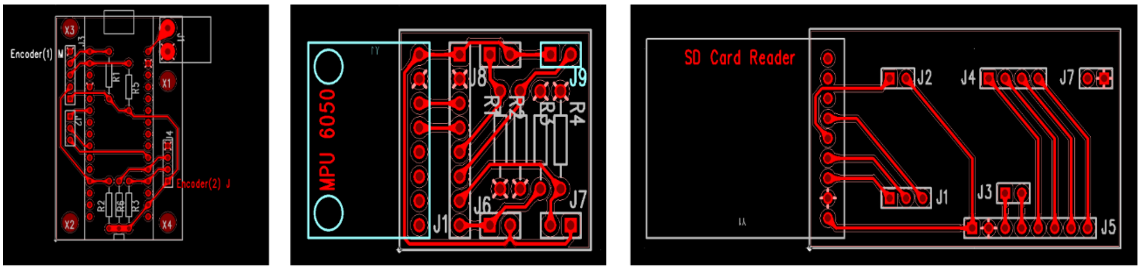

(a) (b) (c)

Figure 55: Circuit Boards: (a) Bottom Shield – Connects the encoders and the motor driver to the STM board; (b) Foot Board – Connects the IMU and the FSRs to the Top Shield; (c) Top Shield – Connects the Foot Board and the SD card to the STM board

5.2.5 Prosthesis Prototype Test Methodology

To test the physical prosthesis prototype, a different set of tests, from the simulation ones, needed to be performed. The different tests center on testing the performance of the prototype and its influence on the Darwin-OP humanoid robot.

To compare the “healthy” humanoid and the humanoid using the prosthesis, the same metrics were used. These are the trajectories and the FSR values from each foot during the entire gait. Since these metrics are measured internally by the Darwin-OP robot and the prosthesis prototype, this test can be performed by simply letting the robot walk with and without the prosthesis.

To test the prosthesis prototype itself, two situations were considered, the prosthesis by itself and the prosthesis while being worn by the robot. With these two situations, it is possible to test the controller and the prosthesis hardware isolated and test the Darwin-OP’s gait impact on the prosthesis controller. The controller test was done manually and perform to check how well the controller and the prosthesis hardware work together. The results of this test are present in this chapter, bellow, while the results of the prosthesis impact on the robot’s gait are presented in the results chapters.

5.3 Results and Discussion

The previous section focused on the prosthetic device and its controller, for the simulated and physical environments. The section showed how the prosthesis was connected to the humanoid robot for the simulated tests and physical ones, also mentioning that the in the simulated tests the simulated prosthesis representation was not used, being replaced by an emulated prosthesis implemented using the existing Darwin-OP joints. The controller for the emulated prosthesis was integrated with the controller for the Darwin-OP robot, in other words, in the simulated tests, the Darwin-Op controller was also responsible for the actuation of the prosthesis. A “Simple Impedance Controller” was used for the prosthesis controller, with its parameters controlled by a finite state machine with two states, corresponding to the main gait phases of Stance and Swing. For the humanoid robot, a CPG controller with a feedback mechanism was chosen. The feedback mechanism is able to increase or decrease the speed of the oscillators and correct the ankle pitch and foot roll to ensure the foot is parallel to the ground during the gait, as well as to correct the robot's turning direction to help the robot to move forward. The chapter ends with the reasoning behind the addition of the foot roll joint to the prosthesis and the choice of having it be passive.

In this section, the work discussed is centered on the results from the prosthesis tests. It discusses results taken from the healthy individual and the individual with the prosthesis, comparing the two of them. This section also discusses the performance of the prosthesis controller and its ability to detect the transitions.

5.3.1 Simulation Results

The results from the Darwin wearing the prosthesis need to be compared to the ones from the healthy Darwin humanoid.

"Healthy" Individual

The simulation tests were performed using the Webots ™ simulation environment Using this environment, the humanoid robot, Darwin-OP, is simulated having its joins controlled by the CPG controller.

When developing a prosthetic device, its final behavior should be compared to a healthy individual, since the objective of the prosthesis is to perform the same way or even outperform its counterpart healthy limb, by generating a natural movement. For this reason, a healthy individual is needed to give a baseline that can be compared to the humanoid robot with the prosthetic device.

The "healthy" individual, in this work, is the humanoid robot controlled solely with the CPG controller and the CPG parameters from before the optimization. These parameters (Table X) were derived from previous works which incorporated the humanoid robot, Darwin-OP, and the same CPG controller (Matos and Santos, 2012; Oliveira, 2012; André, Santos and Costa, 2016) and was able to demonstrate stable forward walking.

TABLE X CPGS PARAMETERS FOR THE WALKING MOTION (SIMULATED)

Name	Value
Amplitudes	
Balancing Hip Roll	14.0
Balancing Ankle Roll	14.0
Flexion Hip	15.0
Flexion Knee	30.0

Flexion Ankle Hip	15.0
Flexion Ankle Knee	30.0
Stance Flexion Knee	0.0
Stance Flexion Ankle	0.0
Pelvis Rotation	0.0
Compass Hip	11.0
Compass Ankle	11.0
Offsets	
Offset Hip Yaw	0.0
Offset Hip Roll	1.5
Offset Hip Pitch	-25.0
Offset Knee Pitch	40.0
Offset Ankle Pitch	20.0
Offset Ankle Roll	-1.5
Feedback Mechanisms	
FSR feedback weight	0.005
Ankle Pitch Correction	0.0025
Ankle Roll Correction	0.005
Turn Correction	4.0

To test the base performance of the “healthy individual, data was collected, which shows the joints trajectories, the foot clearance and the FSR values for each foot and the COM motion throughout the simulation run. This data can then be used for the comparison with the individual with the prosthesis, and the assessment of the impact the prosthetic device has on the gait of the humanoid robot.

The figure 56 and 57 show the angles of the joints of the left and right leg, throughout the gait cycle. The first three graphs from both figures are the joint angles of the hip roll, foot roll, and hip pitch respectively, while the second set of three graphs are the knee pitch, ankle pitch and hip yaw respectively. In these figures, is clear to see that, the CPG controller is able to provide simple curves for the joints position references, such as the ones for the roll joint and the hip yaw, as well generate more complex curves for the pitch joints.

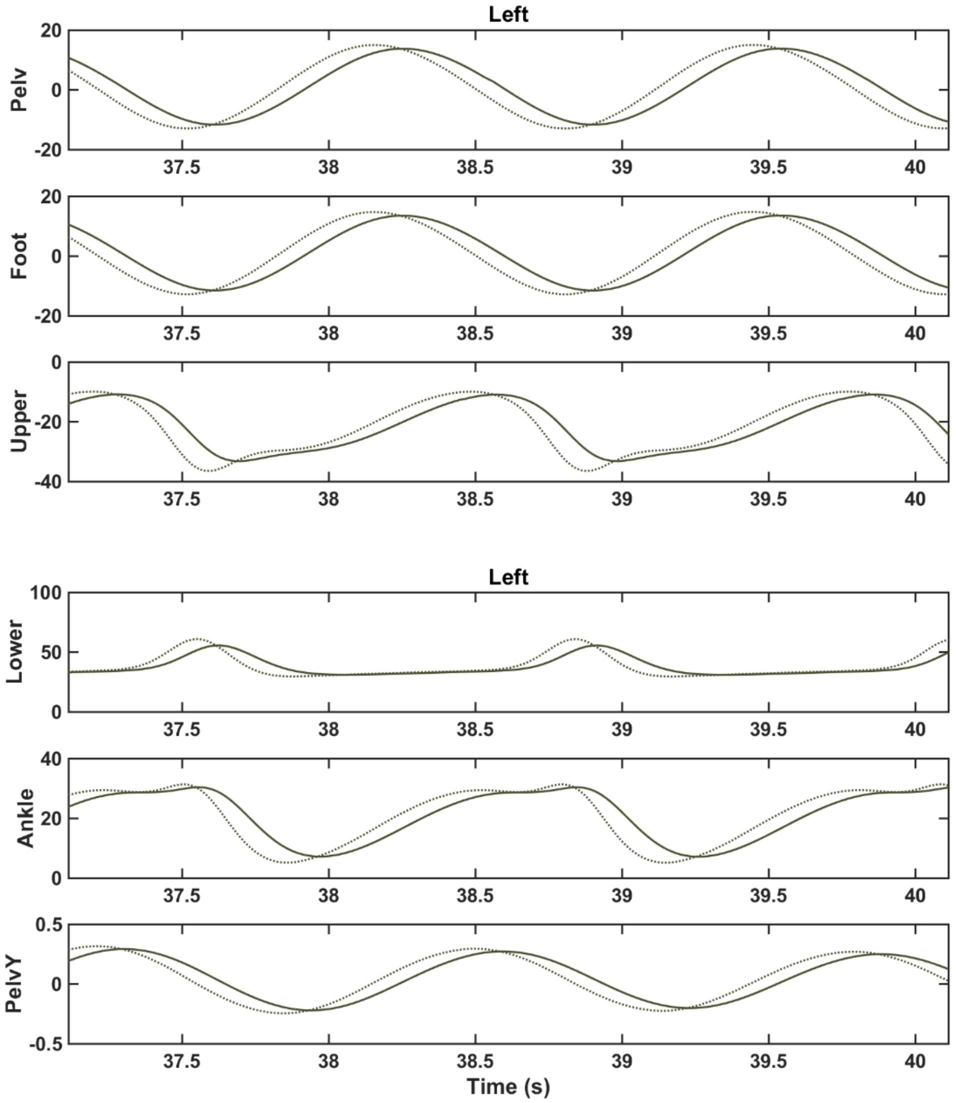

Figure 56: "Healthy" Left Leg (From top to bottom – Hip Roll, Foot Roll, Hip Pitch, Knee Pitch, Ankle Pitch, Hip Yaw) (Dotted line – Desired Joint Position; Solid line – Real Joint Position)

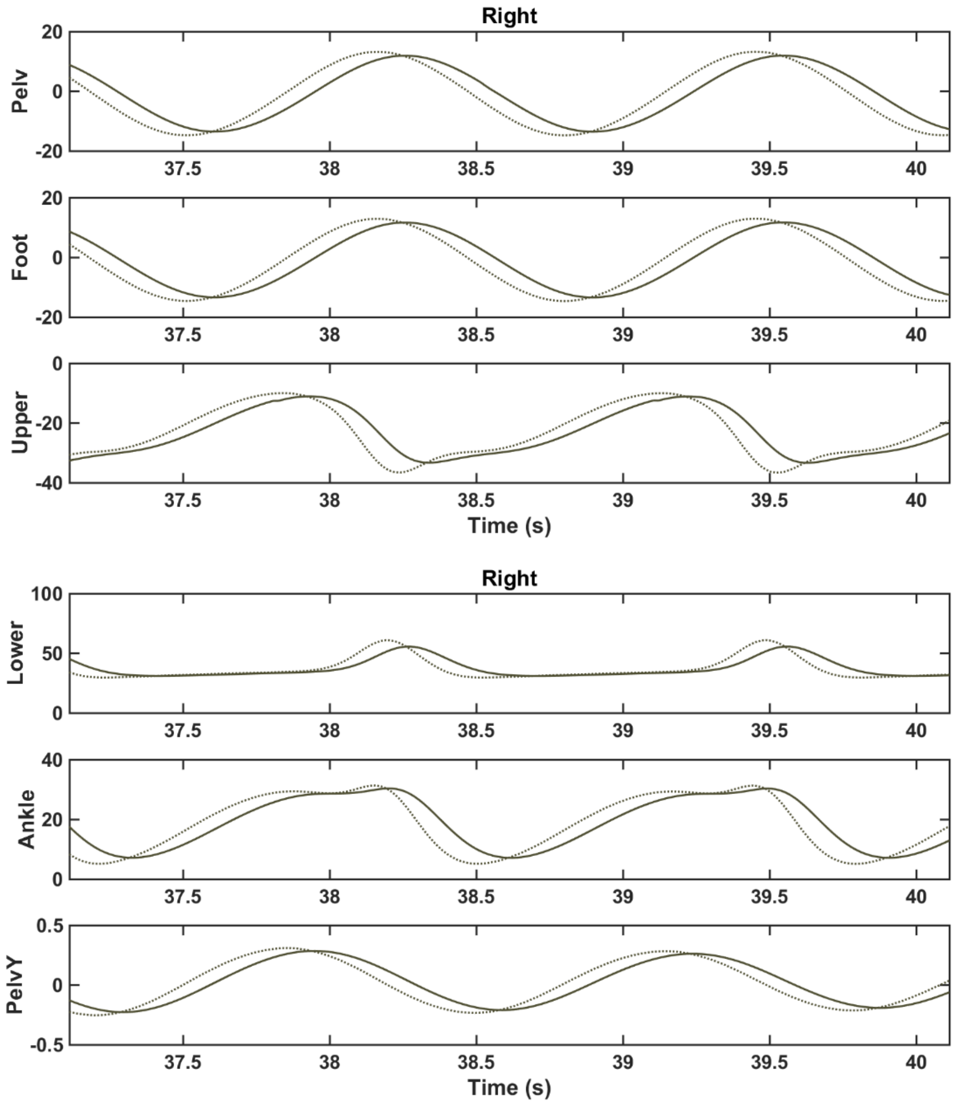

Figure 57: "Healthy" Right Leg (From top to bottom – Hip Roll, Foot Roll, Hip Pitch, Knee Pitch, Ankle Pitch, Hip Yaw) (Dotted line – Desired Joint Position; Solid line – Real Joint Position)

Figure 58 shows the sum of the FSR from each foot, filter with a low pass filter, combine with its foot y position or foot clearance. From the FSR sum, instead of having a curve resembling a square wave, with the FSR sum being its maximum value while the leg's state is in stance and zero when it is in swing, the FSR sum, of both feet, has moments where its value changes significantly from a square wave. These spikes can be attributed to the rigid nature of the CPG controller and the humanoid robot. When a foot reaches the ground, thereby ending its swing, the resulting forward motion is not properly handled. The forward motion of the robot causes the other foot to rise in the air, which explains the last drop of the FSR sum when the stance is finishing. The first drop is the result of the same situation from the other leg. This forward motion causes oscillations in the entire robot's body. When finishing a swing motion, the resulting forward force is also enough to lift the other leg from the ground.

In regards to the foot clearance, the results are what is expected of the movement, a foot takes during the swing state. With a maximum of 1.7 cm off the ground, the foot starts rising at the beginning of the swing and moves in a controlled fashion until the end of its motion.

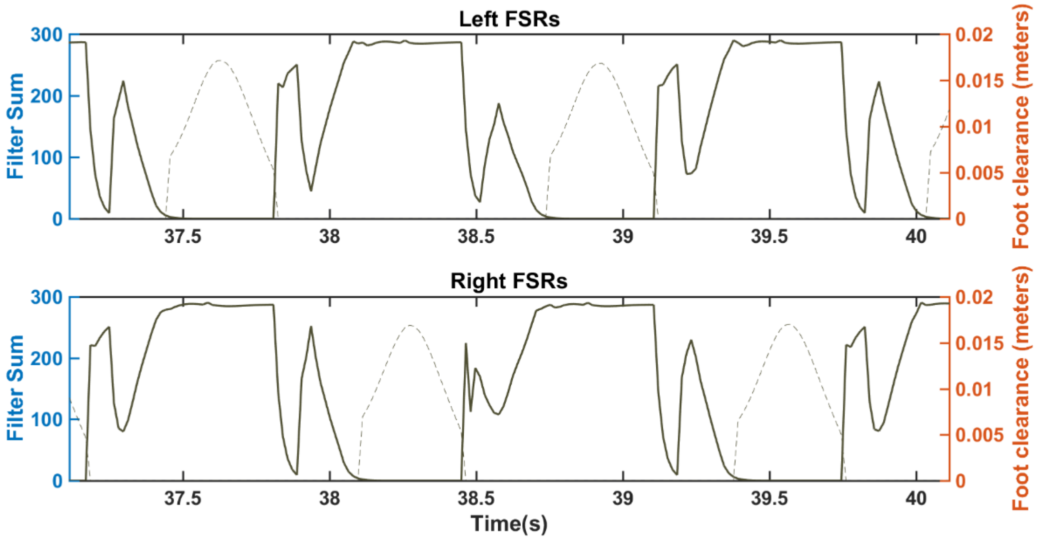

Figure 58: "Healthy" Filtered FSR Values (solid line) and the Foot Clearance (dashed line)

In figure 59, the COM position during the individual run of 40.1 seconds is shown. In this time the humanoid robot was able to move 2.25 meters which equates to a speed of 0.056 meters per second. It is also shown the motion the COM makes during the gait cycles. As expected the COM displays a side to side motion, shifting its center of gravity to move forward. In the graph, is also clear to see the effects of the turn correction added to the CPG controller, when the robot corrects its direction after 1 meter and again at about 1.75 meters.

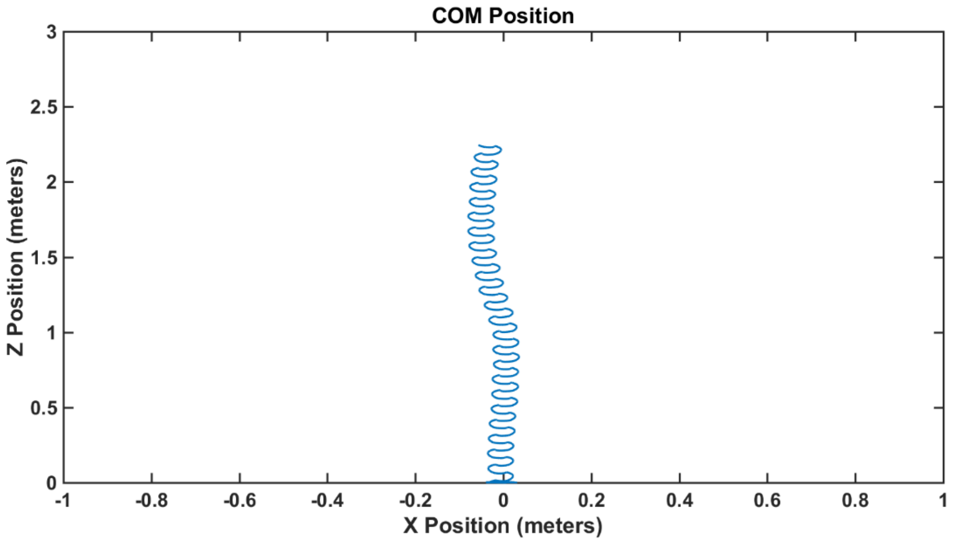

Figure 59: "Healthy" COM Position over time

Individual with the Prosthesis

Has it has been mentioned before, to simulate the prosthesis for the simulation tests, the control for the ankle pitch and the foot roll, on the right leg, instead of being given by the CPG controller, were instead provided by the prosthesis controller. This controller uses a two-state finite state machine to change the stiffness, the damping and the equilibrium position parameters of the impedance controller, thereby actuating the device. The parameters were optimized by a GA optimizer

The optimization of the humanoid robot and the prosthesis controller system took several iterations of optimizations. This is due to the robot being sensitive to slight variations of the parameters, which could result in the robot's fall. The first good results were only achieved after the robot was able to move forward, even if just slightly, and optimize from that result until a satisfactory controller was obtained.

The figure 60 and 61 show the joint trajectories for the left and right leg, respectively, of the humanoid robot, when wearing the prosthesis.

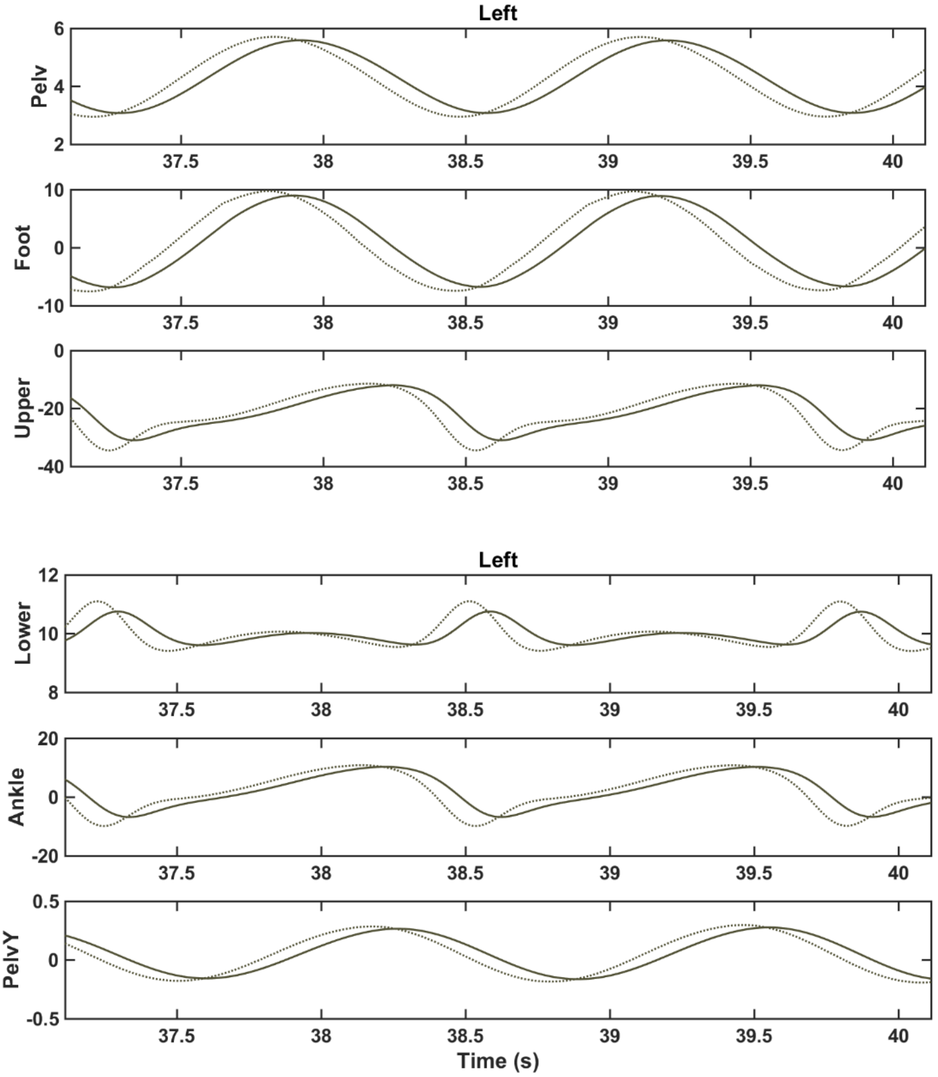

Figure 60: (Prosthesis User) Left Leg (From top to bottom – Hip Roll, Foot Roll, Hip Pitch, Knee Pitch, Ankle Pitch, Hip Yaw) (Dotted line – Desired Joint Position; Solid line – Real Joint Position)

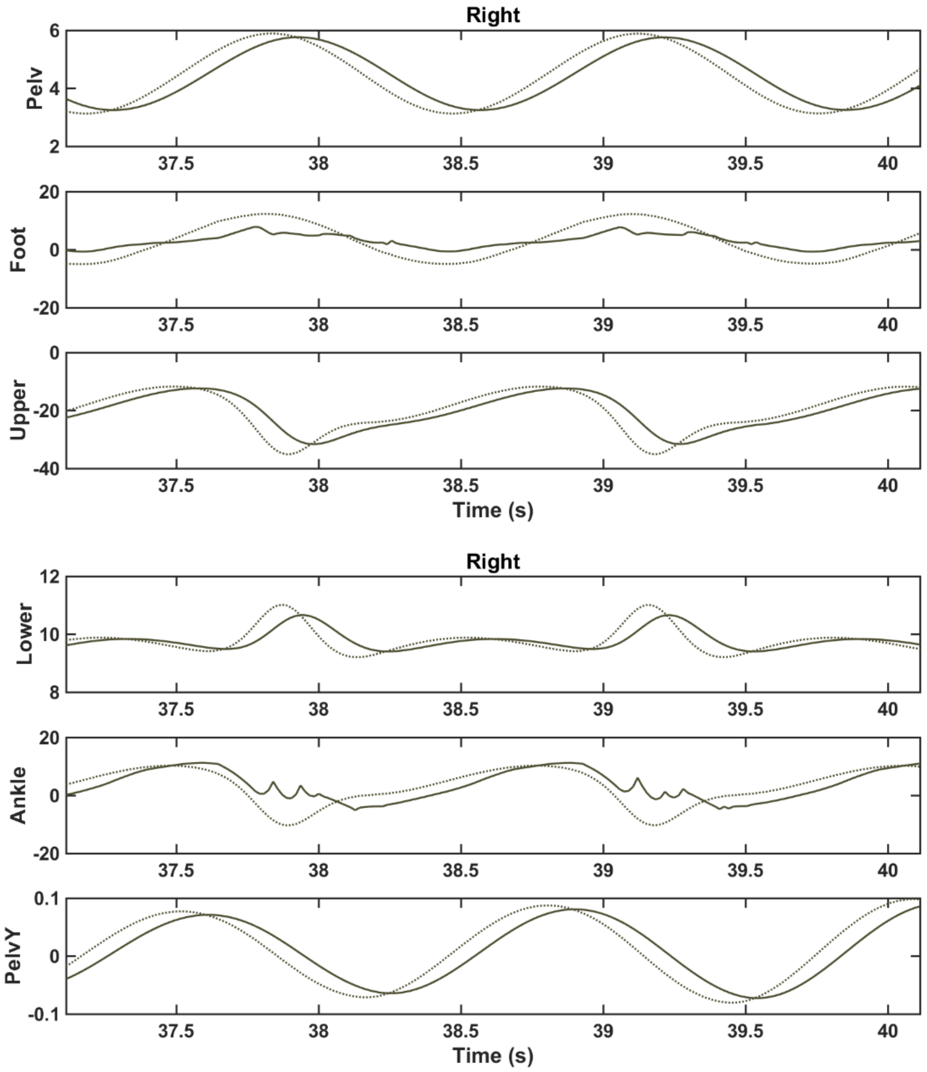

Figure 61: (Prosthesis User) Right Leg -Leg with the prosthesis - (From top to bottom – Hip Roll, Foot Roll, Hip Pitch, Knee Pitch, Ankle Pitch, Hip Yaw) (Dotted line – Desired Joint Position; Solid line – Real Joint Position)

The major differences between these trajectories and the “healthy” trajectories are found in the right leg, more specifically the ankle and foot from the right leg, i.e. the ones controlled by the prosthesis. The rest of the joints do differ from the “healthy” ones but only in amplitude and their offset. The right ankle is able to closely follow the CPG trajectory, except during the swing. During the swing, the joint oscillates due to a high damping gain. Although there are oscillations, they do not appear to affect the balance of the robot during swing. The passive foot, on the other hand, does not follow the CPG trajectory, staying somewhat constant through the gait cycle. Since this joint was made to be passive, it requires outside forces to be able to follow a trajectory and in this situation, this outside force was to be provided by the balancing motion from the left leg. With these optimized parameters, the walking motion of the robot was focus on keeping the COM close to the healthy leg, thereby keeping the balancing motion to a minimum.

Unlike the FSR values from the healthy individual, the values from the prosthesis user from both legs, are not as similar, as shown in figure 62. Since this individual is wearing the prosthesis, this is not unexpected, however, in this case, the left leg (i.e. the leg without the prosthesis) does a less clear distinction between the stance and swing states. The left leg is also shown to never fully lift the foot from the ground, having at least one of its FSRs in contact with the floor. While this does not influence the tests performed in this work, it would prevent the foot clearing a small obstacle if needed. In the leg with the prosthesis, there is a significant foot clearance, which would allow for the foot to overcome small obstacles, however, the prosthesis presents a high amount of vibrations, which could cause problems in a different scenario. In the same way as the left foot, this does not affect the tests perform here.

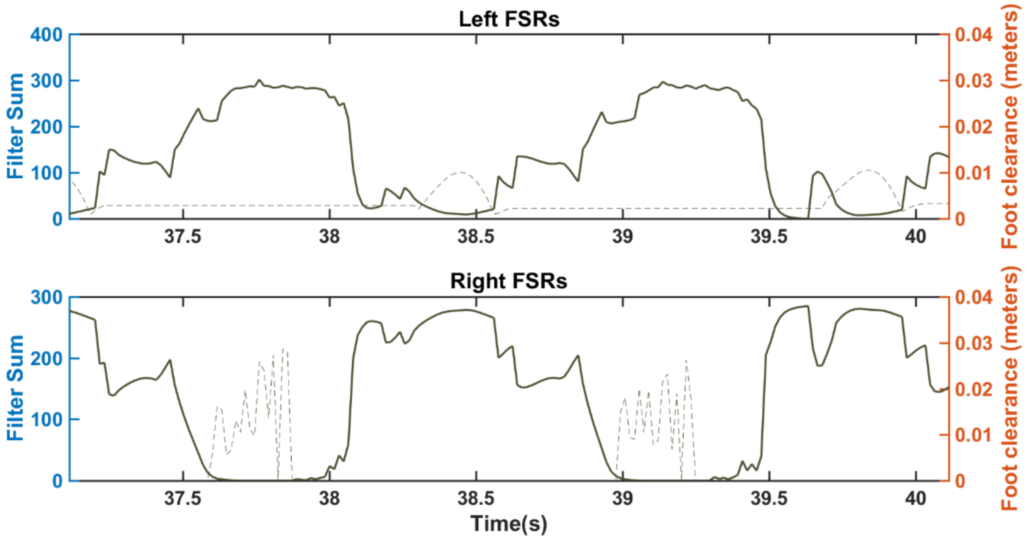

Figure 62: (Prosthesis User) Filtered FSR Values (solid line) and the Foot Clearance (dashed line)

The COM position, figure 63, of this prosthesis controller, also differs from the healthy one by having a smaller motion range in the X-axis, meaning that the COM does not sway from side to side as much as the healthy individual. The COM trajectory is also less smooth, presenting sharper changes in direction. The turn correction is also not as pronounced as in the healthy individual, however, it is still able to correct the forward trajectory of the robot at about the 0.75 meters.

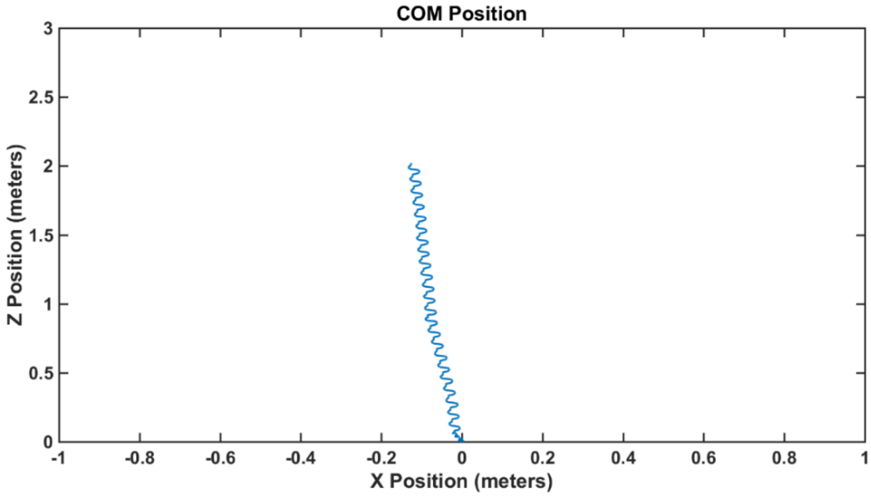

Figure 63: (Prosthesis User) COM Position over time

Although, in this case, the left leg is always in contact with the ground, the right leg raises and lowers properly, shown by the difference in the FSR values throughout the gait cycle. As such, the prosthesis controller is still able to actuate properly. In figure 64, the FSR values from the right leg are shown with the prosthesis state. The figure shows that the controller is able to detect the transitions from stance to swing and vice-versa, with no delay.

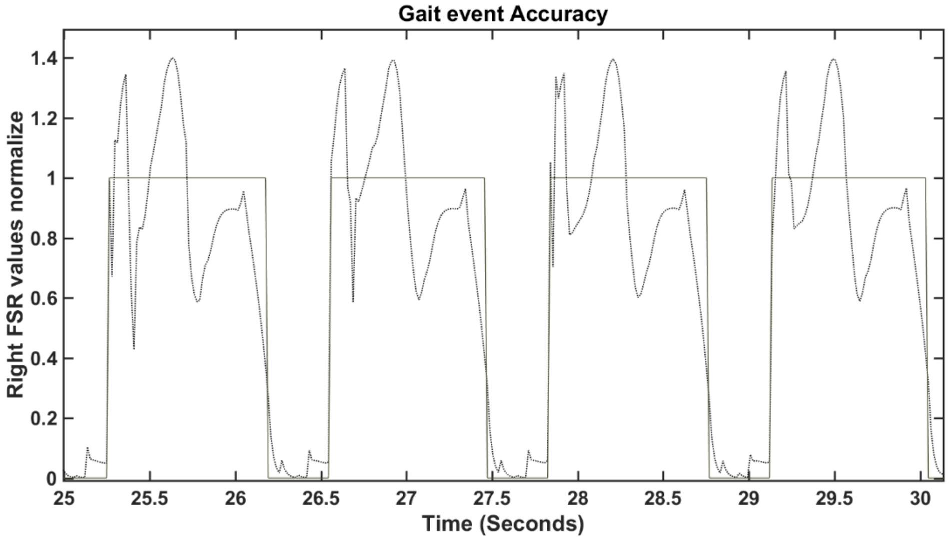

Figure 64: Gait Event Accuracy (1 – Stance, 0 - Swing) (Solid line) and the Filter FSR values (Dotted line)

CHAPTER 6 CONCLUSIONS AND FUTURE WORK

In this chapter, the conclusions of the dissertation and the future work are presented. In the conclusions section, the research questions asked in Chapter 1 are answered, whereas in the future work section, possible improvements to the prototype and controller are mentioned as well as future tests to be performed to the prosthesis.

6.1 Conclusions

In this thesis, a prosthesis controller for a transtibial powered prosthesis was developed. This controller is based on the impedance control developed by Hogan and is used to provide torque commands instead of position commands. To determine the parameters of the prosthesis controller, a genetic algorithm was used. A comparison between the use or not of the device model on the controller is also provided, showing the benefits the model offers versus the problems that arise from its use.

(RQ1): What are the advantages and disadvantages of using a dynamic model on an impedance controller?

From the comparison, it can be concluded that the use of a dynamic model can improve the performance of the controller by decreasing the time of stabilization and decreasing the steady state error of the actuator. This improvement allows for a decrease in the stiffness and damping values for the actuator, which results in a more adaptable and less restrictive motion. As it was mentioned, by lowering the stiffness and damping values, the amount of force present in the interaction points can also be lower and resulting in a safer manipulator, for both the device and the environment.

Although the inclusion of a dynamic model in the controller can be a significant improvement in the end, it does have problems. The main obstacle, when using a model, is the determination of the model itself, which can be a difficult task when the manipulator is complex. The complexity of a manipulator is connected to the number of links, the degrees of freedom, the constraints, the complexity of the joints and the complexity of the environment. With the number of factors required for a dynamic model is easy to have an inaccurate model. The inaccurate model, in turn, can lead to high interaction forces, which might damage the manipulator and or the environment, and even lead to instability.

(RQ2): Is it possible to substitute the ankle pitch joint of the Darwin-OP robot with an impedance-controlled prosthesis?

In this thesis, a design for an impedance-controlled prosthesis for the humanoid robot Darwin-OP was tested. The tests showed that it is possible to substitute the joints of the Darwin-OP robot with an impedance-controlled prosthesis since the robot was able to walk forward without difficulties. Although possible the tests showed that the prosthesis was not able to fully reproduce the motions it was replacing and therefore the prosthesis had a worse performance overall. These results, however, were to be expected since the original or healthy gait differs from that of a human's. In a human gait, the ankle pitch provides most of the energy necessary to walk, with the ankle roll providing stability to irregular grounds. In the Darwin-OP robot, the ankle pitch and roll work together with the rest of the leg joints to position the leg correctly in the ground. Unlike a human's gait, the CPG controller used shifts the COM from side to side to the leg in stance and swings the other leg without requiring push-off power. In this type of walking control, a more accurate controller, such as the CPG controller is more adequate, than a more complaint controller, like the impedance controller.

(RQ3): Is a two-state finite state machine impedance controller sufficient to control the transitions of the prosthesis for the humanoid robot?

The impedance-based controller designed for the prosthesis was controlled by a two-state finite state machine, one for the gait phase stance and the other for the swing. The parameters for the impedance control were different, changing when the states transitions. Since the CPG control gait, in the Darwin-OP robot, moved the feet parallel to the ground, and also considering the manner in which the CPG controller moves the legs forward, the basic transitions of stance and swing do not have the same sub-transitions (i.e. heel-strike, foot flat or toe off) as a human. As such the division of the Darwin-OP gait in just the stance and swing phases is more than sufficient to control the prosthesis.

The prosthesis impedance control had parameters that needed to be determined for the controller to function properly, these being the stiffness, the damping and the equilibrium point, for both stance and swing phases. The Darwin-OP walking controller also had parameters to that also need to be determined, for the humanoid to walk, the CPG parameters The CPG parameters for the healthy individual were already found in previous works, however, with the substitution of the control of the ankle and foot joints to the prosthesis controller, new parameters for the Darwin-OP's CPG controller needed to be found. These new parameters are important since they will allow the Darwin-OP humanoid to adapt its walking gait to the prosthesis, as the prosthesis is not able to fully emulate the missing joints. To determine the parameters, for the prosthesis controller and the humanoid, a genetic algorithm was employed, which uses concepts from evolution to optimize a problem. The GA optimizer was able to successfully find the required parameters to be used in the simulation tests.

6.2 Future Work

The main goal of this work was the creation of an impedance-based controller for a transtibial prosthetic device, and its test in a simulation environment, as well as the delineation of the hardware for the physical prototype of the prosthesis. The work, however, can be improved in the following manner.

The controller should be made more robust, by employing a larger variety of sensors, such as a torque sensor for the controlled joints. The addition of different sensors can be argued against since this thesis does not utilize them, however, the tests performed in this work, focused only on forward walking. Other motions such as turning, walking up and down slopes and stairs and others, could pose difficult to the current controller and the inclusion of other sensors might help.

Relating to the previous point, the controller should be tested in different situations like the ones mentioned. The prosthetic device and its controller must be able to operate properly in different scenarios.

Regarding the prototype itself, it could also be subject to improving, the main one being the addition of a parallel spring, which, according to the literature review, is a common way to increase the torque provided by the device. The parallel spring can supply an extra amount of force, allowing for a smaller motor.

The prototype could also be used to test other types of controller, such as positions or bio-inspired controllers. By testing these controllers on the prototype, comparisons can be drawn against the impedance-based controller.

BIBLIOGRAPHY

Alcaide-Aguirre, R. E., Morgenroth, D. C. and Ferris, D. P. (2013) 'Motor control and learning with lower-limb myoelectric control in amputees', *Journal of rehabilitation research and development*. Superintendent of Documents, 50(5), p. 687.

Alimusaj, M. *et al.* (2009) 'Kinematics and kinetics with an adaptive ankle foot system during stair ambulation of transtibial amputees', *Gait and Posture*, 30(3), pp. 356–363. doi: 10.1016/j.gaitpost.2009.06.009.

Alves, J. (2017) *Dynamic Model of a Transtibial Prosthesis*.

André, J., Santos, C. and Costa, L. (2016) 'Skill Memory in Biped Locomotion: Using Perceptual Information to Predict Task Outcome', *Journal of Intelligent and Robotic Systems: Theory and Applications*, 82(3–4), pp. 379–397. doi: 10.1007/s10846-015-0197-z.

Aoi, S. and Tsuchiya, K. (2006) 'Stability analysis of a simple walking model driven by an oscillator with a phase reset using sensory feedback', *IEEE Transactions on Robotics*, 22(2), pp. 391–397. doi: 10.1109/TRO.2006.870671.

Arshavsky, Y. I., Deliagina, T. G. and Orlovsky, G. N. (1997) 'Pattern generation', *Current Opinion in Neurobiology*. Elsevier Current Trends, 7(6), pp. 781–789. doi: 10.1016/S0959-4388(97)80136-5.

Au, S., Berniker, M. and Herr, H. (2008) 'Powered ankle-foot prosthesis to assist level-ground and stair-descent gaits', *Neural Networks*, 21(4), pp. 654–666. doi: 10.1016/j.neunet.2008.03.006.

Au, S. K. *et al.* (2007) 'Powered ankle-foot prosthesis for the improvement of amputee ambulation', *Annual International Conference of the IEEE Engineering in Medicine and Biology - Proceedings*, pp. 3020–3026. doi: 10.1109/IEMBS.2007.4352965.

Au, S. K., Dilworth, P. and Herr, H. (2006) 'An Ankel-Foot Emulation System for the Study of Human Walking Biomechanics', *Proceedings of the 2006 IEEE International Conference on Robotics and Automation*, (May), pp. 2939–2945. doi: http://dx.doi.org/10.1109/ROBOT.2006.1642148.

Au, S. K. and Herr, H. M. (2008) 'Powered ankle-foot prosthesis', *IEEE Robotics & Automation Magazine*. IEEE, 15(3).

Au, S. K., Weber, J. and Herr, H. (2009) 'Powered Ankle--Foot Prosthesis Improves Walking Metabolic Economy', *Robotics, IEEE Transactions on*, 25(1), pp. 51–66.

Behnke, S. (2006) 'Online trajectory generation for omnidirectional biped walking', *Proceedings - IEEE International Conference on Robotics and Automation*, pp. 1597–1603. doi: 10.1109/ROBOT.2006.1641935.

Bellman, R. D., Holgate, M. A. and Sugar, T. G. (2008) 'SPARKy 3: Design of an active robotic ankle prosthesis with two actuated degrees of freedom using regenerative kinetics', *Proceedings of the 2nd Biennial IEEE/RAS-EMBS International Conference on Biomedical Robotics and Biomechatronics, BioRob 2008*, (November 2008), pp. 511–516. doi: 10.1109/BIOROB.2008.4762887.

Bizzi, E. *et al.* (2008) 'Combining modules for movement', *Brain Research Reviews*. Elsevier, pp. 125–133. doi: 10.1016/j.brainresrev.2007.08.004.

Boaventura, T. *et al.* (2013) 'Stability and performance of the compliance controller of the quadruped robot hyq', in *Intelligent Robots and Systems (IROS), 2013 IEEE/RSJ International Conference on*, pp. 1458–1464.

Bonitz, R. G. and Hsia, T. C. (1996) 'Internal force-based impedance control for cooperating manipulators', *IEEE Transactions on Robotics and Automation*, 12(1), pp. 78–89. doi: 10.1109/70.481752.

Brown, T. G. (1911) 'The intrinsic factors in the act of progression in the mammal', *Proceedings of the Royal Society of London. Series B, Containing Papers of a Biological Character*. The Royal Society, 84(572), pp. 308–319. doi: 10.1098/rspb.1911.0077.

Buchli, J. *et al.* (2009) 'Compliant quadruped locomotion over rough terrain', in *2009 IEEE/RSJ International Conference on Intelligent Robots and Systems, IROS 2009*. IEEE, pp. 814–820. doi: 10.1109/IROS.2009.5354681.

Buehler, M. *et al.* (1998) 'SCOUT: a simple quadruped that walks, climbs, and runs', in *Proceedings. 1998 IEEE International Conference on Robotics and Automation (Cat. No.98CH36146)*. IEEE, pp. 1707–1712. doi: 10.1109/ROBOT.1998.677408.

Burdet, E. *et al.* (2001) 'The central nervous system stabilizes unstable dynamics by learning optimal impedance', *Nature*. Nature Publishing Group, 414(6862), pp. 446–449. doi: 10.1038/35106566.

Caputo, J. and Collins, S. H. (2011) 'Externally powered and controlled ankle-foot prosthesis', *6th Annual Conference on Dynamic Walking, Jena Germany*.

Cherelle, P. *et al.* (2012) 'The AMP-Foot 2.0:Mimicking Intact Ankle Behavior with a Powered Transtibial Prosthesis', *Biomedical Robotics and Biomechatronics (BioRob), 2012 4th IEEE RAS & EMBS International Conference on*, pp. 544–549.

Cherelle, P. *et al.* (2014) 'Advances in propulsive bionic feet and their actuation principles', *Advances in Mechanical Engineering*, 2014. doi: 10.1155/2014/984046.

Cherelle, P. *et al.* (2016) 'The AMP-Foot 3, new generation propulsive prosthetic feet with explosive motion characteristics: Design and validation', *BioMedical Engineering Online*. BioMed Central, 15(3), pp. 21–36. doi: 10.1186/s12938-016-0285-8.

Colgate, J. E. (1988) *The control of dynamically interacting systems*. Massachusetts Institute of Technology.

Collins, S. H. and Kuo, A. D. (2005) ‘Controlled Energy Storage and Return Prostheses Reduces Metabolic Cost of Walking’, *ISB XXth Congress - ASB 29th Annual Meeting*, p. 804.

Craig, J. J. (2004) ‘Introduction to Robotics: Mechanics and Control 3rd’, *Prentice Hall*, 1(3), p. 408. doi: 10.1109/MEX.1986.4306961.

Deb, K. and Bhushan Agrawal, R. (1995) *Simulated Binary Crossover for Continuous Search Space*. Available at: https://pdfs.semanticscholar.org/b8ee/6b68520ae0291075cb1408046a7dff9dd9ad.pdf (Accessed: 6 December 2018).

Eilenberg, M. F., Geyer, H. and Herr, H. (2010) ‘Control of a powered ankle-foot prosthesis based on a neuromuscular model’, *IEEE Transactions on Neural Systems and Rehabilitation Engineering*, 18(2), pp. 164–173. doi: 10.1109/TNSRE.2009.2039620.

Fedele, A., Fioretti, A. and Ulivi, G. (1992) *Implementation of a Hybrid Force-Position Controller using Sliding Mode Techniques*, *IEEE Intcmatiaul Wcrcnce on Robotics and Automation Nice*. Available at: https://www.computer.org/csdl/proceedings/robot/1992/2720/00/00219967.pdf (Accessed: 2 August 2018).

Ferreira, C., Reis, L. P. and Santos, C. P. (2016) ‘Review of Control Strategies for Lower Limb Prostheses’, pp. 209–220. doi: 10.1007/978-3-319-27149-1_17.

Ferreira, C. and Santos, C. P. (2015) ‘Combining central pattern generators and reflexes’, *Neurocomputing*, 170, pp. 79–91. doi: 10.1016/j.neucom.2015.05.113.

Figueiredo, J. *et al.* (2016) ‘Real-Time Gait Events Detection during Walking of Biped Model and Humanoid Robot through Adaptive Thresholds’, *Proceedings - 2016 International Conference on Autonomous Robot Systems and Competitions, ICARSC 2016*, pp. 66–71. doi: 10.1109/ICARSC.2016.58.

Flash, T. and Hochner, B. (2005) ‘Motor primitives in vertebrates and invertebrates’, *Current Opinion in Neurobiology*. Elsevier Current Trends, pp. 660–666. doi: 10.1016/j.conb.2005.10.011.

Franklin, D. W. *et al.* (2003) ‘Functional significance of stiffness in adaptation of multijoint arm movements to stable and unstable dynamics’, *Experimental Brain Research*. Springer-Verlag, 151(2), pp. 145–157. doi: 10.1007/s00221-003-1443-3.

Gao, Z., Huang, Y. and Han, J. (2001) ‘An alternative paradigm for control system design’, *Proceedings of the IEEE Conference on Decision and Control*, 5(February), pp. 4578–4585. doi: 10.1109/CDC.2001.980926.

Geeroms, J. *et al.* (2013) ‘Ankle-Knee prosthesis with powered ankle and energy transfer for CYBERLEGs α-prototype’, *IEEE International Conference on Rehabilitation Robotics*. doi: 10.1109/ICORR.2013.6650352.

Geyer, H. and Herr, H. (2010) ‘A Muscle-reflex model that encodes principles of legged mechanics produces human walking dynamics and muscle activities’, *IEEE Transactions on*

Neural Systems and Rehabilitation Engineering, 18(3), pp. 263–273. doi: 10.1109/TNSRE.2010.2047592.

Goldberg, D. E. (1989) ‘Genetic algorithms in search, optimization, and machine learning/David E’, *Goldberg.–[USA]: Addison-Wesley*.

Goldenberg, A. A. (1992) ‘Analysis of force control based on linear models’, in *Proceedings 1992 IEEE International Conference on Robotics and Automation*, pp. 1348–1353.

Grabbe, M. T. *et al.* (1992) ‘Robust control of robot manipulators during constrained and unconstrained motion’, in *Robotics and Automation, 1992. Proceedings., 1992 IEEE International Conference on*, pp. 2146–2151.

Gregg, R. D. and Sensinger, J. W. (2014) ‘Towards biomimetic virtual constraint control of a powered prosthetic leg’, *IEEE Transactions on Control Systems Technology*, 22(1), pp. 246–254. doi: 10.1109/TCST.2012.2236840.

Grillner, S. *et al.* (2008) ‘Neural bases of goal-directed locomotion in vertebrates-An overview’, *Brain Research Reviews*. Elsevier, pp. 2–12. doi: 10.1016/j.brainresrev.2007.06.027.

Grimes, D. L. (1979) ‘An active multi mode above knee prosthesis controller’, pp. 1–180.

Grizzle, J. W. *et al.* (2009) ‘MABEL, a new robotic bipedal walker and runner’, *Proceedings of the American Control Conference*, pp. 2030–2036. doi: 10.1109/ACC.2009.5160550.

Van Ham, R. *et al.* (2007) ‘MACCEPA, the mechanically adjustable compliance and controllable equilibrium position actuator: Design and implementation in a biped robot’, *Robotics and Autonomous Systems*, 55(10), pp. 761–768. doi: 10.1016/j.robot.2007.03.001.

Herr, H. M. and Grabowski, A. M. (2012) ‘Bionic ankle-foot prosthesis normalizes walking gait for persons with leg amputation’, *Proceedings of the Royal Society B: Biological Sciences*, 279(1728), pp. 457–464. doi: 10.1098/rspb.2011.1194.

Herzog, A. *et al.* (2014) ‘Balancing experiments on a torque-controlled humanoid with hierarchical inverse dynamics’, in *Intelligent Robots and Systems (IROS 2014), 2014 IEEE/RSJ International Conference on*, pp. 981–988.

Hirzinger, G. *et al.* (2001) ‘On a new generation of torque controlled light-weight robots’, in *Robotics and Automation, 2001. Proceedings 2001 ICRA. IEEE International Conference on*, pp. 3356–3363.

Hogan, N. (1984) ‘Adaptive Control of Mechanical Impedance by Coactivation of Antagonist Muscles’, *IEEE Transactions on Automatic Control*, 29(8), pp. 681–690. doi: 10.1109/TAC.1984.1103644.

Hogan, N. (1985) ‘Impedance Control: An Approach to Manipulation: Part I—Theory’, *Journal of Dynamic Systems, Measurement, and Control*. ASME, 107(1), pp. 8–16. Available at: http://dx.doi.org/10.1115/1.3140702.

Hogan, N. (1990) ‘Mechanical impedance of single-and multi-articular systems’, in *Multiple muscle systems*. Springer, pp. 149–164.

Hogan, N. and Buerger, S. P. (2005) ‘Impedance and Interaction Control 19.1’, *Robotics and automation handbook*, pp. 19–1. doi: doi:10.1201/9781420039733.ch19.

Holland, J. H. (1975) ‘Adaptation in natural and artificial systems. An introductory analysis with application to biology, control, and artificial intelligence’, *Ann Arbor, MI: University of Michigan Press*, pp. 439–444.

Hong-Liu, Y. *et al.* (2010) ‘Dynamics modeling and analysis for hydraulic intelligent prosthetic leg’, *Journal of Prosthetics and Orthotics*, pp. 177–182. doi: 10.1097/JPO.0b013e3181eaf2da.

Huang, H. (Helen), Kuiken, T. A. and Lipschutz, R. D. (2011) ‘A Strategy for Identifying Locomotion Modes Using Surface Electromyography He’, 56(1), pp. 65–73. doi: 10.1109/TBME.2008.2003293.A.

Hyon, S.-H. (2009) ‘Compliant terrain adaptation for biped humanoids without measuring ground surface and contact forces’, *IEEE Transactions on Robotics*. IEEE, 25(1), pp. 171–178.

Hyon, S.-H., Morimoto, J. and Cheng, G. (2008) ‘Hierarchical motor learning and synthesis with passivity-based controller and phase oscillator’, in *Robotics and Automation, 2008. ICRA 2008. IEEE International Conference on*, pp. 2705–2710.

Hyon, S.-H., Morimoto, J. and Kawato, M. (2010) ‘From compliant balancing to dynamic walking on humanoid robot: Integration of CNS and CPG’, in *Robotics and Automation (ICRA), 2010 IEEE International Conference on*, pp. 1084–1085.

Hyun, D. J. *et al.* (2014) ‘High speed trot-running: Implementation of a hierarchical controller using proprioceptive impedance control on the MIT Cheetah’, *International Journal of Robotics Research*, 33(11), pp. 1417–1445. doi: 10.1177/0278364914532150.

Kandel, E. R. *et al.* (2000) *Principles of neural science*. McGraw-hill New York.

Kenneth Klute, G. (1999) *Artificial Muscles: Actuators for Biorobotic Systems*. Washington.

Khatib, O. (1987) ‘A unified approach for motion and force control of robot manipulators: The operational space formulation’, *IEEE Journal on Robotics and Automation*, 3(1), pp. 43–53. doi: 10.1109/JRA.1987.1087068.

Kiehn, O. (2006) ‘LOCOMOTOR CIRCUITS IN THE MAMMALIAN SPINAL CORD’, *Annual Review of Neuroscience*. Annual Reviews, 29(1), pp. 279–306. doi: 10.1146/annurev.neuro.29.051605.112910.

Kimura, H., Fukuoka, Y. and Cohen, A. H. (2007) ‘Adaptive dynamic walking of a quadruped robot on natural ground based on biological concepts’, *The International Journal of Robotics Research*. Sage Publications Sage UK: London, England, 26(5), pp. 475–490.

King, J. P. *et al.* (2017) ‘Design, modeling, and control of pneumatic artificial muscles with integrated soft sensing', in *Robotics and Automation (ICRA), 2017 IEEE International Conference on*, pp. 4985–4990.

Kirkpatrick, S., Gelatt, ; C D and Vecchi, ; M P (1983) *Optimization by Simulated Annealing*, *New Series*. Available at: https://sci2s.ugr.es/sites/default/files/files/Teaching/GraduatesCourses/Metaheuristicas/Bibliography/1983-Science-Kirkpatrick-sim_anneal.pdf (Accessed: 6 December 2018).

Lafreniere-Roula, M. and McCrea, D. A. (2005) 'Deletions of Rhythmic Motoneuron Activity During Fictive Locomotion and Scratch Provide Clues to the Organization of the Mammalian Central Pattern Generator', *Journal of Neurophysiology*. American Physiological Society, 94(2), pp. 1120–1132. doi: 10.1152/jn.00216.2005.

Lapre, A. K. and Sup, F. (2011) 'Simulation of a slope adapting ankle prosthesis provided by semi-active damping', *Proceedings of the Annual International Conference of the IEEE Engineering in Medicine and Biology Society, EMBS*, (August 2011), pp. 587–590. doi: 10.1109/IEMBS.2011.6090110.

Lawson, B. E. *et al.* (2013) 'Control of stair ascent and descent with a powered transfemoral prosthesis', *IEEE Transactions on Neural Systems and Rehabilitation Engineering*. IEEE, 21(3), pp. 466–473.

Levine, W. S. (1996) 'The Control Handbook', *The Control Handbook*, p. 1566. doi: www.copyright.com (http:// www.copyright.com/).

Liu, M. *et al.* (2014) 'Improving Finite State Impedance Control of Active-Transfemoral Prosthesis Using Dempster-Shafer Based State Transition Rules', *Journal of Intelligent and Robotic Systems: Theory and Applications*, 76(3–4), pp. 461–474. doi: 10.1007/s10846-013-9979-3.

Macedo, J. F. F. (2014) *Towards the Improvement of Robot Motion Learning Techniques*.

Maki, H. K. (2007) *Bioinspiration and Robotics: Walking and Climbing Robots*. doi: 10.5772/46.

Marder, E. *et al.* (2005) 'Invertebrate central pattern generation moves along', *Current Biology*. Cell Press, pp. R685–R699. doi: 10.1016/j.cub.2005.08.022.

Martinez-Villalpando, E. C. and Herr, H. (2009) 'Agonist-antagonist active knee prosthesis: A preliminary study in level-ground walking', *The Journal of Rehabilitation Research and Development*, 46(3), p. 361. doi: 10.1682/JRRD.2008.09.0131.

Mason, M. T. (1981) 'Compliance and force control for computer controlled manipulators', *IEEE Transactions on Systems, Man, and Cybernetics*. IEEE, 11(6), pp. 418–432.

Mathias, J. R. *et al.* (2010) 'Concept Through Preliminary Bench Testing of a Powered Lower Limb Prosthetic Device', 33(11), pp. 1212–1217. doi: 10.1016/j.dci.2009.07.003.Characterization.

Matos, V. and Santos, C. (2012) 'Central Pattern Generators with Phase Regulation for the Control of Humanoid Locomotion', pp. 134–139.

Matos, V. and Santos, C. P. (2014) 'Towards goal-directed biped locomotion: Combining CPGs and motion primitives', *Robotics and Autonomous Systems*. Elsevier B.V., 62(12), pp. 1669–1690. doi: 10.1016/j.robot.2014.08.010.

McCrea, D. A. and Rybak, I. A. (2008) 'Organization of mammalian locomotor rhythm and pattern generation', *Brain Research Reviews*. Elsevier, pp. 134–146. doi: 10.1016/j.brainresrev.2007.08.006.

Michel, O. (2004) 'Cyberbotics Ltd. Webots^{TM}: professional mobile robot simulation', *International Journal of Advanced Robotic Systems*. SAGE Publications Sage UK: London, England, 1(1), p. 5.

Morimoto, J. *et al.* (2008) 'A Biologically Inspired Biped Locomotion Strategy for Humanoid Robots: Modulation of Sinusoidal Patterns by a Coupled Oscillator Model', *IEEE Transactions on Robotics*, 24(1), pp. 185–191. doi: 10.1109/TRO.2008.915457.

Murray, R. M., Li, Z. and Sastry, S. S. (1994) 'A Mathematical Introduction to Robotic Manipulation CRC Press, Boca Raton, FL, 1994', *Google Scholar*.

Nakanishi, J. *et al.* (2004) 'Learning from demonstration and adaptation of biped locomotion', *Robotics and Autonomous Systems*, pp. 79–91. doi: 10.1016/j.robot.2004.03.003.

Nandi, G. C., Ijspeert, A. and Nandi, A. (2008) 'Biologically inspired CPG based above knee active prosthesis', *2008 IEEE/RSJ International Conference on Intelligent Robots and Systems, IROS*, pp. 2368–2373. doi: 10.1109/IROS.2008.4650600.

Nevins, J. L. and Whitney, D. E. (1972) 'The force vector assembler concept', in *On Theory and Practice of Robots and Manipulators*. Springer, pp. 273–288.

Newman, W. S. (1992) 'Stability and Performance Limits of Interaction Controllers', *Journal of Dynamic Systems, Measurement, and Control*. ASME, 114(4), pp. 563–570. Available at: http://dx.doi.org/10.1115/1.2897725.

Oliveira, M. (2012) 'Locomotion biped Optimization', pp. 0–34.

Orlovskii, G. N., Deliagina, T. G. and Grillner, S. (1999) *Neuronal control of locomotion : from mollusc to man*. New York: Oxford University Press.

Ott, C. *et al.* (2012) 'Hardware and Control Concept for an Experimental Bipedal Robot with Joint Torque Sensors', *Journal of the Robotics Society of Japan*. The Robotics Society of Japan, 30(4), pp. 378–382. doi: 10.7210/jrsj.30.378.

Paine, N., Oh, S. and Sentis, L. (2014) 'Design and control considerations for high-performance series elastic actuators', *IEEE/ASME Transactions on Mechatronics*, 19(3), pp. 1080–1091. doi: 10.1109/TMECH.2013.2270435.

Paljug, E. *et al.* (1992) 'Important Considerations in Force Control with Applications to Multi-Arm Manipulation', in *IEEE International Conference on Robotics and Automation*, pp. 1270–1275. Available at: http://repository.upenn.edu/cis_reports (Accessed: 2 August 2018).

Paul, R. P. (1981) *Robot manipulators: mathematics, programming, and control: the computer control of robot manipulators*. Richard Paul.

Pratt, G. A. A. and Williamson, M. M. M. (1995) 'Series elastic actuators', in *Proceedings 1995 IEEE/RSJ International Conference on Intelligent Robots and Systems. Human Robot Interaction and Cooperative Robots*. IEEE Comput. Soc. Press, pp. 399–406 vol.1. doi: 10.1109/IROS.1995.525827.

Pratt, J. *et al.* (2001) 'Virtual Model Control: An Intuitive Approach for Bipedal Locomotion', *The International Journal of Robotics Research*. SAGE Publications, 20(2), pp. 129–143. doi: 10.1177/02783640122067309.

Pratt, J. and Krupp, B. (2008) 'Design of a bipedal walking robot', (December), p. 69621F. doi: 10.1117/12.777973.

Prof. De Luca, A. (2016) *Dynamic model of robots: Lagrangian approach*. Available at: http://www.dis.uniroma1.it/~deluca/rob2_en/03_LagrangianDynamics_1.pdf (Accessed: 7 December 2017).

Prosthetic Technology – Ottobock, Ossur | MCOP Prosthetics (no date). Available at: https://mcopro.com/prosthetics/technology/ (Accessed: 8 September 2018).

R., D. M., YURI, G. and M., P. M. (2006) 'Evidence for a Spinal Central Pattern Generator in Humansa', *Annals of the New York Academy of Sciences*. Wiley/Blackwell (10.1111), 860(1), pp. 360–376. doi: 10.1111/j.1749-6632.1998.tb09062.x.

Raibert, M. H. (1986) *Legged robots that balance*. MIT press.

Raibert, M. H. and Craig, J. J. (1981) 'Hybrid position/force control of manipulators', *Journal of Dynamic Systems, Measurement, and Control*, 102(127), pp. 126–133.

Richter, H. *et al.* (2015) 'Dynamic modeling, parameter estimation and control of a leg prosthesis test robot', *Applied Mathematical Modelling*. Elsevier, 39(2), pp. 559–573. doi: 10.1016/j.apm.2014.06.006.

Rossignol, S., Dubuc, R. and Gossard, J.-P. (2006) 'Dynamic Sensorimotor Interactions in Locomotion', *Physiological Reviews*. American Physiological Society, 86(1), pp. 89–154. doi: 10.1152/physrev.00028.2005.

Ryu, J. K. *et al.* (2009) 'Adaptive CPG based coordinated control of healthy and robotic lower limb movements', *Proceedings - IEEE International Workshop on Robot and Human Interactive Communication*, (1), pp. 122–127. doi: 10.1109/ROMAN.2009.5326045.

Al Salami, N. M. A. and Salami, N. M. A. Al (2009) 'Ant Colony Optimization Algorithm', 4(3), pp. 823–826. Available at: http://www.ubicc.org/files/pdf/10_336.pdf (Accessed: 6 December 2018).

Santos, C. P. and Ferreira, C. (2016) 'Impedance Control'.

Schaal, S. and Schweighofer, N. (2005) ‘Computational motor control in humans and robots’, *Current Opinion in Neurobiology*. Elsevier Current Trends, pp. 675–682. doi: 10.1016/j.conb.2005.10.009.

Selen, L. P. J., Franklin, D. W. and Wolpert, D. M. (2009) ‘Impedance Control Reduces Instability That Arises from Motor Noise’, *Journal of Neuroscience*, 29(40), pp. 12606–12616. doi: 10.1523/JNEUROSCI.2826-09.2009.

Semini, C. *et al.* (2011) ‘Design of HyQ--a hydraulically and electrically actuated quadruped robot’, *Proceedings of the Institution of Mechanical Engineers, Part I: Journal of Systems and Control Engineering*. SAGE Publications Sage UK: London, England, 225(6), pp. 831–849.

Semini, C. *et al.* (2015) ‘Towards versatile legged robots through active impedance control’, *International Journal of Robotics Research*, 34(7), pp. 1003–1020. doi: 10.1177/0278364915578839.

Shadmehr, R. and Arbib, M. A. (1992) ‘A mathematical analysis of the force-stiffness characteristics of muscles in control of a single joint system’, *Biological Cybernetics*. Springer-Verlag, 66(6), pp. 463–477. doi: 10.1007/BF00204111.

Sharon, A., Hogan, N. and Hardt, D. E. (1988) ‘High bandwidth force regulation and inertia reduction using a macro/micro manipulator system’, in *Robotics and Automation, 1988. Proceedings., 1988 IEEE International Conference on*, pp. 126–132.

Shi, Y. (2015) ‘Particle swarm optimization : Development , applications and resources’, (February 2001). doi: 10.1109/CEC.2001.934374.

Shorter, K. A. *et al.* (2012) ‘Modeling, control, and analysis of a robotic assist device’, *Mechatronics*, pp. 1067–1077. doi: 10.1016/j.mechatronics.2012.09.002.

Spong, M. W. *et al.* (2006) *Robot modeling and control*. Wiley New York.

SpringActive – Innovative Solutions to Powered Human Assistance (no date). Available at: https://springactive.com/ (Accessed: 8 September 2018).

Stephens, B. J. and Atkeson, C. G. (2010) ‘Push recovery by stepping for humanoid robots with force controlled joints’, *2010 10th IEEE-RAS International Conference on Humanoid Robots, Humanoids 2010*, pp. 52–59. doi: 10.1109/ICHR.2010.5686288.

Sup, F. *et al.* (2010) ‘Preliminary Evaluations of a Self-Contained Anthropomorphic Transfemoral Prosthesis’, 14(6), pp. 667–676. doi: 10.1109/TMECH.2009.2032688.Preliminary.

Sup, F., Bohara, A. and Goldfarb, M. (2009) ‘Design and Control of a Powered Transfemoral Prosthesis’, 129(1), pp. 77–83. doi: 10.1021/ja064902x.Brilliant.

Sup, F., Varol, H. A. and Goldfarb, M. (2011) ‘Upslope walking with a powered knee and ankle prosthesis: initial results with an amputee subject’, *IEEE Transactions on Neural Systems and Rehabilitation Engineering*. IEEE, 19(1), pp. 71–78.

Taga, G. (1998) ‘A model of the neuro-musculo-skeletal system for anticipatory adjustment of human locomotion during obstacle avoidance’, *Biological Cybernetics*, 78(1), pp. 9–17. doi: 10.1007/s004220050408.

Taga, G., Yamaguchi, Y. and Shimizu, H. (1991) ‘Self-organized control of bipedal locomotion by neural oscillators in unpredictable environment’, *Biological Cybernetics*, 65(3), pp. 147–159. doi: 10.1007/BF00198086.

Tee, K. P. *et al.* (2010) ‘Concurrent adaptation of force and impedance in the redundant muscle system’, *Biological Cybernetics*. Springer-Verlag, 102(1), pp. 31–44. doi: 10.1007/s00422-009-0348-z.

Thavai, R. (2016) ‘Dynamic Modelling of Biped Robot’. P and R Engineering Consultancy Publication.

Tilley, S. W. and Cannon Jr, R. H. (1986) ‘End point position and force control of a flexible manipulator with a quick wrist’, in *Proc. AIAA Guidance, Navigation and Control Conference*, pp. 41–49.

Torrealba, R. R. *et al.* (2010) ‘Through the development of a biomechatronic knee prosthesis for transfemoral amputees: Mechanical design and manufacture, human gait characterization, intelligent control strategies and tests’, *Proceedings - IEEE International Conference on Robotics and Automation*, (January), pp. 2934–2939. doi: 10.1109/ROBOT.2010.5509674.

Torrealba, R. R. *et al.* (2012) ‘Cybernetic knee prosthesis: Application of an adaptive central pattern generator’, *Kybernetes*, 41(1–2), pp. 192–205. doi: 10.1108/03684921211213034.

Torrealba, R. R., Fernández-López, G. and Grieco, J. C. (2008) ‘Towards the development of knee prostheses: review of current researches’, *Kybernetes*. Emerald Group Publishing Limited, 37(9/10), pp. 1561–1576.

Vanderborght, B. *et al.* (2013) ‘Variable impedance actuators: A review’, *Robotics and autonomous systems*. Elsevier, 61(12), pp. 1601–1614.

Varol, H. A. and Goldfarb, M. (2007) ‘Decomposition-based control for a powered knee and ankle transfemoral prosthesis’, in *Rehabilitation robotics, 2007. ICORR 2007. IEEE 10th international conference on*, pp. 783–789.

Wang, J., Kannape, O. A. and Herr, H. M. (2013) ‘Proportional EMG Control of Ankle Plantar Flexion in a Powered Transtibial Prosthesis’, *MIT Open Access Articles*, pp. 1–5. doi: 10.1109/ICORR.2013.6650391.

Whitney, D. E. (1977) ‘Force Feedback Control of Manipulator Fine Motions’, *Journal of Dynamic Systems, Measurement, and Control*. ASME, 99(2), pp. 91–97. Available at: http://dx.doi.org/10.1115/1.3427095.

Windrich, M. *et al.* (2016) ‘Active lower limb prosthetics: A systematic review of design issues and solutions’, *BioMedical Engineering Online*. BioMed Central, 15(3), pp. 5–19. doi: 10.1186/s12938-016-0284-9.

Winter, D. A. *et al.* (1990) ‘Biomechanical walking pattern changes in the fit and healthy elderly’, *Physical Therapy*, 70(6), pp. 340–347. doi: 10.1093/ptj/70.6.340.

Wu, S. K., Waycaster, G. and Shen, X. (2011) ‘Electromyography-based control of active above-knee prostheses’, *Control Engineering Practice*. Elsevier, 19(8), pp. 875–882. doi: 10.1016/j.conengprac.2011.04.017.

Zhang, J., Chien Chern, C. and Collins, S. (2016) ‘Torque control in legged locomotion’, *Bio-Inspired Legged Locomotion: Concepts, Control and Implementation*.

Zhiqiang Gao (2006) ‘Active disturbance rejection control: a paradigm shift in feedback control system design’, *2006 American Control Conference*, p. 7 pp. doi: 10.1109/ACC.2006.1656579.

Zhu, J., Wang, Q. and Wang, L. (2014) ‘On the design of a powered transtibial prosthesis with stiffness adaptable ankle and toe joints’, *IEEE Transactions on Industrial Electronics*, 61(9), pp. 4797–4807. doi: 10.1109/TIE.2013.2293691.

Zitzler, E. and Thiele, L. (1999) ‘Multiobjective Evolutionary Algorithms : A Comparative Case Study and the Strength Pareto Approach’, *IEEE TRANSACTIONS ON EVOLUTIONARY COMPUTATION*, 3(4), pp. 257–271. Available at: https://www.cse.unr.edu/~sushil/class/gas/papers/StrengthParetoEA.pdf (Accessed: 6 December 2018).